UNIVERSITY OF CALIFORNIA, SAN DIEGO

# Measurement of the Magnetic and Temperature Dependence of the Electron-Electron Anisotropic Temperature Relaxation Rate

A dissertation submitted in partial satisfaction of the

requirements for the degree Doctor of Philosophy

in Physics

by

Bret Robert Beck

Committee in charge:

Professor John H. Malmberg, Chairman
Professor Thomas M. O'Neil
Professor Carl E. McIlwain
Professor Hassan Aref
Professor Joel Fajans (U. C., Berkeley)

1990

The dissertation of Bret Robert Beck is approved, and it is acceptable in quality and form for publication on microfilm:

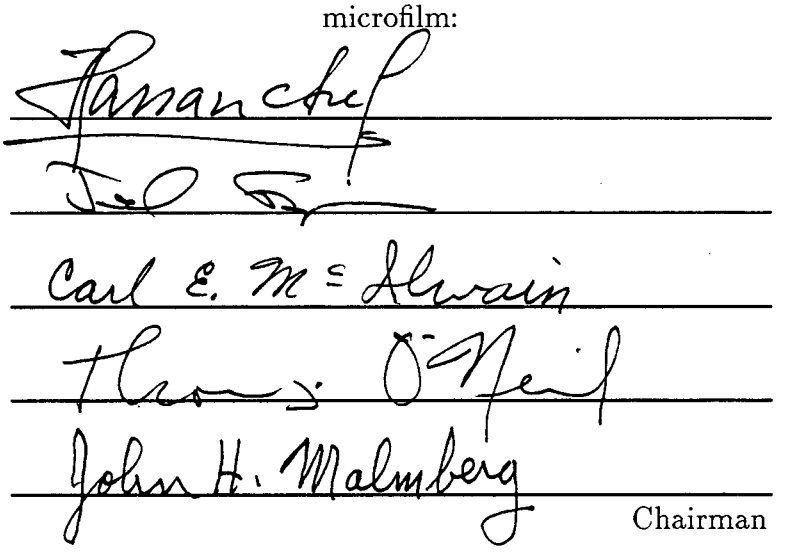

Chairman

University of California, San Diego

1990

*This thesis is dedicated to my parents,*

*Robert and Bonna*

# Contents

# List of Figures

# List of Tables

# Acknowledgements

They say that the road is long and windy; I think the road is straight, and that at times I am inebriated. And, if I could follow the road the journey would be brief. Fortunately, I have had the opportunity to watch, learn and converse with people whom provide a wagon for me to jump on at times when I stray.

I wish the thank Prof. John Malmberg. He hired a farm boy and has, hopefully, produced a scientist (which is not an easy task, ask him). I must provide the ability to think and create new science; his job has been to reprogram the errors in my naive logical and produces an almost finished product. Fortunately, for Dr. Malmberg, he has had help. There have been many who have contributed to my education but I will only thank a few. The help received from Dr. Fred Driscoll has contributed significantly to my education.

I owe a special thanks to Prof. Joel Fajans, who was my accomplice on the experiment described in this thesis. We spent many a late nights arguing physics; and he won a few of them. When I started working for Dr. Malmberg on the CV experiment, Al Hyatt, along with Dr. Malmberg, had all ready built the main parts of the apparatus. For the first few years Al and I worked together on this apparatus before he graduated and Joel joined the group.

From the theoretical side, I would like to especially thank Prof. Dan Dubin and Prof. Tom O'Neil. Dan has answer many of my stupid question, and has also been a great friend. He is also a good guitars player, singer and song writer. The

theory of thermal relaxation for a strongly magnetized plasma is the creation of Dr. O'Neil, and it has been a pleasure discussing this theory with him. I also had the pleasure of taking several classes from him.

From the physics side, I would finally like to thank the rest of the people that I have worked with in the Malmberg group. Dr. Kevin Fine, Dirk Hartmann, Xiao-Pei Huang, Tim Mitchell (he also proofread parts of this thesis), and Poul Hjorth. In addition, there is the much appreciated technical support; thanks to Ralph Dawson and Bob Bongard (electronic technicians); and JoAnn Christina (group secretary) whom does an excellent job.

Physics is fun, but there are times when one must escape and put ones mind to rest. I wish to thank Karl Klose, David Lesmes, Ron Estes , Mike Smith, John Neumeiyer Saeid Ghamaty. The UCSD scuba club, in particular Bert Kobayashi. The friendship of Rick Hobbs, Rita Klabacha and Steve Buchsbaum has been most enjoyable.

Finally, I wish to thank my parents, siblings and their families for there love and support.

Financial support for this research was provided by ONR Contract N00014-82-K-0621, NSF Grant PHY87-06358 and DOE Grant DE-FG03-85ER53199.

# Vita, Publications and Fields of Study

## Vita

| | |
|---|---|
| 23 September 1958 | Born, Bellingham, Washington |
| 1977-1981 | B.S., Western Washington University |
| 1981-1990 | Ph.D., University of California, San Diego |

# Publications

1. A. W. Hyatt, J. H. Malmberg, C. F. Driscoll, K. S. Fine, B. R. Beck and D. L. Eggleston. Observation of anisotropic temperature relaxation. *Bull. Am. Phys. Soc.*, 30:1552 (1985).

2. B. R. Beck. Measurement of coulomb collision frequency over a wide and novel parameter range. *Bull. Am. Phys. Soc* 33:2004 (1988).

3. J. H. Malmberg, C. F. Driscoll, B. R. Beck, D. L. Eggleston, J. Fajans, K. S. Fine, X.-P. Huang and A. W. Hyatt. Experiments with pure electron plasmas. *Nonneutral plasma physics* (C. W. Roberson and C. F. Driscoll, eds.), AIP Conf. Proceedings 175:34, (1988).

4. T. M. O'Neil, P. G. Hjorth, B. R. Beck, J. Fajans and J. H. Malmberg. Collisional Relaxation of a Strongly Magnetized Pure Electron Plasmas. To appear in *Proceedings of the Yamada Conference on Strongly Coupled Plasma Physics* (S. Ichimaru, editor), Tokyo, Japan (1989).

# Fields of Study

Major Field: Physics

Studies in Plasma Physics
Professor Nicholas A. Krall

Studies in Mechanics
Professor Thomas M. O'Neil

Studies in Electromagnetism
Professors Robert A. Swanson, Shang-keng Ma and Thomas M. O'Neil

Studies in Quantum Mechanics
Professor Harry Suhl

Studies in Statistical Mechanics
Professors Shang-keng Ma and Ed Reyayi

Studies in Nuclear Physics
Professor Keith A. Brueckner

Studies in General Relativity and Cosmology
Professor Francis R. Halpern

Studies in Astrophysics
Professor Robert J. Gould

Studies in Mathematical Physics
Professor Frank B. Thiess

# Abstract of the Dissertation

## Measurement of the Magnetic and Temperature Dependence of the Electron-electron Anisotropic Temperature Relaxation Rate

by

Bret Robert Beck

Doctor of Philosophy in Physics

University of California, San Diego, 1990

Professor John H. Malmberg, Chairman

Using a pure electron plasma, the magnetic field and temperature dependences of the electron-electron anisotropic temperature relaxation rate are measured. The anisotropy is characterized by $T_{\|} \neq T_{\perp}$, the temperatures associated with the degrees of freedom parallel and perpendicular to the applied magnetic field. The relaxation rate is measured for large magnetic fields (30 kG to 60 kG) and for an unusual plasma temperature range (25 K to $10^4$ K). In this parameter regime, the ratio of the gyroradius, $r_c$, to the classical distance of closest approach, $b$, plays an important role in determining the relaxation rate.

At high temperatures the plasma is in the regime $r_c/b > 1$. (At all temperatures $\lambda_D \gg r_c$ where $\lambda_D$ is the Debye length.) In this regime the measured rates are compared to a Fokker-Planck prediction as modified by a strong magnetic field approximation due to Montgomery, Joyce and Turner. The rates are also compared to a Fokker-Planck prediction without this approximation. The modified prediction

yields much better agreement to the measured rates.

For temperatures where $r_c/b \sim 1$, the measured rate peaks. As the temperature is lowered below this point, the plasma enters a regime where $r_c/b < 1$. Here, as $r_c/b$ goes from about 1 to about 0.03 the measured rate normalized by $T^{3/2}$ drops by a factor of $10^4$. (Whereas, for $r_c/b \gg 1$ the normalized rate is essentially independent of temperature.) This rapid decrease is consistent with a theoretical prediction of O'Neil and Hjorth, who argue that the collisional dynamics is constrained by a many electron adiabatic invariant in the regime $r_c/b \ll 1$.

The plasma is contained axially by a potential well and radially by the magnetic field. To measure the relaxation rate the shape of the potential well is modulated sinusoidally which similarly modulates the plasma length parallel to the magnetic field. If the modulation frequency is neither slow nor rapid compared to the relaxation rate the compression is irreversible and the plasma is heated. Maximum heating per cycle is predicted to occur when $2\pi f = 3\nu$, where $\nu$ is the relaxation rate and $f$ is the modulating frequency. The relaxation rate is thus determined by measuring which modulating frequency produces the most heating per cycle.

# Chapter 1

# Introduction and Summary

This thesis describes an experiment in which the anisotropic temperature relaxation rate for a pure electron plasma is measured. The anisotropy is characterized by $T_{||} \neq T_{\perp}$, where these are the temperatures associated with the degrees of freedom parallel and perpendicular to an applied magnetic field. $T_{||}$ and $T_{\perp}$ are isotropized to an equilibrium temperature by electron-electron collisions. We have measured the magnetic field and temperature dependence of the anisotropic temperature relaxation rate (henceforth to be called the relaxation rate.) over a range from a magnetized regime ( $\lambda_D > r_c > b$ ) to a strongly magnetized regime ( $\lambda_D > b > r_c$ ). Here, $\lambda_D$ is the Debye length, $r_c$ is the gyroradius and $b$ is the classical distance of closest approach[1].

The first calculations of velocity space scattering in plasmas treat collisions as isolated, two particle events (i.e. binary collisions), and considered a nonmagnetized plasma. These assumptions allow the calculations to employ the differential scattering cross section for a two particle coulomb collision. In addition, it is common (even in more recent calculations) to assume that a collision produces only a small perturbation to a particle's orbit, and then calculate the perturbation by integrating along unperturbed particle orbits. The procedure of integrating along

[1]Commonly used symbols are listed in Appendix A.9. In this thesis we use Gaussian units.

unperturbed orbits will be called the unperturbed orbit approximation. As a consequence of the binary collision assumption and the unperturbed orbit approximation, the first calculated velocity space scattering rates diverge logarithmically at both small and large impact parameters. (The impact parameter is the distance of closest approach that two particles would achieve if there were no interaction between the particles.) This logarithmic dependence of the relaxation rate on the small and large impact parameters is written as $\log(p_{\max}/p_{\min})$ where $p_{\max}$ is some maximum impact distance, $p_{\min}$ is some minimum impact distance, and $\log(p_{\max}/p_{\min})$ is called the coulomb logarithm factor.

The divergence of the calculated velocity scattering rates at small impact parameters can be traced back to the unperturbed orbit approximation. One expects this approximation to break down when $p_{\min} \sim b$, and for this reason one typically lets $p_{\min} = b$. Of course, this implies that collisions with impact distances less than $p_{\min}$ are ignored in these calculations. It can be shown that when collisions with impact distances less than $b$ are neglected, the error in the calculated velocity scattering rates are small as long as $p_{\max} \gg b$ (see reference [6]).

The divergence of the calculated velocity scattering rates at large impact parameters can be traced back to the binary collision assumption. The binary collision assumption neglects effects such as plasma shielding which will reduce the interaction between two particles when they are separated by large distances. This reduction results in less scattering at large impact distances than the binary collision approximation predicts, and would cause the calculations to converge at large impact distances if properly included. For a plasma in the regime $r_c \gg \lambda_D \gg b$, $p_{\max}$ is typically set to $\lambda_D$. The coulomb logarithm factor then becomes $\log(\lambda_D/b)$.

Note that on the first calculations the minimum and maximum impact distances, $b$ and $\lambda_D$, are introduced in an ad hoc manner. However, slightly more

rigorous calculations, such as the Lenard-Balescu approach which includes plasma correlation effects to lowest order in the plasma parameter $g = 1/(n\lambda_D^3)$, also predict a $p_{max}$ of about $\lambda_D$.

For the regime $\lambda_D \gg r_c \gg b$, Montgomery, Joyce and Turner show that $p_{max}$ is about $r_c$, so that the coulomb logarithm becomes $\log(r_c/b)$. For the plasmas studied in this thesis $\lambda_D$ is always much greater than $r_c$.

When $\lambda_D$ is much larger than both $r_c$ and $b$, but $r_c$ is not much larger than $b$, traditional calculations are expected to fail. However, O'Neil and Hjorth [48] have recently calculated the anisotropic temperature relaxation rate due to electron-electron collisions for a pure electron plasma in the strongly magnetized regime (i.e. $r_c \ll b$), with the assumption that the plasma is weakly correlated (i.e. $n^{-1/3} \gg b$). The O'Neil-Hjorth calculation uses a Boltzmann equation, and thus properly treats collisions with small impact distances. They predict a rapid decrease in the relaxation rate as $r_c/b$ is decreased.

The rapid decrease in the relaxation rate as $r_c/b$ is decreased is due to a many electron adiabatic invariant, which for uniform magnetic field simplifies to the total perpendicular energy of the electrons. Were the adiabatic invariant an exact constant of the motion, no exchange of energy would be possible between the parallel and the perpendicular degrees of freedom. However, an adiabatic invariant is not strictly conserved, and there is an exponentially small exchange of energy between the parallel and the perpendicular degrees of freedom per collision as a result of the adiabatic invariant. The smaller $r_c/b$ the smaller the exchange of energy per collision on the average; hence a rapid decrease in the relaxation rate as $r_c/b$ is decreased.

In Fig. 1.1 we show our most important result. In this figure we have plotted relaxation rates versus $r_c/b$. We have normalized the relaxation rate by $nb^2v_T$ where $n$ is the density and $v_T$ is the thermal velocity. The diamond points, $\diamond$, in Fig. 1.1 are

our data. The square points, □, are results previously obtained by Hyatt, Driscoll and Malmberg (we discuss their results on page 7). The dashed line is a Fokker-Planck prediction of the relaxation rate due to Ichimaru and Rosenbluth [28]. We have modified the Ichimaru-Rosenbluth prediction as per Montgomery, Turner and Joyce [41] by effectively cutting off the coulomb interaction at a distance of $r_c$ (i.e. the coulomb logarithm is $\log(r_c/b)$). The solid line is a plot of the O'Neil-Hjorth prediction. Note that the comparison between the experimental data (both our results and the Hyatt, Driscoll and Malmberg results) and the predictions are absolute (i.e. there are no adjustable parameters in either the experimental data or the theories).

Our results are consistent with the Fokker-Planck prediction when $r_c/b \gg 1$, provided the coulomb interaction is effectively cut off at a distance of $r_c$ instead of $\lambda_D$. And, our results clearly demonstrates that a rapid decrease in the normalized relaxation rate occurs as $r_c/b$ is decreased below the point $r_c/b \approx 1$. This rapid decrease is consistent with the O'Neil-Hjorth prediction when $r_c/b \ll 1$. This, as O'Neil [44] has argued, is most likely due to a many electron adiabatic invariant which constrains the exchange of perpendicular and parallel energy.

We should warn the reader that the close agreement between our data and the O'Neil-Hjorth prediction for $0.02 \lesssim r_c/b \lesssim 0.2$ may be fortuitous. Recent calculations [19] of the relaxation rate yield a rate which is about a factor of 4 larger than the O'Neil-Hjorth prediction when $r_c/b \sim 0.01$. Note that for $r_c/b \ll 1$ the normalized relaxation rate is such a rapidly decreasing function of $r_c/b \propto T^{3/2}$, that changing the temperature by about 30% results in a factor of 4 change in the normalized relaxation rate. Consequently, this factor of 4 disagreement between the predictions, does not alter the conclusions we make regarding the experimental data. In other words, our measured normalized relaxation rates vary by about 4.5 decades as $r_c/b$ is varied, and even with a factor of 4 error we are still observing a rapid

decrease in the normalized relaxation rate as $r_c/b$ is decrease below $r_c/b \approx 1$. But, more importantly, the discrepancy between the recent calculations and our results are within the estimated error of the temperature diagnostic.

For low temperatures we estimate that systematic errors in the measured temperature may be as much as 30%. In addition, we believe that the measured temperatures in this region are most likely too high. Since the normalized relaxation rate is a rapidly increasing function of temperature (i.e. $r_c/b$ for fixed magnetic field) in the regime $r_c/b \ll 1$, a 30% reduction in the measured temperature is sufficient to reconcile the recent calculations with our data in the region $0.02 \lesssim r_c/b \lesssim 0.2$.

To measure the relaxation rate we modulate the plasma length essentially sinusoidally. The amount of heating as a function of the modulation frequency is measured. If the modulation is slow compared to the relaxation rate, the compression is three-dimensional and reversible so there is no heating. If the modulation is rapid compared to the relaxation rate, then the modulation is one-dimensional and reversible, and again there is no heating. If the modulation frequency is neither slow nor rapid compared to the relaxation rate, the compression is irreversible and the plasma is heated. At all times the modulation frequency is low compared to the bounce time and to the lowest plasma mode frequency. A model of this heating process shows that maximum heating per cycle occurs when $2\pi f = 3\nu$, where $\nu$ is the relaxation rate and $f$ is the modulating frequency.

We observe the heating as a function of the modulating frequency. The frequency, $f_{\max}$, which produces the most heating per cycle is determined, and the relaxation rate is then obtained from the relation $2\pi f_{\max} = 3\nu$. We have measured the relaxation rate for three magnetic fields, 30, 40 and 60 kG, and for temperatures from about 26 K to about $10^4$ K. This gives a range in $r_c/b$ of about $1/35 < r_c/b < 450$.

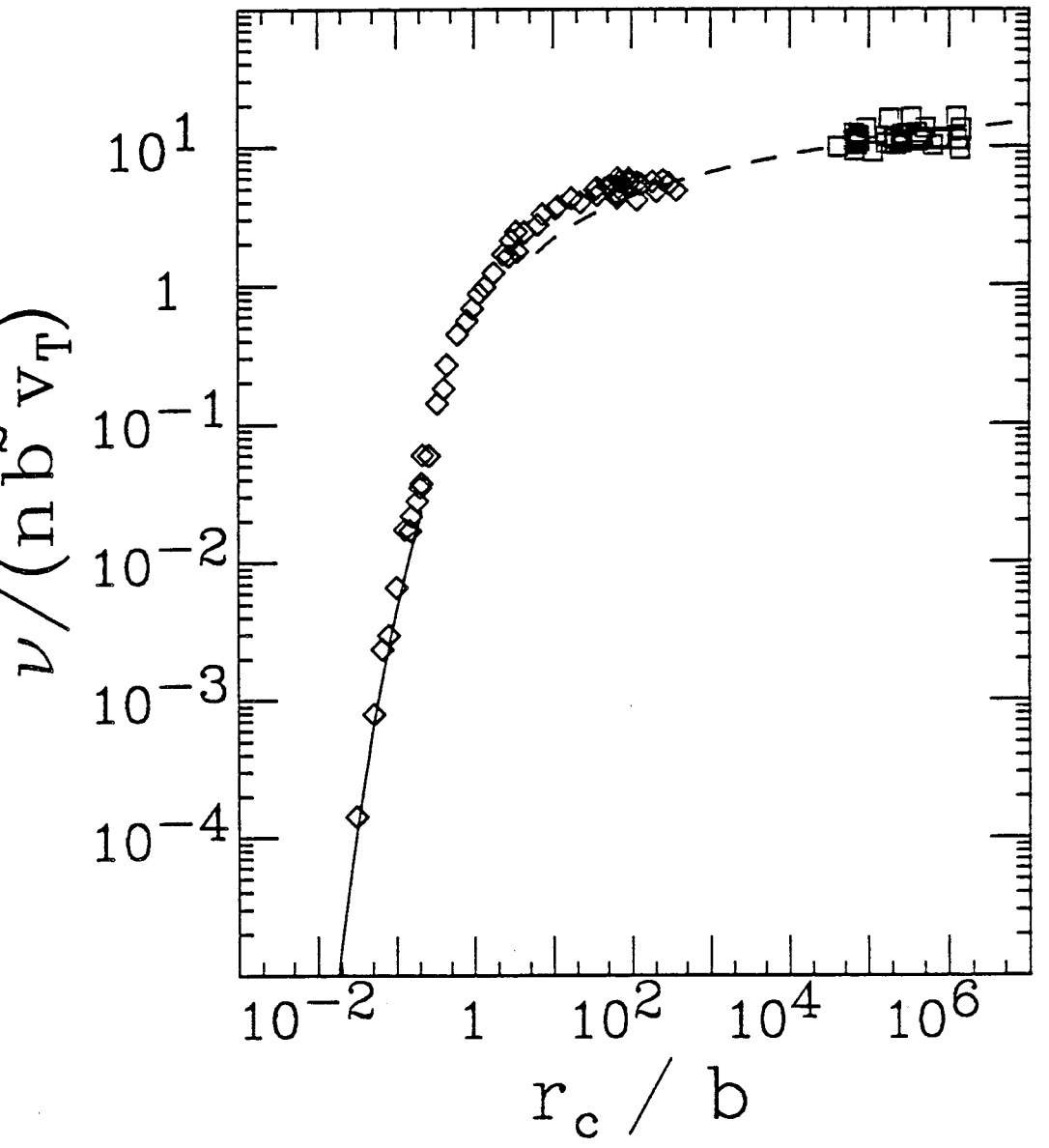


**Figure 1.1:** The diamond points, $\diamond$, are our experimentally measured relaxation rates normalized by $n\,b^2\,v_T$, and plotted versus $r_c/b$. The solid curve is the O'Neil-Hjorth prediction. The dash curve is a Fokker-Planck prediction with the coulomb interaction effectively cut off at a distance of $r_c$. The square data points are prior results obtained by Hyatt, Driscoll and Malmberg.

A prior measurement of the relaxation rate for a pure electron plasma has been made by Hyatt, Driscoll and Malmberg [26, 25]. They used a pure electron plasma trap which is similar to the one we have used; however, their magnetic field was much lower (281 G) and their plasma temperatures were around $10^4$ K. This places their experiment in the regime $3 \times 10^4 \lesssim r_c/b \lesssim 10^6$, with $\lambda_D \approx 30\, r_c$. In their experiment the parallel temperature, $T_{||}$, was changed by a single axial compression or expansion. The subsequent time evolution of $T_{||}$ and $T_\perp$ was then measured as these temperatures relaxed to an isotropic temperature. Relaxation rate as a function of density and temperature were measured over a two decade range, with uncertainties in the measured rate of about 10%. Since they were in the regime $r_c/b \gg 1$, they compared their results to an absolute (no adjustable parameters) Fokker-Planck prediction using $r_c$ instead of $\lambda_D$ as the cutoff distance and found absolute agreement to about 10%.

Their results clearly demonstrate the $n/T^{3/2}$ dependence of the relaxation rate. However, since they are in the regime $r_c/b \gg 1$, an order of magnitude change in $r_c/b$ has only about a 20% change in $\log(r_c/b)$. This, combined with the fact that their data has errors of about 10% and the Fokker-Planck theory has an uncertainty of about 10%, means that their data is not suited to test the $\log(r_c/b)$ dependence of the predicted relaxation rate. Second, their data was taken at a single magnetic field, so that they are unable to give conclusive data showing that $r_c$ is the proper cutoff instead of $\lambda_D$. This is again due to the fact that the predicted coulomb logarithm term is a very slow function of its argument.

There are additional experimental results of collisional velocity space transport[2]. Hiskes and Futch [22] present measurements of the rate at which ions are transported into the loss cone of a magnetic mirror for several devices, and find

[2]Here we essentially reproduce the conclusions of A. W. Hyatt on other collision velocity space transport rate experiments (see pages 2 to 3 in reference [25]).

that at best the agreement with collisional theory is about a factor-of-two. The theoretical rates are generated by a Fokker-Planck code which requires the input of initial conditions, and in some cases, there are free parameters which are adjusted to bring the output of the code into agreement with some measured quantity. Burke and Post [4] present the results of their experiments on fast test ions slowing in a neutral plasma, and contrast these results with those of other similar experiments. Their results differ from theory by a factor of 3 with uncertainties of order unity. The other experimental results referred to by Burke and Post differ from theory by factors of 1/3 to 8.

The resistivity measurements of Lin el al. [55] and Mohler [39] together agree quite well with the theoretical predictions of Spitzer and Härm [58] over a reasonable range of temperatures and densities, with experimental accuracies on the order of 10-20%. They measure the average conductivity in the shock wave front of a gas. This shock wave is produced in a shock tube. The average charge density and shock wave temperature are calculated from the measured Mach number. Although a resistivity measurement does not measure a scattering rate per se, it does measure one of the bedrocks of collisional velocity space scattering in plasmas - the effective cross-section for momentum transfer between charged particles in a plasma.

The remainder of this thesis is organized as follows. In Chapter 2, we present the basic ideas and assumptions used to theoretically predict the relaxation rate. In particular, we estimate for what regions of $r_c/b$ one should expect the different theories to be valid and then estimate their uncertainties when possible. Also included in this chapter is an argument due to O'Neil [44] which shows that a many electron adiabatic invariant exists in the regime $r_c/b \ll 1$. In Chapter 3, we explain how a pure electron plasma can be confined by static magnetic and electric fields. We also describe the design of the experiment and how it is typically operated. We end this

chapter by explaining how we determine the plasma density and length.

We start Chapter 4 by showing that one expects the plasma to cool via cyclotron radiation with an e-folding time of about $4 \times 10^8 \, B^{-2}$ sec. We then compare the calculated temperature versus time to the measured temperature versus time. Next we present possible ways to heat the plasma, one of which we use to measure the relaxation rate. We then present the temperature measurement method. The plasma temperature is determined by measuring the number of electrons which escape as the potential on an axial confinement gate is slowly raised to ground. The temperature is obtained by comparing the number of electrons that escape as a function of the confining gate potential to a model which predicts how many electrons should escape as a function of the confining gate potential. The assumptions built into this model are presented in this chapter as well as why we believe these assumptions are satisfied by the experiment. In Chapter 5, we present the compressional heating model and its assumptions. Compressional heating data is then presented for two simple heating schemes. This data is compared to the model's prediction. We also present our experimental relaxation rate data and compare this data with theory. Finally, we estimate the uncertainties in the measured relaxation rates.

In Appendix A.1 we elaborate on the cyclotron radiation rate calculation presented in section 4.2. This calculation includes quantum effects (i.e. Landau levels) and the effect of a background, thermal equilibrium, radiation field. In Appendix A.2 we show that for a Maxwellian distribution, $\langle dE_i/dt \rangle = d\langle E_i \rangle/dt = (k_B/2)dT_i/dt$ when $dE_i/dt = C'E_i$. Here $E_i$ is the kinetic energy of an electron along an axis $i$, the brackets means an average over the distribution, and $C'$ is a constant.

The model for the compression heating assumes that the plasma length is modulated sinusoidally. This assumption combined with a few other assumptions predicts that maximum heating per cycle will occur when $2\pi f = 3\nu$. If harmonics are

added to the sinusoidal modulation then maximum heating per cycle will no longer occur when $2\pi f = 3\nu$. In Appendix A.3 we estimate the size of the fundamental and first harmonic modulations for a well confined plasma (one in which the potentials on the confining gates are much greater than the plasma space charge potential) when a confining gate is modulated sinusoidally. In Appendix A.4 the compressional heating model is reanalyzed to determine which frequency produces maximum heating when the first harmonic of the plasma length modulation is included. Combining the results of this appendix with those of Appendix A.3, we conclude that the first harmonic adds at most a 1% error to the measured relaxation rate.

O'Neil and Hjorth obtain a simple formula for the relaxation rate when $r_c/b \ll 1$; however, this formula is an approximation, and there is no indication of how small $r_c/b$ must be before this simple formula is a good approximation to the relaxation rate. In Appendix A.5 we show how this simple formula was calculated. In Appendix A.6 we estimate the rate at which one might expect three-body collisions to relax the distribution of parallel velocities to a Maxwellian. For small $r_c/b$ the three-body collision rate may be larger than the relaxation rate; in which case, the rate at which the parallel velocity distribution relaxes to a Maxwellian is the three-body collision rate.

When a plasma expands radially the electrostatic potential energy of the plasma decreases, and this can heat the plasma. In Appendix A.7 we calculate the rate of change in the electrostatic potential energy for a plasma density which is varying in time as $n(r,t) = n(r/x(t))/x^2(t)$. In Appendix A.8 the experimental relaxation rate data as well as other relevant parameters are presented. Finally, in Appendix A.9 we present symbols which are frequently used in this thesis.

# Chapter 2

# Theory

## 2.1 Introduction

In this chapter we will present the basic ideas and assumptions used to calculate the relaxation rate. In particular, we will focus on those theories that are pertinent to the experimental data presented in this thesis. In the parameter range $r_c/b \gg 1$ a Fokker-Planck [28] equation is used to calculate the relaxation rate. For $r_c/b \ll 1$, a recent theory by O'Neil and Hjorth [48] which uses a Boltzmann-like collision operator is used to calculate the relaxation rate. This latter theory predicts a rapid decrease in the relaxation rate as $r_c/b$ is decreased. For the region $r_c/b \sim 1$ all current theories become invalid. However, recently the relaxation rate has been calculated numerically for the range $10^{-4} < r_c/b < 10^4$ [19].

In the early days of plasma physics attempts were made to calculate velocity space scattering using the Boltzmann equation. This was, in part, due to the numerous relatively accurate calculations which had been made for molecular gases using the Boltzmann equation. However, it was soon realized that the Boltzmann equation is ill-suited to describe velocity space scattering of charged particles. This failure is due to the fact that the force between charged particles falls off as $1/r^2$; in contrast to molecular forces which fall off as $1/r^6$ or $1/r^7$. Hence, it is not appropriate to assume that a collision between charged particles is an isolated two particles event (binary

collision assumption); an assumption which is valid for many molecular gases.

It is rather simple to show that unphysical results are obtained when one naively treats collisions between charged particles as isolated events. For example, the electron-electron cross section for momentum transfer is (see section 1.2 in reference [27])

$$Q_{\mathrm{m}} = \frac{\pi}{4} b_{||}^2 \left[ \log(p_{\mathrm{max}}/b_{||}) + \vartheta(b_{||}/p_{\mathrm{max}}) \right]$$

where $b_{||} = 4e^2/(mu_0^2)$, $u_0$ is the relative velocity between two electrons when they are separated by an infinite distance, $p_{\mathrm{max}}$ is the maximum impact parameter and $p_{\mathrm{max}} \gg b_{||}$. Obviously, $p_{\mathrm{max}}$ must be finite or $Q_{\mathrm{m}}$, which is known to be finite, would be infinite. The binary collision assumption alone does not limit the value of $p_{\mathrm{max}}$. Also, when $p_{\mathrm{max}} \gg n^{1/3}$ the binary collision assumption is clearly invalid.

More elaborate theories of velocity space scattering have since been developed. These theories include correlation effects to lowest order in the plasma parameter, $g = 1/(n\lambda_{\mathrm{D}}^3)$, and predict an effective cutoff of the coulomb interaction at a distances of about the Debye length (i.e. $p_{\mathrm{max}} \sim \lambda_{\mathrm{D}}$).

When a plasma is immersed in a magnetic field the cutoff distance is still believed to be $\lambda_{\mathrm{D}}$ as long as $r_{\mathrm{c}} \gg \lambda_{\mathrm{D}} \gg b$. However, when $\lambda_{\mathrm{D}} \gg r_{\mathrm{c}} \gg b$, Montgomery, Joyce and Turner argue that the coulomb cutoff distance is about $r_{\mathrm{c}}$. To understand the physics of this cutoff distance, consider a collision between two electrons, electron 1 and electron 2. Let $\mathbf{u} = \mathbf{v}_1 - \mathbf{v}_2$ be the relative velocity between electron 1 and electron 2, and let $u_{||}$ be the component of $\mathbf{u}$ parallel to the magnetic field. Now consider the case $\Omega \gg u_{||}/p$ where $\Omega$ is the electron gyrofrequency. (For electrons with thermal velocities, the condition $\Omega \gg u_{||}/p$ is equivalent to $p \gg r_{\mathrm{c}}$.)

During the collision, electron 2 will produce a time varying field felt by electron 1 which has two essential time scales. One time scale is about $p/u_{||}$ and is much slower than the gyromotion. If this were the only time varying field felt by electron 1

during the collision, then the magnetic moment of electron 1 would be an adiabatic invariant. However, the gyromotion of electron 2 introduces a second time scale with frequency $\Omega$ to the interaction field felt by electron 1, and this breaks the adiabatic invariant of electron 1. Likewise the invariant of electron 2 is broken by the time varying field produce by the gyromotion of electron 1. Although separately neither magnetic moment is an adiabatic invariant, O'Neil [44] has shown that the sum of the two magnetic moments is an adiabatic invariant. For a uniform magnetic field, this simply states that the total perpendicular kinetic energy of the two electrons is an adiabatic invariant. As a consequence of this two electron adiabatic invariant there is essentially no scattering of perpendicular energy into parallel energy or vise versa for collisions where $\Omega \gg u_{||}/p$. Therefore, one concludes that collisions with $\Omega \gg u_{||}/p$ contribute a negligible amount to the relaxation rate, and for a Maxwellian plasma this is essentially collisions with $p \gg r_c$, so that the coulomb cutoff distance is about $r_c$.

When $r_c \gg b$ many collisions have an impact distance which is much less than $r_c$. For these collisions the gyromotion can be ignored when calculating the velocity space scattering, so that a Fokker-Planck formalism is expected to be valid as long as the coulomb interaction is cut off at a distance of about $r_c$.

On the other hand, when $r_c \ll b$ there will be an exponentially small number of collisions with an impact distance less than a gyroradius. Basically, the relative velocity of two electrons must be such that $mu_{||}^2/2 \gtrsim e^2/r_c$, which can be written in terms of the thermal velocity,$v_T$, as $u_{||} \gtrsim v_T(b/r_c)^{1/2}$. For a Maxwellian distribution there are an exponentially small number of collision such that $u_{||} \gtrsim v_T(b/r_c)^{1/2}$. In addition, there are only an exponentially small number of collisions in which the rearrangement of $v_{||}$ and $v_\perp$ is not constrained by the previously described adiabatic invariant (for $r_c \ll b$ most collision satisfy $v_{||}/p \ll \Omega$). The result of all these expo-

nentially small quantities (of course, the adiabatic invariant predicts an exponentially small rearrangement of $v_{||}$ and $v_{\perp}$ per collision), is an exponentially small relaxation rate when $r_c \ll b$.

This chapter is arranged as follows. In section 2.2 we give a short overview of the history of velocity space scattering. In particular, we present the assumptions used in the different velocity space scattering theories. We will not derive any of the formulas here; these derivations can be found in the references. In section 2.3 we present the actual formulas that will be compared in section 5.4 to the experimental results. We will make some attempt at determining the validity of such comparisons. Section 2.3.1 contains the formula for $r_c/b \gg 1$ and section 2.3.2 contains the formula for $r_c/b \ll 1$. Finally, in section 2.4 we reproduce an argument by O'Neil [44] which shows a many electron adiabatic invariant exist in the regime $r_c/b \ll 1$.

## 2.2 Historical Review of Velocity Space Scattering

The Boltzmann equation [3, 42], describes the evolution of the one-particle distribution function, $f = f(\mathbf{x}, \mathbf{v}, t)$ for a gas when the interaction range is much smaller than the mean interparticle spacing, $n^{-1/3}$ (i.e. binary collisions). For a gas composed of like-particles (i.e. a single species) the Boltzmann equation is

$$\frac{\partial f}{\partial t} + \mathbf{v} \cdot \frac{\partial f}{\partial \mathbf{x}} + \frac{\mathbf{F}}{m} \cdot \frac{\partial f}{\partial \mathbf{v}} = \left.\frac{\partial f}{\partial t}\right|_c \tag{2.1}$$

where $\mathbf{F}$ is the external force. The right-hand side gives the evolution of the one-particle distribution function due to the discrete nature of the gas and is called the collision term.

Consider a binary elastic collision, and write the velocities before the collision as $\mathbf{v}$ and $\mathbf{v}_1$, and the velocities after the collision as $\mathbf{v}'$ and $\mathbf{v}_1'$. Then, for the

Boltzmann equation the collision term is

$$\left.\frac{\partial f}{\partial t}\right|_c = n \int d\mathbf{v}_1 \int d\Omega \frac{d\sigma}{d\Omega} \{ f(\mathbf{x}, \mathbf{v}_1') f(\mathbf{x}, \mathbf{v}') - f(\mathbf{x}, \mathbf{v}_1) f(\mathbf{x}, \mathbf{v}) \} |\mathbf{v}_1 - \mathbf{v}| \qquad (2.2)$$

where $d\sigma/d\Omega$ is the differential scattering cross section and $d\Omega$ is an element of solid angle. Note that a collision transforms the unprimed velocities into the prime velocities so that $\mathbf{v}' = \mathbf{v}'(\mathbf{v}, \mathbf{v}_1)$. A similar expression holds for $\mathbf{v}_1'$. The term containing $f(\mathbf{x}, \mathbf{v}_1) f(\mathbf{x}, \mathbf{v})$ is the rate at which particles scatter out of the range $\mathbf{v}$ to $\mathbf{v} + d\mathbf{v}$, and the term containing $f(\mathbf{x}', \mathbf{v}_1') f(\mathbf{x}', \mathbf{v}')$ is the rate at which collisions scatter particles into this range. In thermal equilibrium these two terms are equal and the collision term vanishes; otherwise, there is a net flux of particles either into or out of the range $\mathbf{v}$ to $\mathbf{v} + d\mathbf{v}$.

The Boltzmann equation has been verified experimentally for cases where the interaction range is much less than $n^{-1/3}$ and spatial and temporal gradients are not too great [5]. In other words, the Boltzmann equation works well for a sparse neutral gas.

Attempts have been made to adapt the Boltzmann equation to plasma and stellar dynamics. This leads to a problem since the Boltzmann equation was derived for particles with short range interactions, and it is, therefore, assumed that only two particles are interacting at any one time. The coulomb and gravitation interactions, on the other hand, are infinite range and many particles, in general, are interacting at any one time (e.g. the number of electrons within the effective interaction range of a given electron is roughly $1/g = n\lambda_D^3$).

A second approach to calculating the evolution of the one-particle distribution function is to use the Fokker-Planck equation [17, 51]. This equation is the same as the Boltzmann equation except for the collision term. In this formalism a particle is assumed to make small random walks in phase-space (often called Brownian motion) in a time $\Delta\tau$. The time $\Delta\tau$ is taken to be much shorter than the time it

takes the distribution function to relax to a local equilibrium and much longer than a typical correlation time (e.g. $\omega_p^{-1}$ for a plasma).

In the Fokker-Planck derivation, one assumes that a function $\Psi(\mathbf{v}, \Delta\mathbf{v})$ can be calculated which gives the probability that a particle with velocity $\mathbf{v}$ acquires a velocity increment $\Delta\mathbf{v}$ during a time interval $\Delta\tau$. One also assumes that $\Psi$ does not depend explicitly on time (this is known as a Markoff process). Given $\Psi$ (and assuming here that the gas is uniform in $\mathbf{x}$, that is, the $\mathbf{x}$ coordinate will be ignored), the distribution will evolve as

$$f(\mathbf{v}, t) = \int f(\mathbf{v} - \Delta\mathbf{v}, t - \Delta t)\Psi(\mathbf{v}, \Delta\mathbf{v})\, d(\Delta\mathbf{v}). \tag{2.3}$$

The collision term is then

$$\left.\frac{\partial f}{\partial t}\right|_c \approx \frac{f(\mathbf{v}, t) - f(\mathbf{v}, t - \Delta t)}{\Delta t}. \tag{2.4}$$

Taylor expanding this equation one obtains

$$\left.\frac{\partial f}{\partial t}\right|_c \approx -\frac{\partial}{\partial \mathbf{v}} \cdot \left(f\frac{\langle\Delta\mathbf{v}\rangle}{\Delta\tau}\right) + \frac{1}{2}\frac{\partial^2}{\partial\mathbf{v}\partial\mathbf{v}} : \left(f\frac{\langle\Delta\mathbf{v}\Delta\mathbf{v}\rangle}{\Delta\tau}\right) \tag{2.5}$$

where

$$\langle\Delta\mathbf{v}\rangle = \int \Delta\mathbf{v}\Psi(\mathbf{v}, \Delta\mathbf{v})\, d(\Delta\mathbf{v}) \tag{2.6}$$

and

$$\langle\Delta\mathbf{v}\Delta\mathbf{v}\rangle = \int \Delta\mathbf{v}\Delta\mathbf{v}\Psi(\mathbf{v}, \Delta\mathbf{v})\, d(\Delta\mathbf{v}). \tag{2.7}$$

Here $\Delta\mathbf{v}$ is assumed to be small and terms of order $\Delta\mathbf{v}\Delta\mathbf{v}\Delta\mathbf{v}$ and greater are ignored. Note that in order to neglect terms of order $\Delta\mathbf{v}\Delta\mathbf{v}\Delta\mathbf{v}$ and greater, $\Delta\tau$ must be short enough so that most particles incur only a small velocity increment.

The term containing a single $\Delta\mathbf{v}$ is called the dynamical friction term and tends to bring all particles to a common velocity. The term containing $\Delta\mathbf{v}\Delta\mathbf{v}$ is called the diffusion term and tends to diffuse the particles in velocity space. In the

absence of external driving forces, these two terms will relax the distribution function to a Maxwellian.

For small impact distances, of order $b$ or less, $\Delta \mathbf{v}$ can be shown to be large. Since the Fokker-Planck equation is derived for small $\Delta \mathbf{v}$ it will not be valid for impact distances of order $b$ or less. This leads to a problem if the main contribution to velocity scattering occurs at small impact distances. It has been shown [6] for $1/r^2$ forces that if $p_{\max} \gg b$ ($p_{\max}$ being the cutoff distance) then the range $b$ to $p_{\max}$ contributes much more to velocity space scattering then does the range 0 to $b$.

One problem with the Fokker-Planck equation is that it does not explicitly present a method for calculating $\langle \Delta \mathbf{v} \rangle$ and $\langle \Delta \mathbf{v} \Delta \mathbf{v} \rangle$. That is, one must still determine the transition probability function $\Psi$. One method of calculating $\langle \Delta \mathbf{v} \rangle$ and $\langle \Delta \mathbf{v} \Delta \mathbf{v} \rangle$ [18] assumes that changes in velocity, $\Delta \mathbf{v}$, can be calculated using the two particle scattering cross section. This method has been employed by Rosenbluth, MacDonald and Judd [54]. Their results can be shown to be equivalent to expanding the Boltzmann collision operator for small $\Delta \mathbf{v}$ (see pages 15-20 in reference [42]). Since the Boltzmann equation is not obviously valid for impact distances greater than $n^{-1/3}$, one may question the validity of this approach in the regime $p_{\max} > n^{-1/3}$. However, if one estimates the change in an electron's velocity as it traverses a distance $p_{\max}$, one can show for a thermal electron that this change is small provided $p_{\max} \gg b$. In this estimate the rare large angle scattering collisions are ignored (i.e. collisions with impact parameters of order $b$ or less), and each collision, although occurring simultaneously, is treated as a binary collision. Each binary collision causes a change in the electron's velocity as it traverses a distance $p_{\max}$, and these changes are statistically summed to obtain the total change in the electron's velocity.

The fact that a particle's trajectory is hardly perturbed by all its surrounding neighbors as it traverses a distance $p_{\max}$ means that to a good approximation the

interaction between any two particles may be treated as if it occurs in isolation. This implies that both the Boltzmann formalism and the Fokker-Planck formalism should be a valid approach to calculating the relaxation rate as long as $p_{\max} \gg b$.

It is worth noting that $r_c \ll n^{-1/3}$ for the plasmas studied in this thesis. This implies that the Fokker-Planck formalism of Rosenbluth, MacDonald and Judd should be valid for the plasmas studied in this thesis as long as $r_c \gg b$. It also implies that a Boltzmann formalism should be valid for all $r_c/b$ as long as the plasma is uncorrelated.

A second method of calculating $\langle \Delta \mathbf{v} \rangle$ and $\langle \Delta \mathbf{v} \Delta \mathbf{v} \rangle$was employed by Thompson and Hubbard [59]. They calculate $\langle \Delta \mathbf{v} \rangle$ and $\langle \Delta \mathbf{v} \Delta \mathbf{v} \rangle$ by calculating the fluctuating electric microfields produced by a weakly correlated plasma. Their results include plasma shielding to lowest order in the plasma parameter, $g$, and thus provide a natural cutoff of the coulomb interaction at a distance of about $\lambda_D$.

The Fokker-Planck equation calculated by Thompson and Hubbard is essentially equivalent to the Lenard-Balescu equation [33, 2]. In this latter formalism, a plasma is consider to be weakly correlated, and again only correlation effects to order $g$ are retained. The Lenard-Balescu collision term can be written as

$$\left.\frac{\partial f}{\partial t}\right|_c = \frac{\pi \omega_p^4}{n} \sum_{\mathbf{k}} \frac{\mathbf{k}}{k^2} \cdot \frac{\partial}{\partial \mathbf{v}} \int d\mathbf{v}' \frac{\mathbf{k}}{k^2} \cdot \left[ \left( \frac{\partial}{\partial \mathbf{v}} - \frac{\partial}{\partial \mathbf{v}'} \right) f(\mathbf{v}) f(\mathbf{v}') \right] \times \frac{\delta(\mathbf{k} \cdot \mathbf{v} - \mathbf{k} \cdot \mathbf{v}')}{|\epsilon(\mathbf{k}, \mathbf{k} \cdot \mathbf{v})|^2} \tag{2.8}$$

where $\epsilon(\mathbf{k}, \omega)$ is the plasma dielectric function, and is given by

$$\epsilon(\mathbf{k}, \omega) = 1 + \frac{\omega_p^2}{k^2} \int d\mathbf{v} \left( \frac{1}{\omega - \mathbf{k} \cdot \mathbf{v}} \right) \mathbf{k} \cdot \frac{\partial}{\partial \mathbf{v}} f(\mathbf{v}). \tag{2.9}$$

Finally, O'Neil [44] considered a strongly magnetized plasma (i.e. $r_c/b \ll 1$, which essentially guarantees that the gyromotion will have the fastest time scale)

and derived a Boltzmann-like[1] collision term as

$$\frac{\partial f}{\partial t} + \mathbf{v}\cdot\frac{\partial f}{\partial \mathbf{x}} - \Omega \mathbf{v}\times\hat{z}\cdot\frac{\partial f}{\partial \mathbf{v}} = n\int d\mathbf{v_1}\int d\Omega \frac{d\sigma}{d\Omega}\{ f(\mathbf{x},\mathbf{v}_1')f(\mathbf{x},\mathbf{v}') - f(\mathbf{x},\mathbf{v}_1)f(\mathbf{x},\mathbf{v})\}|v_{\|_1} - v_{\|}| \qquad (2.10)$$

This collision term is derived assuming that the plasma is spatially homogeneous (i.e. $f(\mathbf{x},\mathbf{v},t) = f(\mathbf{v},t)$), that the main contribution to perpendicular velocity scattering occurs for impact distances of order $b$ or less, and that $b \ll n^{-1/3}$ (i.e. uncorrelated plasma).

## 2.3 Validity of a Comparison Between Theory and Experimental Data

Simple arguments show that the relaxation rate should be proportional to[2] $n\,b^2\,v_{\mathrm{T}}$. This has a simple analogy to collisions between hard spheres if one interprets $b^2$ as the total cross section. We therefore choose to write the relaxation rate as

$$\nu = nb^2 v_{\mathrm{T}}\,\bar{I}(r_c/b) \qquad (2.11)$$

In this section we present the predicted relaxation rates that are plotted in section 5.4. Here we assume that $\bar{I}$ is a function only of $r_c/b$ in the regime $\lambda_{\mathrm{D}} > r_c$, $g \ll 1$. This is predicted by theory for $r_c/b \gg 1$ and for $r_c/b \ll 1$. We will assume that it is also true for the region $r_c/b \sim 1$, which seems reasonable. This implies that a plot of $\nu/(n\,b^2\,v_{\mathrm{T}})$ versus $r_c/b$ should lie on a single curve for all temperatures, magnetic fields, and densities (see Fig. 5.8).

[1] O'Neil has called this equation Boltzmann-like since it is essentially the Boltzmann collision term except that the charged particles basically follow the magnetic field lines during a collision.

[2] For the regime $r_c/b \ll 1$ this is not so obvious, and one might guess that the relaxation rate is proportional to $nb^s\,r_c^t v_{\mathrm{T}}$ where $s+t=2$ instead of $nb^2 v_{\mathrm{T}}$.

### 2.3.1 Theory For $r_c/b \gg 1$

For the region $r_c/b \gg 1$ we use an $\bar{I}$ as calculated from a Fokker-Planck equation (see Eq. 76 in reference [28] or page 33 in reference [7]) which gives

$$\bar{I}(r_c/b) = \frac{8\sqrt{\pi}}{15} \log(r_c/b) \tag{2.12}$$

Here we have substituted $\log(r_c/b)$ for $\log(\lambda_D/b)$ as per the Montgomery, Joyce and Turner [41, 40] approximation. That is, the coulomb cutoff distance, $p_{max}$, is $r_c$, and not $\lambda_D$, when $\lambda_D \gg r_c$.

This predicted relaxation rate breaks down as $r_c/b$ approaches 1 for two reasons. First, the calculated relaxation rate involves integrals that contain $\mathbf{r}_e$ and $\mathbf{v}_e$ where $\mathbf{r}_e$ and $\mathbf{v}_e$ are the exact orbits traced by the particles during a collision. When a plasma is immersed in a magnetic field these integrals are too complicated to calculate analytically. To simplify the integrals one ignores the particle interaction when calculating $\mathbf{r}_{e\perp}$ and $\mathbf{v}_{e\perp}$ (i.e. the particle interactions are assume to make negligible changes to $\mathbf{r}_e$ and $\mathbf{v}_e$ during a collision). This is sometimes called unperturbed or noninteracting orbit assumption. Such an approximation is valid only for collisions in which either $p \gg b$ (i.e. small $\Delta\mathbf{v}$) or $\Omega \gg u_{||}/p$ (i.e. the sum of the electrons' magnetic moment is an adiabatic invariant). Using the argument that the main contribution to velocity space scattering occurs for $p > b$ when $p_{max} \gg b$ and the argument that $p_{max} \sim r_c$, one concludes that the unperturbed orbit assumption should be valid as long as $r_c/b \gg 1$.

Second, the Fokker-Planck equation was derived assuming $\Delta\mathbf{v}$ is small so that terms containing $\Delta\mathbf{v}\Delta\mathbf{v}\Delta\mathbf{v}$ and higher orders of $\Delta\mathbf{v}$ can be ignored. It can be shown (see reference [54]) that terms containing $\Delta\mathbf{v}\Delta\mathbf{v}\Delta\mathbf{v}$ and higher orders of $\Delta\mathbf{v}$ are about $1/\log(r_c/b)$ smaller than the terms containing $\Delta\mathbf{v}$ and $\Delta\mathbf{v}\Delta\mathbf{v}$. In other words, this calculation employs the dominant term approximation which neglects terms that do not contain the coulomb logarithm factor, $\log(p_{max}/b)$. Thus, the

uncertainty in this Fokker-Planck relaxation rate calculation is at least $1/\log(r_c/b)$, and this uncertainty becomes very large when $r_c/b \sim 1$.

### 2.3.2 Theory For $r_c/b \ll 1$

Consider a binary collision between electrons that are immersed in a uniform magnetic field. Assume that the magnetic field is strong in the sense that $\Omega \gg u_{0_\parallel}/d_{\max}$ where $u_{0_\parallel}$ is the initial relative velocity parallel to the magnetic field, $d_{\max}$ is the larger of $p$ and $b_\parallel$, and $b_\parallel = 4e^2/(mu_{0_\parallel})$. In this case, O'Neil argues that the sum of the perpendicular energy of the two electrons, $\Xi_\perp$, is an adiabatic invariant. Thus, the collision is expected to cause an exponentially small change to $\Xi_\perp$, and using unperturbed orbits, O'Neil and Hjorth calculate this change to be[3]

$$\Delta\Xi_\perp \approx \frac{e^2 v_\perp p \cos(\delta)}{v_\parallel b_\parallel^2} \int_{-\infty}^{\infty} \frac{d\xi \cos(\kappa'\xi)}{[\eta^2 + \zeta(\xi)^2]^{3/2}} \tag{2.13}$$

where $\delta$ corresponds to the phase angle between $\mathbf{v}_{1_\perp}$ and $\mathbf{v}_{2_\perp}$, $\zeta = z/b_\parallel$, $\eta = p/b_\parallel$, $\xi = u_{0_\parallel}t/b_\parallel$ and $\kappa' = \Omega b_\parallel/u_{0_\parallel}$. From conservation of energy and letting $\Delta\Xi_\perp = 0$, the normalized relative parallel velocity, $\partial\zeta/\partial\xi$, must satisfy the equation

$$\left(\frac{\partial\zeta}{\partial\xi}\right)^2 = 1 - \frac{1}{[\eta^2 + \zeta(\xi)^2]^{1/2}} \tag{2.14}$$

Since $\kappa' \gg 1$ (i.e. $\Omega \gg u_{0_\parallel}/b_\parallel$) the integral in Eq. 2.13 involves the product of a rapidly oscillating function and a slowly varying function[4]. Consequently, this integral can be shown to be of the form

$$\int_{-\infty}^{\infty} \frac{d\xi \cos(\kappa'\xi)}{[\eta^2 + \zeta(\xi)^2]^{3/2}} = h(\kappa', \eta) \exp(-\kappa' g(\eta)) \tag{2.15}$$

where $g(\eta)$ is an increasing function of $\eta$ with $g(0) = \pi/2$, and $h(\kappa', \eta)$ is neither exponentially small nor exponentially large as long as $\kappa' \gg 1$ or $\kappa'\eta \gg 1$.

[3]All the equations in this section are derived in reference [48].

[4]This is also true when $\kappa' \not\gg 1$, as long as $\kappa'\eta = \Omega p/u_{0_\parallel} \gg 1$.

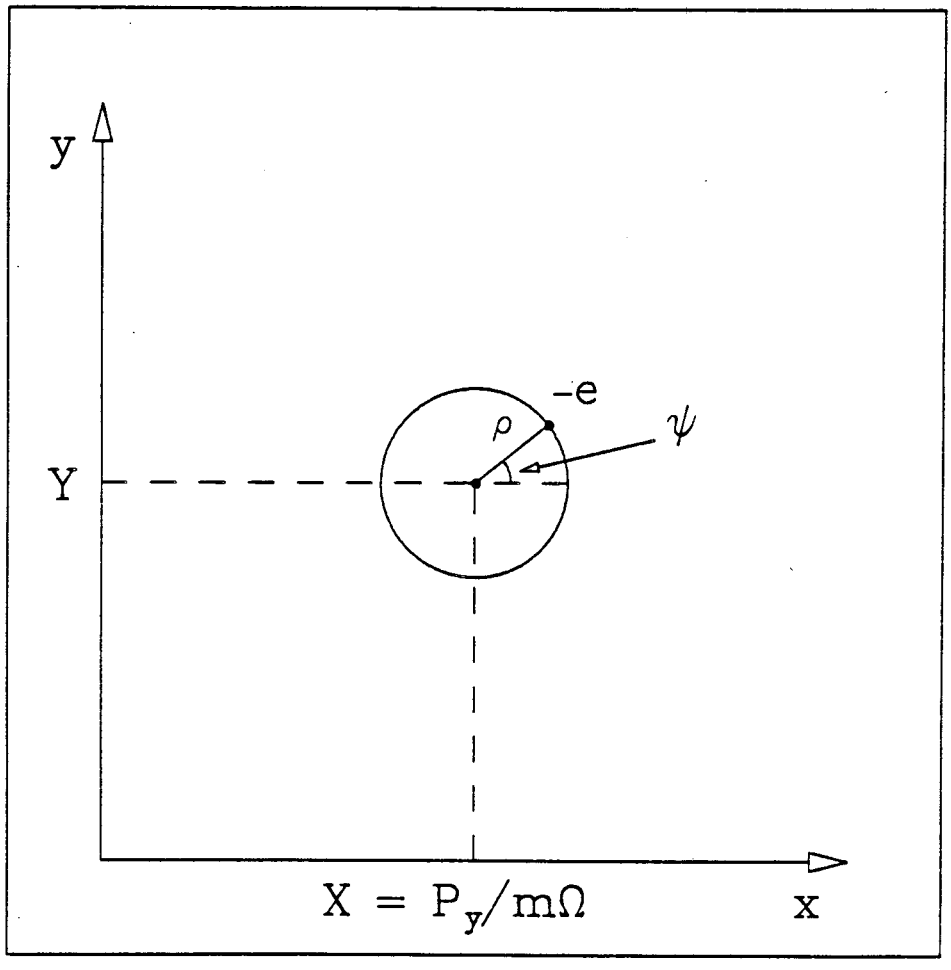


**Figure 2.1:** Guiding center and gyroangle coordinates for a single electron.

For $r_c/b \ll 1$, O'Neil and Hjorth calculate $\bar{I}(r_c/b)$ using Eq. 2.13 for $\Delta\Xi_\perp$ and the Boltzmann-like equation, Eq. 2.10, and obtain

$$\bar{I}(r_c/b) = \sqrt{\pi} \int_0^\infty \frac{d\sigma}{\sigma} \exp(-\sigma^2/2) \int_0^\infty d\eta\, \eta^3\, h^2(\kappa/\sigma^3, \eta)\, \exp(-2\kappa g(\eta)/\sigma^3) \quad (2.16)$$

where $\kappa = \sqrt{2}\,\Omega b/v_{T_\parallel}$, $v_{T_\parallel} = \sqrt{k_B T_\parallel/m}$, $v_{T_\perp} = \sqrt{k_B T_\perp/m}$, $\sigma = u_\parallel/(\sqrt{2}\,v_{T_\parallel})$ and $k_B$ is the Boltzmann constant. This derivation also assumes that $T_\parallel \simeq T_\perp$ at all times. (For the experimental data present in this thesis $T_\parallel \simeq T_\perp$, so that $v_{T_\parallel} \simeq v_{T_\perp}$. In this case $\kappa \simeq \sqrt{2}b/r_c$.)

When $r_c/b \ll 1$, O'Neil and Hjorth argue that the main contribution to the relaxation rate comes from collisions with small impact distances (i.e. small $\eta$), and give $h(\kappa/\sigma^3, \eta)$ and $g(\eta)$ as

$$h(\kappa/\sigma^3, \eta) \approx 2.79\kappa/\sigma^3, \quad (2.17)$$

$$g(\eta) \approx \pi/2 + 0.675\eta^2. \quad (2.18)$$

With these approximations $\bar{I}$ becomes

$$\bar{I}(r_c/b) \approx 3.79 \int_0^\infty d\sigma\, \frac{\exp(-\sigma^2/2)}{\sigma} \exp(-\pi\kappa/\sigma^3). \quad (2.19)$$

This equation has a simple interpretation. The factor $\exp(-\sigma^2/2)$ is just the Maxwellian distribution in $u_\parallel$ which dies off quickly for large $\sigma$. The factor $\exp(-\pi\kappa/\sigma^3)$ dies off quickly at low relative velocities, and implies that only high relative velocity collisions contribute significantly to velocity space scatter. These two terms produce a peak in the integrand near $\sigma^5 = 3\pi\kappa$. Using a saddle point method to evaluate Eq. 2.19, one finds that the range $v_T((3\pi\kappa)^{1/5}-1) < u_\parallel < v_T((3\pi\kappa)^{1/5}+1)$ contributes the most to velocity space scattering (see AppendixA.5).

A saddle point evaluation of Eq. 2.19 yields

$$\bar{I}(r_c/b) \approx 2.66\, \frac{\exp(-2.04\,\kappa^{2/5})}{\kappa^{1/5}}. \quad (2.20)$$

We have numerically integrated Eq. 2.19 for various values of $r_c/b$, and find that Eq. 2.20 is a good approximation to Eq. 2.19 as long as $r_c/b \lesssim 1$. Note that these equations are not valid unless $r_c/b \ll 1$. When comparing theory to the experimental data, we will use Eq. 2.20 for $\bar{I}(r_c/b)$ in the region $r_c/b < 1$.

## 2.4 Many Electron Adiabatic Invariant

In this section we will essentially reproduce an argument by O'Neil [44] which shows that when $r_c/b \ll 1$, there is a many electron adiabatic invariant which prevents the energy exchange of parallel and perpendicular velocity components. This is a novel invariant since it involves many electrons. First, consider the canonical coordinates and momenta [57] $(z, p_z, Y, m\Omega X, \psi, p_\psi)$ of each electron where

$$\tan(\psi) = -\frac{v_x}{v_y} \tag{2.21}$$

$$p_\psi = \frac{m\,(v_x^2 + v_y^2)}{2\Omega} \tag{2.22}$$

$$X = x - \frac{v_y}{\Omega}, \quad Y = y - \frac{v_x}{\Omega}. \tag{2.23}$$

Here $\psi$ is the gyroangle and $p_\psi$ is its conjugate momentum, $(X, Y)$ are the guiding center coordinates, and $P_Y = m\Omega X$ is the momentum conjugate to $Y$. Figure 2.1 shows what these coordinates would look like for a single electron.

The Hamiltonian for $N$ electrons is given by

$$H = \sum_{j=1}^{N} \left( \frac{p_z^2}{2m} + \Omega p_{\psi_j} \right) + \sum_{i<j} \frac{e^2}{|\mathbf{r}_i - \mathbf{r}_j|} \tag{2.24}$$

where

$$\begin{aligned} |\mathbf{r}_i - \mathbf{r}_j|^2 \;=\; & (\, X_i + \rho_i \cos(\psi_i) - X_j - \rho_j \cos(\psi_j)\,)^2 + \\ & (\, Y_i + \rho_i \sin(\psi_i) - Y_j - \rho_j \sin(\psi_j)\,)^2 + \\ & (z_i - z_j)^2. \end{aligned}$$

The quantity $\rho = (2p_\psi/(m\Omega))^{1/2}$ is the gyroradius for an electron with perpendicular energy $p_\psi\Omega$.

The inequality $\Omega \gg (v_\perp/b, v_\parallel/b)$ implies that the $\psi_j$'s are rapidly varying compared to the other variables. Next, a transformation to a new set of variables is made such that only one of the variables is rapidly varying. The transformation takes $\{(\psi_j, p_{\psi_j})|\ j = 1,\ldots,N\}$ into $\{(\theta_j, p_{\theta_j})|\ j = 1,\ldots,N\}$ via the generating function (see chapter 9 in reference [20]),

$$F_2 = p_{\theta_1}\psi_1 + \sum_{j=2}^{N} p_{\theta_j}(\psi_j - \psi_1) \tag{2.25}$$

and leaves the variables $(z_j, p_{z_j}, Y_j, m\Omega Y_j)$ unchanged. The new variables are related to the old by

$$\theta_1 = \frac{\partial F_2}{\partial p_{\theta_1}} = \psi_1, \quad \theta_j = \frac{\partial F_2}{\partial p_{\theta_j}} = \psi_j - \psi_1, \quad \text{for } j > 1, \tag{2.26}$$

$$p_{\psi_1} = \frac{\partial F_2}{\partial \psi_1} = p_{\theta_1} - \sum_{j=2}^{N} p_{\theta_j}, \quad p_{\psi_j} = \frac{\partial F_2}{\partial \psi_j} = p_{\theta_j}, \quad \text{for } j > 1. \tag{2.27}$$

From these equations it follows that $p_{\theta_1} = \sum_{j=1}^{N} p_{\psi_j}$ so that the Hamiltonian takes the form

$$H = \Omega p_{\theta_1} + \sum_{j=1}^{N} \frac{p_z^2}{2m} + \sum_{i<j} \frac{e^2}{|\mathbf{r}_i - \mathbf{r}_j|}. \tag{2.28}$$

From this Hamiltonian, one sees that $\theta_1$ is the only rapidly varying variable. Thus,

$$p_{\theta_1} = \sum_{j=1}^{N} p_{\psi_j} = \sum_{j=1}^{N} \left(\frac{m}{2\Omega}\right)(v_{x_j}^2 + v_{y_j}^2) \tag{2.29}$$

is the desired adiabatic invariant.

For a uniform magnetic field, this adiabatic invariant is the total perpendicular kinetic energy of the electrons. To the degree that this adiabatic invariant is conserved there is no exchange of energy between the parallel and perpendicular velocity components.

# Chapter 3

# Experiment Apparatus and Measurement Methods

## 3.1 Introduction

This chapter describes the design of the experimental apparatus, how a plasma is produced, and the density and length measurements. The apparatus described here is unique in the world although similar to other pure electron plasma traps which have been employed by Malmberg el al. [53]. This particular pure electron trap has been given the name CV which stands for Cryogenic plasma, Voltage contained. A more exact name for CV would be CVM where the "M" stands for Magnetic contained, since CV uses both magnetic and electric fields to trap the electrons. However, we will stick with the name CV.

A schematic of the CV trap is shown in Fig. 3.1. This simple drawing is all one needs for a quantitative understanding of the data in this thesis. In Fig. 3.1 there are three conducting cylinders, called gates. Each gate is electrically isolated from the other gates, and all the gates are aligned along a common axis, designated the $z$-axis. These gates are called $G_6$, $G_7$, and $G_8$. Also aligned with the cylinders are an electron source and five collecting rings, $R_1$, $R_2$, $R_3$, $R_4$ and $R_5$. Finally, a uniform magnetic field is aligned along the $z$-axis. The magnetic field provides radial confinement.

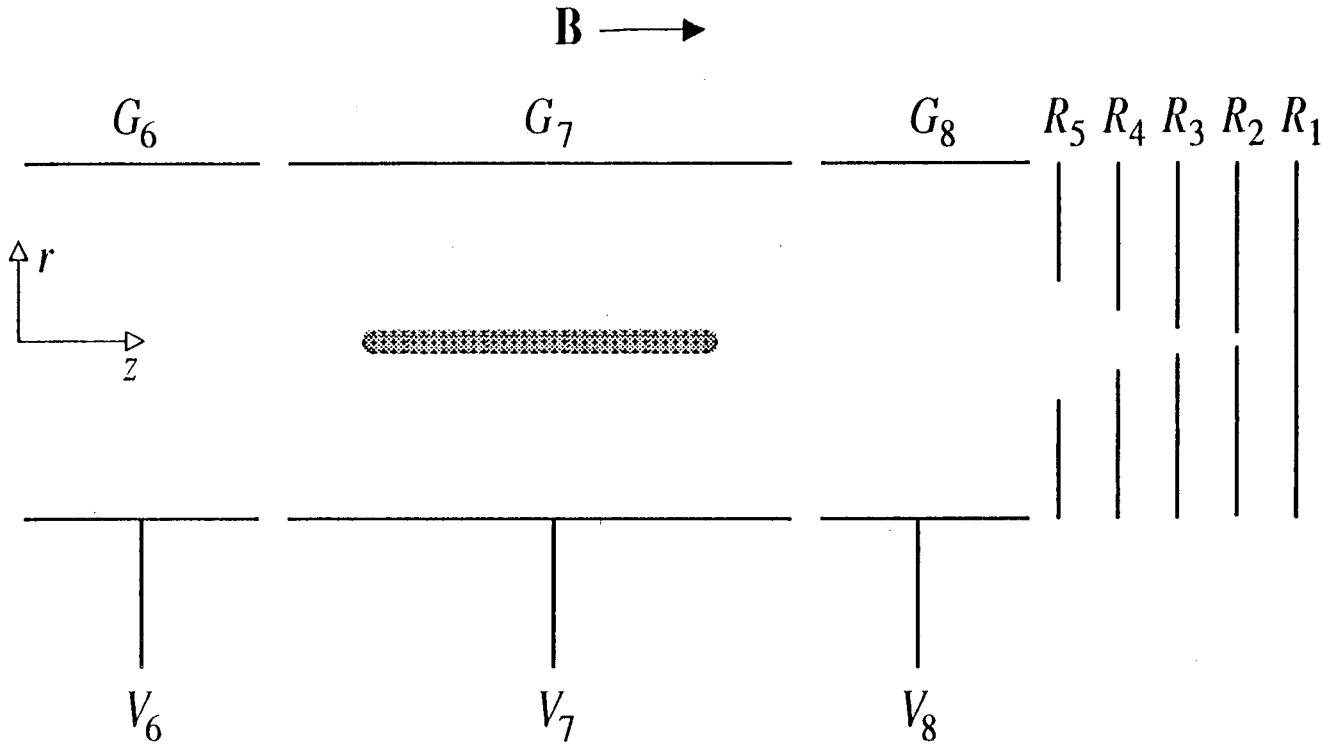


**Figure 3.1:** Schematic of CV pure electron plasma trap. The magnetic field is aligned with the $z$-axis. The shaded area represents a trapped plasma when $G_6$ and $G_8$ are at $-V$ and $G_7$ is grounded.

Note that the plasmas described in this thesis are pure electron plasmas. There are no ions[1] and the background neutral pressure is assumed to be ignorable for times less than about 1000 sec. This implies that the plasma can be cooled to very low temperatures (much less than 1 eV) without recombination.

In section 3.2 we explain how a pure electron plasma can be confined for long times by static magnetic and electric fields. The electric field provides confinement along the magnetic field, axially, by creating a potential energy well. The electric field produced by the plasma together with the external magnetic field produces a field angular momentum along the $z$ axis (see page 604 in reference [29]). This angular momentum is much larger than the plasma mechanical angular momentum for a typical plasma in CV. The field angular momentum is proportional to $\sum_j (R_w^2 - r_j^2)$ where the sum is over all the electrons, $r_j$ is the radial position of the $j^{th}$ electron and $R_w$ is the radius of the cylindrical gates. If external torques are small a plasma in CV can be confined for a long time due to the constraint on the allowed radial position of the electrons (i.e. $\sum_j r_j^2 \simeq$ const). Plasmas used to acquire the relaxation rate data had lifetimes, $\tau_{\text{lifetime}}$, much greater than 100 sec where $\tau_{\text{lifetime}} \equiv n\,(dn(r=0)/dt)^{-1}$.

In section 3.3 several adiabatic invariants are introduced which will be used in different sections of this thesis. In section 3.4 an overview of the basic experimental apparatus is presented. The actual electron source, conducting gates and end collectors are presented as well as the approximate magnetic field strength versus axial position. The magnetic field at the electron source is about 20 times smaller than the magnetic field where the plasma is ultimately contained. This is done to protect the electron source which can not be operated in large magnetic fields. In sections 3.4 and 3.5 we explain what it takes to produce a stable, repeatable plasma.

The apparatus is operated in an inject, hold, dump and measure cycle (hence-

[1] Axially, only negative charges are trapped. In fact, positive charges see a potential energy hill which accelerates them out of the trap region.

forth this cycle will be called a shot). During the dump and measurement phase the potential on $G_8$ is raised to ground, causing the confined electrons to stream along the magnetic field to the end collectors. Depending on the rate at which the potential on $G_8$ is raised to ground, information about either the plasma density profile or the plasma temperature obtained. However, only one of these measurements can be made per shot. Fortunately, with the proper apparatus setup the shot to shot repeatability of both the number of electrons collected on the end collectors and the plasma temperature can be greater than 97%.

In section 3.6 we first describe some of the properties of a global thermal equilibrium plasma, then compare this to what is presently known about a CV plasma. Finally, we discuss particle transport times for a CV plasma.

In section 3.7 the density and length measurements are presented. In this section we show that the average density, $\langle n \rangle$, seen by an electron as it traverses axially will depend on the electron's radial position (i.e. $d\langle n \rangle / dr \neq 0$). Also dependent on the radial position of an electron is an electron's axial bounce length, the axial distance between an electron's axial reflection points. Furthermore, at high temperature and for the same radial position, an electron's axial bounce length will depend significantly upon the electron's axial velocity, $v_{||}$. The radial variation of the average axial density combined with an unknown radial energy transport time contribute the largest uncertainty to the measured relaxation rate.

## 3.2 Electric and Magnetic Confinement of a Pure Electron Plasma

In this section we will explain how a pure electron plasma can be confined with static electric and magnetic fields.

| | CV | Others[a] |
|---|---|---|
| magnetic field (kG) | $10 - 60$ | $0.05 - 0.5$ |
| plasma length (cm) | $0.5 - 10.0$ | $4 - 40$ |
| plasma radius (cm) | 0.1 | $1 - 2.5$ |
| plasma density ($e/cm^3$) | $10^7 - 10^{10}$ | $10^6 - 10^7$ |
| plasma lifetime $\tau_{\text{lifetime}}$ (sec) | $10^2 - 10^4+$ | $1 - 2 \times 10^3$ |
| plasma temperature (Kelvin) (eV) | $30 - 2,000,000$ $0.003 - 200$ | $5,000 - 80,000$ $0.5 - 8$ |

**Table 3.1:** Comparison between CV plasmas and other pure electron plasmas studied by Malmberg et al.

[a]Other pure electron plasmas studied by Malmberg et al.

### 3.2.1 Magnetic Field and Radial Confinement

It is the axial magnetic field together with very small external torques that provide the long radial confinement times for a pure electron plasma in the CV trap [45]. To understand how the magnetic field confines the plasma, one must consider the total angular momentum of the system, $P_\theta$, which has two parts, the mechanical angular momentum of the electrons and the field angular momentum,

$$P_\theta = \sum_j m\, v_{\theta j} r_j + \int d\mathbf{V}\, r\, \hat{\theta} \cdot (\mathbf{E} \times \mathbf{B})/(4\pi c). \tag{3.1}$$

Here we have taken $v_j \ll c$ (the speed of light), the sum is over all particles and $d\mathbf{V} = r\, dr\, d\theta\, dz$. To calculate the field angular momentum term let the potential on $G_6$ and $G_8$ be $-V$ and the potential on $G_7$ be ground. To simplify the problem we will consider the case where the lengths of $G_6$ and $G_8$ are much longer than the radius of the gates. For the magnetic field we write $\mathbf{B} = B\hat{z}$ where $B$ is a constant. Also, we will ignore the diamagnetic field produced by the electrons since the electron velocities are small compared with the speed of light and since the density is well

below the Brillouin limit[2]. We then obtain $\hat{\theta} \cdot (\mathbf{E} \times \mathbf{B}) = -E_r B = B\partial\phi/\partial r$, so that

$$\int d\mathbf{V}\, r\, \hat{\theta} \cdot (\mathbf{E} \times \mathbf{B}) = B \int d\mathbf{V}\, r \frac{\partial \phi}{\partial r}. \tag{3.2}$$

After some manipulation and using Green's theorem we find that

$$\frac{1}{4\pi c} \int d\mathbf{V}\, r\, \hat{\theta} \cdot (\mathbf{E} \times \mathbf{B}) = -\frac{B}{2c} \left( R_w^2 \sum_j q_j - \sum_j q_j r_j^2 \right). \tag{3.3}$$

We next assume that no electrons hit the gate walls[3] (i.e. $r_j < R_w$), that the mechanical angular momentum term is ignorable and let $q_j = -e$. To the extent that the plasma angular momentum is conserved, the allowed radial positions of the electrons is constrained by the relation $\sum_j r_j^2 = \text{const}$. Of course, the plasma angular momentum is conserved by electrostatic interactions between the electrons. The only way to change $\sum_j r_j^2$ is to apply external torques to the plasma.

Sources of external torques include neutral particles, external fields with $\theta$ components, finite wall resistance, and electromagnetic coupling between the plasma and the external world. For this reason the plasma is contained in a high vacuum and all external fields seen by the plasma are designed to be independent of $\theta$ (e.g. cylindrical gates). Of course, it is impossible to make the field completely independent of $\theta$ or to have a perfect vacuum. However, to measure the relaxation rate we only require that the density profile remain essentially the same for about 20 sec, which is the case for the plasmas studied in this thesis (it takes about 1000 sec for the central density to drop a factor of two).

For a typical CV plasma it is easy to show that the mechanical angular momentum term is much smaller than $eB/(2c)\sum_j r_j^2$. Let $v_\theta$ be decomposed into two parts. One part is the gyrocenter drift velocity, $v_f$ (see section 3.3), which for a zero temperature plasma is $v_E = c\mathbf{E} \times \mathbf{B}/B^2$. For a constant density plasma

[2]For a uniform density pure electron plasma, the density must satisfy the relation $r_c \leq \lambda_D/\sqrt{2}$ (see reference [38] and references therein).

[3]This first assumption is not necessary, but it simplifies the following explanation.

$v_E = r\omega_p^2/(2\Omega)$ so that $\sum_j 2r_j v_{f,j}/(\Omega \sum_j r_j^2) \approx (\omega_p/\Omega)^2$. For the plasmas studied in this thesis, $(\omega_p/\Omega)_{max} \approx 0.003$. The second part is the $\hat{\theta}$ component of the electron's gyrovelocity, $v_c$, about the gyrocenter. One can overestimate this term by letting $v_c$ equal the thermal velocity $v_T$. Thus, $\sum_j 2r_j v_{T,j}/(\Omega \sum_j r_j^2) \approx r_c/\langle r_p \rangle$, where $r_c$ is the electron gyroradius and $\langle r_p \rangle$ is essentially the average plasma radius. For CV $\langle r_p \rangle \approx 0.04\,\text{cm}$ so that $(r_c/\langle r_p \rangle)_{max} \approx 0.01$. Thus, the field angular momentum term is much larger than the mechanical angular momentum term for the plasma in CV.

Note that for a neutral plasma the field angular momentum will not constrain the plasma radially. This can be seen from Eq. 3.3. Consider two charges at a radius $r$ with charge $e$ and $-e$. These two charges can wander together in $r$ without changing the field angular momentum.

### 3.2.2 Electric Field and Axial Confinement

Electrostatic potentials are used to confine the plasma axially by creating, for electrons, a potential energy well along the $z$-axis. This well is created, for example, by applying negative potentials to gates $G_6$ and $G_8$ with $G_7$ at ground (see Fig. 3.1). The actual potential, $\phi$, seen by the electrons is the sum of the potentials from the gates (called vacuum potential) and the potential from the confined electrons (called space charge potential). The total potential can be calculated from Poisson's equation,

$$\nabla^2\phi(r,z) = 4\pi e\, n(r,z), \tag{3.4}$$

where $n(r,z)$ is the electron density, and $\phi$ must satisfy the appropriate boundary condition, which for CV is to good approximate the potentials applied to the gates and end collectors. Also, we assume that the plasma and fields are independent of $\theta$. To confine the plasma axially one requires that $-e(V_b - \phi_0) \gg k_B T$ where $V_b$ is the maximum potential along the axis and $\phi_0$ is the total potential at the center of the plasma. Note, because of the finite length of the gates, the potential $V_b$ is less

than the potential applied to the confining gates.

## 3.3 Adiabatic Invariants

Before discussing the operation of CV and the plasma measurements, it is useful to present three important adiabatic invariants and the guiding center drift approximation.

If a system has a periodic motion, the action integral, $\oint p\,dq$, taken over a period is a constant of the motion where $q$ is a generalized coordinate and $p$ is its conjugate canonical momentum. If the system changes slowly compared to the periodicity of the $q$ motion then to good approximation the action integral is a constant, and in standard nomenclature is called an adiabatic invariant [20, 43].

One good adiabatic invariant for the plasmas studied in this thesis is an electron's gyromotion, which has an angular frequency $\Omega = eB/(mc) \approx 1.76 \times 10^7\, B$ rad/sec. With the exception of close collisions (which can cause the interaction fields to vary on time scales that are short compared to $\Omega^{-1}$), all fields seen by the electrons vary on time scales which are long compared to $\Omega^{-1}$. In fact, at low temperature even the collision time becomes slow compared to $\Omega^{-1}$, thus reducing the exchange of energy between the parallel and perpendicular motion which is one of the main themes of this thesis.

Integrating $\oint p\,dq$ for an electron's gyromotion yields

$$\mu \propto \frac{mv_\perp^2}{2B} = \frac{E_\perp}{B}, \tag{3.5}$$

as the adiabatic invariant where $\mu$ is usually called the magnetic moment of the electron. For uniform $B$ one sees that $E_\perp$ is then an adiabatic invariant. It has been pointed out by O'Neil [44] that when $r_c/b \ll 1$, which occurs for some of the plasmas described in this thesis, it is not the magnetic moment of a single electron that is conserved but the sum of all the magnetic moments (see section 2.4).

Another useful approximation is to ignore the gyromotion of the electrons. To lowest order in this approximation, called the guiding center drift theory, an electron's motion perpendicular to the applied magnetic field is given by [43]

$$\frac{d\mathbf{r_g}}{dt} = \mathbf{v_f}(\mathbf{r_g}) = \frac{-c}{e}\frac{(\mathbf{F}\times\mathbf{B})}{B^2}, \tag{3.6}$$

where $\mathbf{r_g}$ is the center of the electron's gyromotion and an electron at $\mathbf{r_g}$ will feel a static force $\mathbf{F}$. Usually, $\mathbf{v_f}$ is called the drift velocity.

Let us calculate the motion perpendicular to an applied magnetic field for an electron embedded in an infinitely long column of charged fluid. Let the charged fluid have a charge density $-en(r)$. The axis of the charged fluid column is aligned with the magnetic field. This charged fluid is essentially equivalent to a plasma in CV with density $n(r)$. Here we assume that the guiding center drift theory is valid, and for the moment we assume that the plasma temperature is zero. The motion of an electron's gyrocenter is given by $\mathbf{v_E}$, where the force on the electron is due to the electric field from all the other electrons. By Gauss' law this field is

$$\mathbf{E}(r_g) = \frac{-4\pi e}{r_g}\int_0^{r_g} n(r')\,r'\,dr'\,\hat{r}, \tag{3.7}$$

which yields

$$\mathbf{v_E}(r_g) = \frac{-4\pi ec}{Br_g}\int_0^{r_g} n(r')\,r'\,dr'\,\hat{\theta}. \tag{3.8}$$

Thus, electrons circle the point $r = 0$ with angular frequency,

$$\omega_E(r_g) = \frac{4\pi ec}{Br_g^2}\int_0^{r_g} n(r')\,r'\,dr'. \tag{3.9}$$

Note, for uniform density profile $\omega_E(r_g)$ is also uniform, and for all other density profile $\omega_E(r_g)$ is a function of $r_g$.

For finite plasma temperature, the angular rotation rate for an electron about the radial axis is [47]

$$\omega_R(r) = \omega_E + \frac{c}{rBen}\frac{\partial(nk_BT)}{\partial r}. \tag{3.10}$$

The second term on the right hand side of Eq. 3.10 is a result of the diamagnetic (or the pressure) drift.

When $\omega_R$ is fast compared to changes in the magnetic field we have another adiabatic invariant, $Z_g$. This adiabatic invariant is the flux enclosed by an electron's guiding center drift motion,

$$Z_g \propto B r_g^2. \tag{3.11}$$

This invariant is useful when determining the plasma density (see section 3.7).

We should also point out at this time what we mean by $v_\perp$. An actual electron's velocity perpendicular to the magnetic field can be essentially written as

$$\mathbf{v}_\perp = \mathbf{v}_R + \Omega\vec{\rho} \tag{3.12}$$

where $\vec{\rho}$ is the position of the electron about its guiding center in the absence of other electrons. Since the plasma and all the fields are assumed to be symmetrical in $\theta$ and $\Omega \gg \omega_R$, we drop the $\mathbf{v}_R$, and write $\mathbf{v}_\perp = \Omega\vec{\rho}$. Thus, when we write the distribution function as $f(\mathbf{v}_{||}, \mathbf{v}_\perp)$ we are using this approximation for $\mathbf{v}_\perp$.

The final adiabatic invariant is usually called the bounce invariant. In this case $q$ is the $z$ coordinate of an electron and $p$ is the momentum along $\hat{z}$, $mv_{||}$. To calculate $\oint p\,dq$, we will assume that the potential is constant along $z$ inside the plasma except for a small region of $z$, where the electrons are reflected. This assumption is good at low temperatures (see section 3.7.1). Thus, $\oint mv_{||}\,dz = 2ml_p v_{||}$. If the potentials on the end gates confining the plasma are changed slowly compared to $v_{||}/l_p$ then $l_p v_{||}$ will be an adiabatic invariant.

## 3.4 Experimental Apparatus

When looking at the CV experimental apparatus one sees two distinct objects; the electronics that control the experiment, and a liquid helium dewar and

its support. The electronic part consist of units for timing events and producing voltages on the different gates, power supplies for the magnetic field, oscilloscopes, function generators and several specialized units. There is also a computer, a DEC LSI 11/73, which is usually used for acquiring data. Although, at times the computer is also used for controlling parts of the experiment. Presently, the main function of the computer is acquiring temperature data and analyzing it if the temperature is high, or transferring the data via a serial port to a VAX where low temperatures are analyzed.

The liquid helium dewar contains a superconducting solenoidal magnet and its support, a vacuum can residing in the magnet bore, leads, and an amplifier that operates at about 100 K. Inside the vacuum can are the cylindrical gates, end collectors, and an electron source[4]. Figure 3.2 shows a schematic of the helium dewar and its contents.

The liquid helium serves three essential functions, all related to its low temperature of 4.2 K. First, it cools the magnet below the temperature at which the magnet becomes superconducting. This allows for a large (up to 72 kG) steady magnetic field. This large field provides radial confinement and cyclotron cooling of the plasma (see section 4.2). Second, it cools the walls of the vacuum can, causing the inside walls of the vacuum can to act as a cryopump. This produces an ultrahigh vacuum, possibly $10^{-13}$ Torr or less, inside the vacuum can. Finally, cyclotron cooling can at most cool the plasma to the background radiation temperature. Since the background radiation temperature is essentially determined by the apparatus temperature[5], we want the apparatus temperature to be as low as reasonably possible.

[4]For the rest of this section we will call the cylindrical gates, end collectors, and electron source by the name "trap".

[5]The plasma and the heated spiral filament (electron source) are additional sources of radiation; however, the radiation from these sources appears to have no effect on the measured plasma temperature.

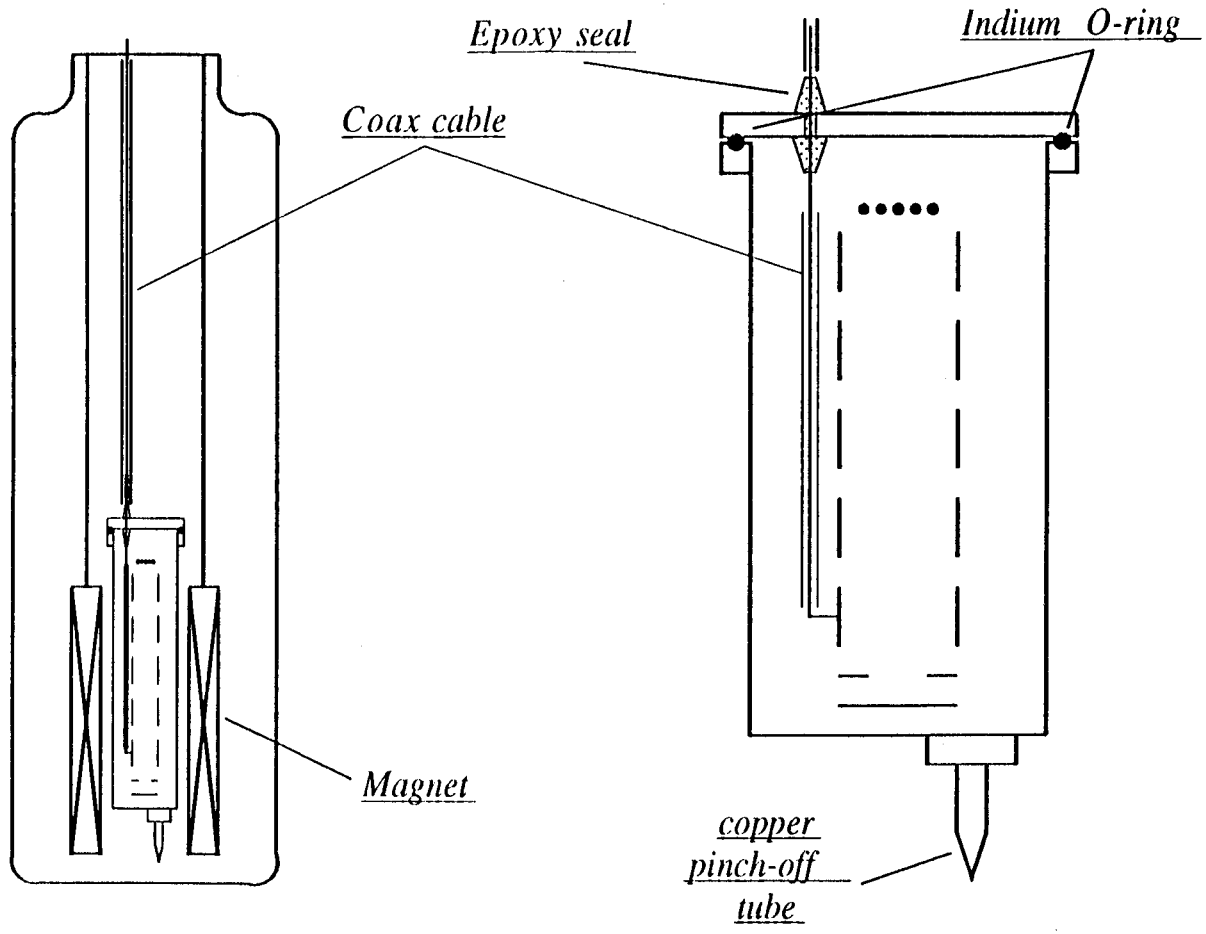


**Figure 3.2:** Schematic of helium dewar and vacuum can. The vacuum can in the dewar is shown in larger scale at the right.

Figure 3.3 shows the actual arrangement of the trap in the vacuum can. The electron source is a 0.006 cm diameter 1% thoriated tungsten wire. Initially the wire was wound in a 0.5 cm diameter spiral. However, the original shape of the wire has since been distorted. To produce electrons a current of about 0.5amps is run through the wire causing it to heat to about 1800 K. At this temperature some electrons are able to overcome the work function of the metal and escape [30].

The number of electrons trapped is mainly determined by three potentials, $V_{\rm fil}$, $V_{\rm bias}$ and $V_{\rm grid}$ [35, 14] and by the length of the initial trapping region. $V_{\rm fil}$ is the potential difference between the center of the spiral filament and the outer edge of the filament. $V_{\rm bias}$ is the potential applied to the center of the spiral filament. In most cases $V_{\rm bias}$ is a negative potential. $V_{\rm grid}$ is the potential applied to the gate $G_0$, which is situated directly in front of the filament. Henceforth, the spiral filament will be called the electron source.

The gates and end collectors are machined from OFHC copper, and are designed so that there is as little asymmetry in the $\theta$ direction as possible. This is done to reduce external torques. All the gates and end collectors are electroplated with palladium and then electroplated with gold. The palladium is used to stop the gold from diffusing into the copper. The gold forms an outer surface which is conducting yet does not oxidize. The original design of CV had pure copper gates. When Malmberg and Hyatt [37] initially operated CV they noticed that the lifetime of a plasma in CV was greatly reduced when electrons were sprayed onto the inner walls of the gates. They concluded that the copper surface had oxidized, and electrons sprayed onto this oxidized surface were stuck there for a long time. This produced a asymmetrical field, and resulted in a decreased plasma lifetime. For this reason the copper surfaces were gold plated, and this effect has since disappeared.

Each gate, each end collector and the electron source are connected to sepa-

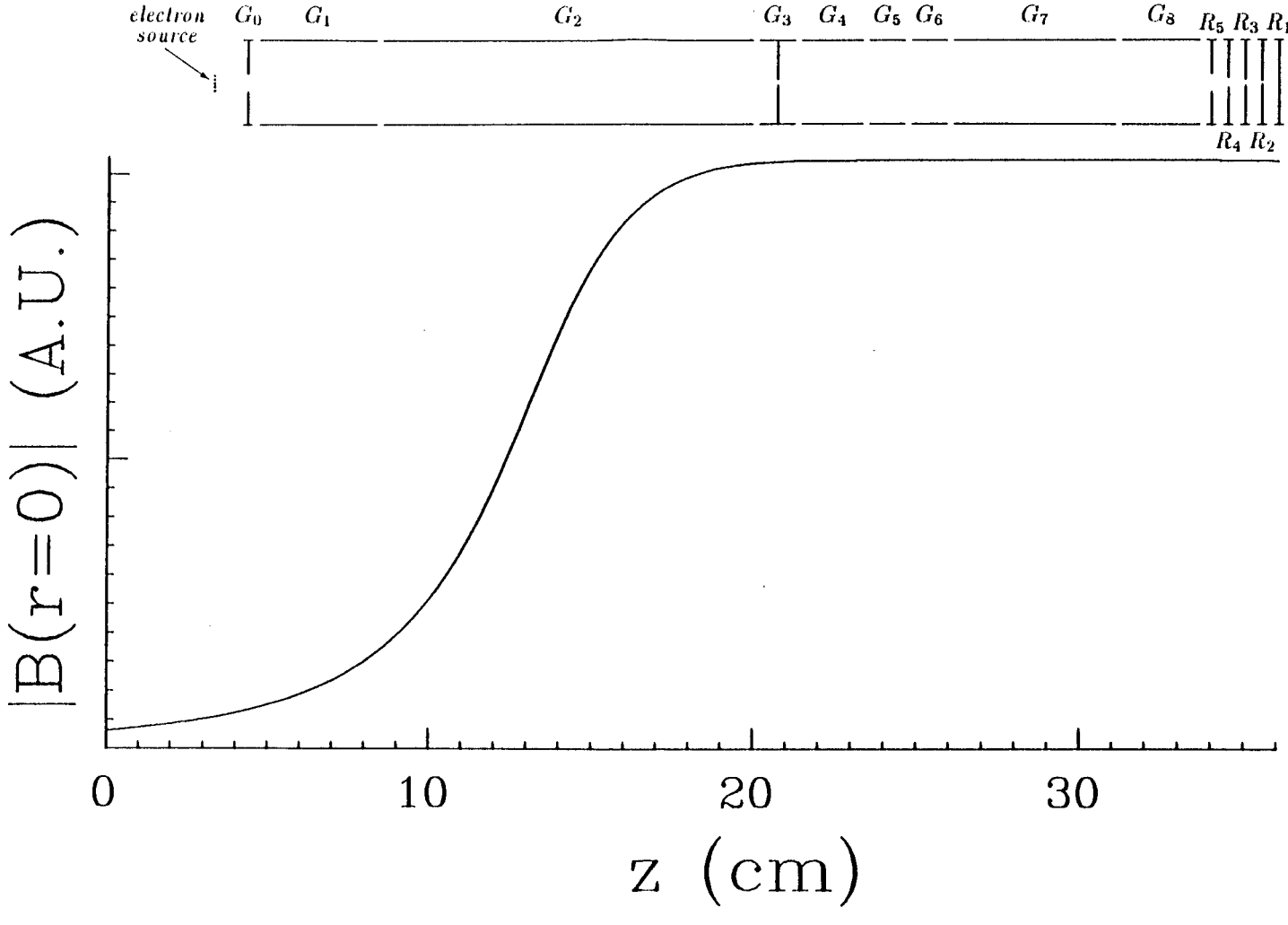


**Figure 3.3:** Actual CV trap layout. The curve is a plot of the magnetic field at $r = 0$ for the different regions of the CV trap.

rate annealed copper leads that feed through the top of the vacuum can. These leads provide two functions. First, they allow voltages to be applied to each gate, each end collector and the electron source. Second, they provide a good thermal path for the heat generated by the electron source to escape into the liquid helium; thus keeping the trap near 4.2 K.

The original design of CV had the electron source and the trapping gates in the constant magnetic field region of the magnet (i.e. near the center of the magnet). One problem with this arrangement is that the electron source could not be on while the large magnetic field is larger than 4 kG. With the electron source hot, the $\mathbf{I} \times \mathbf{B}$ force will destroy the electron source if the magnetic field is too large. To capture a plasma in a large magnetic field, we first had to trap a plasma in a low field, typically 1 kG, and then ramp the magnetic field up to the desired field. The self inductance of the magnet is 22 H, making the ramp time about 5 min (a maximum of about 5 V can be applied across the magnet leads).

To speed the injection process the electron source was moved outside the bore of the magnetic, but still aligned with the bore, into a region where the magnetic field is about 1/20 the field in the center of the magnet. With this new arrangement electrons emitted from the source, where the magnetic field is less than 3 kG, can be quickly (a repetition rate of 100 Hz is achievable) and easily transported to the center of the magnetic. This greatly increases the amount of data that can be taken, which was necessary to take the relaxation rate data in this thesis.

Another advantage of placing the electron source outside the magnet is that the electrons follow the magnetic field lines as they travel into the center of the magnet. This produces a higher density, by about a factor of 20, inside the magnet than exists around the electron source. Note that, this also happens when the magnetic field is ramped up by a factor of 20 (see section 3.3).

### 3.4.1 Achieving a High Vacuum

The top of the vacuum can may be removed to overhaul the CV trap. An indium O-ring is used to seal the top of the vacuum can to the rest of the vacuum can (see Fig. 3.2). The copper wires that feed through the top of the vacuum can are sealed with epoxy. At the bottom of the vacuum can is a 3/8″ OFHC copper tube. To obtain a good vacuum, the vacuum can is first removed from the dewar and attached via the copper tube to a pumping station. The inside of the vacuum can is pumped down to about $10^{-6}$ Torr and then tested for leaks. The vacuum can is then sealed by pinching the copper tube with a special pinching tool. This cold welds the end of the copper tube, thus sealing the vacuum can with a partial vacuum.

The vacuum can is then placed back into the dewar and all necessary mechanical and electrical connections are made. Next the dewar is filled with liquid nitrogen to precool the dewar and its contents. After about a day the nitrogen is removed from the dewar, and liquid helium is added to the dewar. At this point, if there are still no leaks, the pressure inside the vacuum can is probably $10^{-13}$ Torr or less.

The actual neutral helium pressure (only helium will be a gas at this temperature) in the vacuum can is too low to measure. However, an upper limit can be set at about $10^{-11}$ Torr (at 4.2 K) or $4 \times 10^7$ atom/cm$^3$. This limit is determined by creating a current of a monoenergetic beam of electrons that travels from the electron source to the end collectors. If the energy of the beam is near the ionization energy for helium, some of the electrons will ionize some of the helium atoms. By measuring the current of the electron beam and the current of the helium ions one can estimate the density of helium atoms. This technique can measure helium densities down to about $4 \times 10^7$ atom/cm$^3$.

## 3.5 Operation of CV

By changing the voltages on the gates, we can capture a plasma (inject), moved the plasma along the $z$-axis, or release it (dump). If $V_{\rm fil}$, $V_{\rm bias}$, $V_{\rm grid}$ and potentials on the gates are adjusted properly, a stable, reproducible plasma can be trapped. In this section we will describe a typical trap, hold, dump cycle.

Figure 3.4 shows a typical timing sequence for the voltages applied to the different gates in Fig. 3.3[6]. At time $t_0$, $G_1$, $G_2$, $G_3$, $G_4$, $G_5$, $G_6$ and $G_7$ are at ground and $G_8$ is at $-V$. For simplicity we will take all the voltages to be either ground or $-V$. The electron source is turned on with a potential $V_{\rm fil}$, and a potential bias $V_{\rm bias}$. Electrons are emitted from the source and fill the region between the electron source and $G_8$. At time $t = t_{\rm i}$, $G_1$ is ramped in about 1 msec to $-V$, capturing some electrons between $G_1$ and $G_8$. After a short time, typically a few msec, $G_2$, $G_3$, $G_4$, $G_5$ and $G_6$ are ramped to $-V$, confining the electrons between $G_6$ and $G_8$ (see Fig 3.1). By capturing a plasma in $G_2 + G_3 + G_4 + G_5 + G_6 + G_7$ and then squeezing the plasma into $G_7$, a plasma with a higher density is captured in $G_7$ than if the plasma is just trapped in $G_7$ initially.

Once confined, the plasma may then be manipulated (e.g. compressionally heated, see chapter 5). Finally, the potential on $G_8$ is ramped to ground. This dumps the plasma onto the end collectors where either the plasma density or plasma temperature is measured. Once the plasma has been dumped, the potential on $G_8$ is ramped to $-V$ and $G_1$, $G_2$, $G_3$, $G_4$, $G_5$ and $G_6$ are ramped to ground, and the process is repeated.

The shot to shot repeatability and the plasma density are essentially determined by $V_{\rm fil}$, $V_{\rm bias}$, $V_{\rm grid}$.

[6]The timing chain described here will capture a plasma in $G_7$. However, typically we capture a plasma in other gates or a combination of gates.

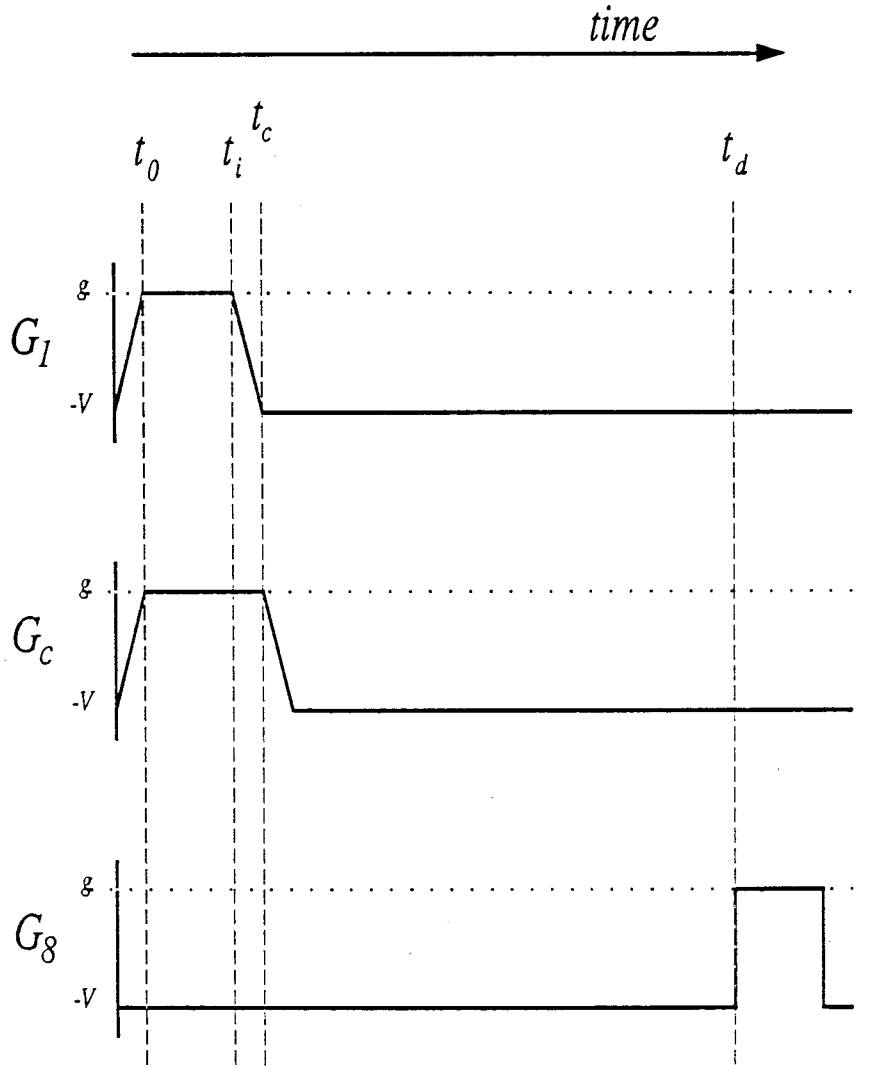


$$G_c = G_2 + G_3 + G_4 + G_5 + G_6$$

$$G_7 = g, \quad g = ground$$

**Figure 3.4:** Typical timing chain sequence.

## 3.6 Thermal Equilibrium and Plasma Transport

In an ideal CV trap (one in which the fields have perfect $\theta$ symmetry, and there are no neutrals or ions) a pure electron plasma can be confined for a time which is long compared to the internal rearrangement[7] time. The plasma will then rearrange itself so that it reaches a state of global thermal equilibrium. However, the internal rearrangement time for a typical CV plasma immersed in a magnetic field of 60 kG appears to be very long (possibly 1000 sec or longer). Since a single relaxation rate measurement requires many shots, waiting 1000sec per shot is unrealistic. Therefore, the plasmas studied in this thesis are most likely not in global thermal equilibrium.

In this section we first describe some of the properties of a global thermal equilibrium plasma, then compare this to what is presently known about a CV plasma. Finally, we discuss particle transport times for a CV plasma.

### 3.6.1 Global Thermal Equilibrium: An Ideal CV Trap

For a global thermal equilibrium CV plasma, the distribution function is (see references [8, 47])

$$f(\mathbf{r}, \mathbf{v}) = Z^{-1} \exp[-(H - \omega P_\theta)/(k_B T)] \tag{3.13}$$

where $H$ is the Hamiltonian for the electrons in a magnetic field and $Z$ is the partition function. This distribution describes 1) a plasma rotating about the radial axis with a uniform angular frequency $\omega$; 2) a density distribution which is a monotonically decreasing function of radius; and 3) in a frame rotating with the plasma, a velocity distribution which is a Maxwellian with uniform temperature $T$.

For a global thermal equilibrium plasma in a CV trap (or similar trap), Prasad and O'Neil [52] have shown that the density profile is essentially uniform except near the plasma edge. At the plasma edge they choose a local coordinate that is

[7] Here rearrangement is a general term implying all possible types of transport in both coordinate and velocity space (e.g. particle and energy transport, and velocity space transport).

perpendicular to the edge, and find that the plasma density decreases monotonically to zero on the scale of a few Debye lengths. At low temperature the Debye length for a plasma in CV is much less than the plasma radius.

### 3.6.2 CV Plasma

The concept of a global thermal equilibrium plasma is a theoretical construct which can never be achieved experimentally (although some plasmas may closely approach global thermal equilibrium). Ideally, one would like to measure the relaxation rate for a global thermal equilibrium plasma, since the temperature and to good approximation the density would be uniform through out the plasma (here we assume that the dimensions of the plasma are large compared to the Debye length). However, it appears that a CV plasma is not in global thermal equilibrium, and this produces some uncertainty in the measured relaxation rates.

When the relaxation rate data was obtained, the density measurement yielded very little information about the density profile (the density measurement will be described in section 3.7). Essentially, the density measurement yields an average density of the plasma which lies inside the radius $r_1$, where $r_1$ is the radius of the collecting region of $R_1$. However, with a new density analysis procedure we have achieved better spatial resolution of the density profile. This new density analysis yields density profiles which decrease to zero on a scale length of many Debye lengths, as opposed to the few Debye length predicted by Prasad and O'Neil for a plasma in global thermal equilibrium.

Figure 3.7 represents a density plot obtained using the new density analysis procedure. Recall that this density profile was obtained after the relaxation data taken (see the last paragraph of this section). Figure 3.7 is a plot of $n(r,z)$ versus $z$ for various $r$. In this figure $T_{||} = 10^3\,\mathrm{K}$ and near the plasma center, $r = 0$, $z = 2.8$, $n(r,z) \approx 10^9 \mathrm{e/cm}^3$ so that $\lambda_{D_0} = \lambda_D(r = 0, z = 2.8) \approx 6.6 \times 10^{-3}\,\mathrm{cm}$. In addition,

we have inserted two small figures near the top of Fig. 3.7 which show the density fall off for two local coordinates which are perpendicular to the local edge of the plasma. The top, left figure is a plot of the density profile versus radius, $r$, for $z = 2.8$. In this small figure $r$ goes from the axis to an $r$ of about $14\,\lambda_{D_0}$. The second small figure, top right, is a plot of the density profile versus $z$ for $r = 0$ and $4.4 < z < 4.8$. In this latter figure the tick marks on the abscissa are separated by a distance of $10\,\lambda_{D_0}$. These small figures represent two cases where the density is not decreasing to zero on a scale of a few Debye length when viewed by a local coordinate that is perpendicular to the local plasma edge. Therefore, we conclude that this plasma is not in global thermal equilibrium. (Note that this results in a non-uniform rotation rate (i.e. $\partial\omega_R/\partial r$ in Eq. 3.10 is not zero).)

Although a CV plasma is not in global thermal equilibrium, the plasma temperature may be uniform. This is possible since an electron can diffuse radially across the plasma much faster than the density rearrangement time. This is simply due to the fact that two electrons can exchange radial position[8] and yet cause no rearrangement of the plasma density. In this type of exchange there is no change in the density profile. However, in such an exchange an electron's energy can remain essentially the same, causing radial energy transport. In general, radial energy transport time will be much shorter than the time it takes for the density profile to relax to a global thermal equilibrium density profile. The energy transport time will be discussed in section 4.5.

[8]For example, one might use guiding center drift theory to calculate the radial positions of the two electrons, electron 1 and electron 2, during a collision. During a collision each electron feels an electric field produced by the other electron. These fields cause the electrons to $\mathbf{E} \times \mathbf{B}$ drift about a common axis. If $\mathbf{a}_1$ ($\mathbf{a}_2$) is the radial position of electron 1 (electron 2), then during the collision one can show that $\mathbf{a}_1 + \mathbf{a}_2 = \text{const}$ and $\mathbf{a}_1^2 + \mathbf{a}_2^2 = \text{const}$.

### 3.6.3 Plasma Density Rearrangement and Loss Times

For the relaxation rate measurement to work, the radial density profile must be essentially stable for up to 20 sec (i.e. $[(1/n(r))(\partial n(r)/\partial t)]^{-1} \gg 20\,\mathrm{sec}$). There are many processes which may cause the radial density profile to vary with time. However, these processes can be divided into two classes. In one class are all processes that change the density profile while conserving the plasma angular momentum. This class of processes we will call the rearrangement class. The second class contains all processes which change the density profile and also change the plasma angular momentum (i.e. transport processes that are a result of external torques). We call this class the plasma loss class. Naturally, the processes in the plasma loss class are due to $\theta$ asymmetries in the fields and/or to background neutrals.

Typically, processes classified under the plasma loss class cause the radial density profile to vary on the time scale of the plasma lifetime, $\tau_{\mathrm{lifetime}}$. Experimentally [13, 15, 36], it is observed that, in general, short plasmas have longer lifetimes than longer plasmas, and the larger the applied magnetic field the longer the plasma lifetime. In addition, on the CV trap we find that low density plasmas in general have longer lifetimes than high density plasmas.

Transport classified under the rearrangement class has been studied on other pure electron traps at the University of California at San Diego (see page 56 in reference [53]). To simplify rearrangement class transport we will consider the transport along the three coordinates axes, $(r, \theta, z)$, separately. Transport along $z$ is fast (about the bounce time) and will be ignored[9].

Recent data [10] indicates that $\theta$ variations in the density profile disappear on a time scale of $\omega_{\mathrm{R}}^{-1}$. For the plasmas studied in the thesis $\omega_{\mathrm{R}}^{-1} \sim 1\,\mu\mathrm{sec}$. After trapping a plasma we wait at least 100 msec before performing any measurements.

[9] Of course, this assumes that there are no plasma waves with finite $k_z$. These waves, or any plasma wave, will cause the density profile to vary in time until such waves are damped away.

This should allow the plasma to come into a local thermal equilibrium (e.g. allowing the plasma distribution to relax to a Boltzmann distribution along the $z$ axis). The time of 100 msec is about $10^5$ $\omega_R^{-1}$ times, and we therefore believe that the density profile is to good approximation independent of $\theta$ during the measurement phrase.

For a CV plasma with $n \approx 10^9 e/cm^3$, rearrangement class, radial particle transport appears to have a time scale of about 1000 sec or greater. (Evidence of this will be presented in section 3.7).

## 3.7 Plasma Density and Length

For a typical plasma in CV, greater than 99% of the electrons, when dumped, hit either $R_1$ or $R_2$, with about an equal number of electrons hitting $R_1$ and $R_2$. This information says very little about the density as a function of radius and nothing about $\theta$ variations in the density. We will assume that the density does not depend on $\theta$ (see section 3.6), that electrons stream along the magnetic field line when they are dumped, and that the magnetic field lines are aligned with the gates and end collectors.

The number of electrons that hit $R_1$, $N_1$, is the number of electrons between $r = 0$ and $r = r_1$ ($r_1$ is the radius of the collecting region of $R_1$) integrated over the length of the plasma[10],

$$N_1 = 2\pi \int_0^{r_1} n(r,z)\, r\, dr\, dz, \tag{3.14}$$

with a similar expression for the number of electrons collected on $R_i$, $N_i$, where $i$ can be 2, 3, 4 or 5. If a good estimate for the plasma length, $l_p$, is known, the average density of the plasma which lies inside the radius $r_1$ would be $N_1/(\pi r_1^2 l_p)$, when the plasma was confined. The plasma length is obtained from a computer program which solves Poisson's equation in $(r,z)$ to obtain a self-consistent $n(r,z)$ and $\phi(r,z)$, given

[10]There is a correction due to the finite size of the gyroradius. This effect is of order $r_c/r_1 \ll 1$ and will be ignored. We estimate that for the worst case this error is about 1%.

$N_1$, $N_2$ and the gate potentials. This yields an average density of the plasma which lies inside the radius $r_1$ to about 20% accuracy.

To achieve better spatial resolution of the density profile we capture a plasma with an initial applied magnetic field $B_i$. Next, the magnetic field is ramped down to $B_f$, and then the plasma is dumped. We assume that the magnetic flux enclosed by an electron's guiding center drift motion is well conserved as the magnetic field is ramped down (see section 3.3). For CV $B\,(dB/dt)^{-1} \approx$ minutes and $\omega_R^{-1} \approx 1$ $\mu$sec, so that $Br_g^2$ for an electron is, to good approximation, a constant while the magnetic field is being varied.

Using $Br_g^2 =$ const one finds that all the electrons that hit $R_1$ were inside the radius $r = r_1\sqrt{B_f/B_i}$ when the magnetic field was $B_i$. Ramping the field back to $B_i$, and repeating this procedure, we find that the number of electrons collected on the various end collectors is repeatable to about 1%. This method is repeated many times with the plasma always injected with an applied magnetic field of $B_i$; however, to get more information about the radial density profile we dump the plasma at various $B_f$'s.

A computer program is employed to estimate $N_l(r)$, where

$$N_l(r) = \int n(r,z)\,dz, \tag{3.15}$$

and $n(r,z)$ is the density when the magnetic field is $B_i$. We assume that $N_l(r) = N_{l_i}$ where $N_{l_i}$ is constant for $(i-1)(\delta r) < r < i(\delta r)$ and is zero otherwise, and where $i = 1, 2...m$ (i.e. we assume that $N_l(r)$ has a histogram shape with $m$ bins out to a radius of $m(\delta r)$ and is zero otherwise). The $N_{l_i}$'s are then determined from the known signals on the end collectors. A least squares method is used to average out the noise. The calculated $N_l(r)$ is accurate to about 10% as long as the radial variation of $N_l(r)$ is gradual.

Figure 3.5 is a plot of $N_l(r)$. To construct $N_l(r)$ we calculated $N_{l_i}$ for $m\delta r =$

$3\ r_1$, and with various number of bins (i.e. $m = 5, 6, 7, 8, 9$). We then average the $N_{1_i}$ to get $N_1(r)$. Finally, a spline algorithm is used to smoothly connect the $N_1(r)$ versus $r$ data points. To construct $N_1(r)$ in Fig. 3.5, the plasma was injected with a $B_i = 60\,\text{kG}$ and dumped at fields of 10, 15, 20, 25, 30 and 40 kG.

To determine $N_1(r)$ we have assumed that the flux enclosed by an electron's guiding center drift motion is well conserved. This assumption will be broken if transport (either from the rearrangement class or from the loss class) causes a change in the density profile. Note, it takes about 200 sec to ramp the magnetic field from 60 kG to 10 kG. To check the problem of particle transport a plasma is injected at 60 kG, the magnetic field is ramped down to $B_f$ (e.g. 20 kG) then the magnetic field is immediately ramped back to 60 kG at the same rate at which it was ramped down. Once the field is back at 60 kG the plasma is dumped and the signals on the end collectors are compared to those where the plasma is injected at 60 kG and then immediately dumped. It is found that the signals on the end collectors are the same, to the accuracy of the plasma's reproducibility, until $B_f$ is about 6 kG. At 6 kG there is a 6% difference in the signal measured on $R_1$; that is, $n(r, z)$ has changed slightly.

Once $N_1(r)$ is known the density $n(r, z)$ can be determined by assuming local thermal equilibrium along a magnetic field line (i.e. along $z$), and using a computer to solve Poisson's equation,

$$\nabla^2\phi(r, z) = 4\pi e\, n(r, z), \tag{3.16}$$

with the appropriate boundary conditions. Local thermal equilibrium along $z$ allows one to write

$$n(r, z) = C(r) \exp(e\phi(r, z)/[k_B T_{||}(r)]), \tag{3.17}$$

where $C(r)$ is determined from Eq. 3.15.

Since we do not know the radial dependence of $T_{||}(r)$, we assume that $T_{||}(r)$ is uniform through out the plasma. At low temperatures this assumption makes little

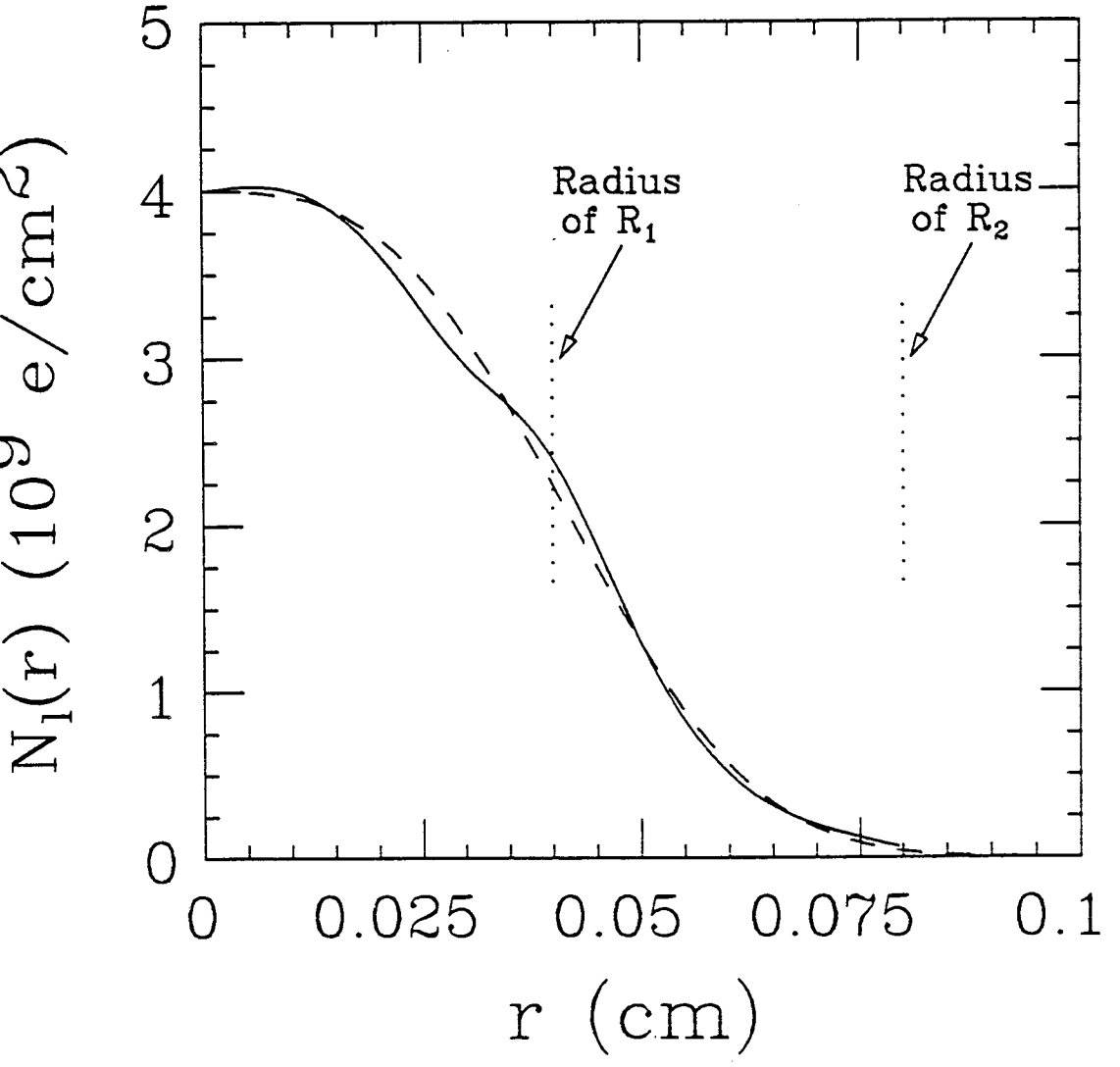


**Figure 3.5:** $N_1(r)$ versus $r$. The solid line is the experimental result and the dashed line is $N_1(r) = 4 \times 10^9 \exp(-(r/0.048\,\mathrm{cm})^3)\,\mathrm{e/cm^2}$, which is used to obtain $n(r,z)$ in Figs. 3.6 and 3.7. The radii of $R_1$ and $R_2$ are marked by the vertical dotted lines.

error (few %) since $n(r,z)$ is essentially uniform along $z$ except near the axial ends of the plasma (i.e. the plasma is a good conductor along $z$ and makes the electric field essential zero along $z$ except near the axial ends). By low temperature one means a temperature such that $\lambda_D(r) \ll l_p(r)$. Here $\lambda_D(r)$ is calculated using $T_{||}(r)$ and an average over $z$ of $n(r,z)$, and $l_p(r)$ is an average length of the plasma at a radius $r$. At the axial ends the density falls off essentially on a scale length of $\lambda_D(r)$ (this statement may not be valid near the maximum radial boundary of the plasma (i.e. $r \approx 2r_1$ for a CV plasma); however, for the plasmas in this thesis there is a fractionally small number of electrons at radii $r \gtrsim 2r_1$). When $\lambda_D(r) \sim l_p(r)$ the predicted density profile may have errors greater than 10% if $T_{||}(r)$ is not uniform through out the plasma.

Figures 3.6 and 3.7 show plots [49, 50] of $n(r,z)$ versus $z$ for various radii. To calculate $n(r,z)$ we used $N_1(r) = 4 \times 10^9 \exp(-(r/0.048\,\mathrm{cm})^3)\ \mathrm{e/cm^2}$, which closely matches the experimentally determined $N_1(r)$ in Fig. 3.5. In Fig. 3.6 $T_{||} = 10^4\,\mathrm{K}$ and in Fig. 3.7 $T_{||} = 10^3\,\mathrm{K}$.

Figures 3.6 and 3.7 illustrate possible density profiles for a CV plasma. However, we should warn the reader that $N_1(r)$ in Fig. 3.5 may not represent the actual $N_1(r)$ for each of the relaxation rate data sets. This method of determining $N_1(r)$ was not implemented until after the relaxation rate data was taken. Although, the experimental setup was essentially the same and the signals on $R_1$, $R_2$ and $R_3$ (in all cases only about 1% of the electrons hit $R_3$) were also very similar. Also, we have worked out many of the analyses with different density profiles and find essentially the same conclusions.

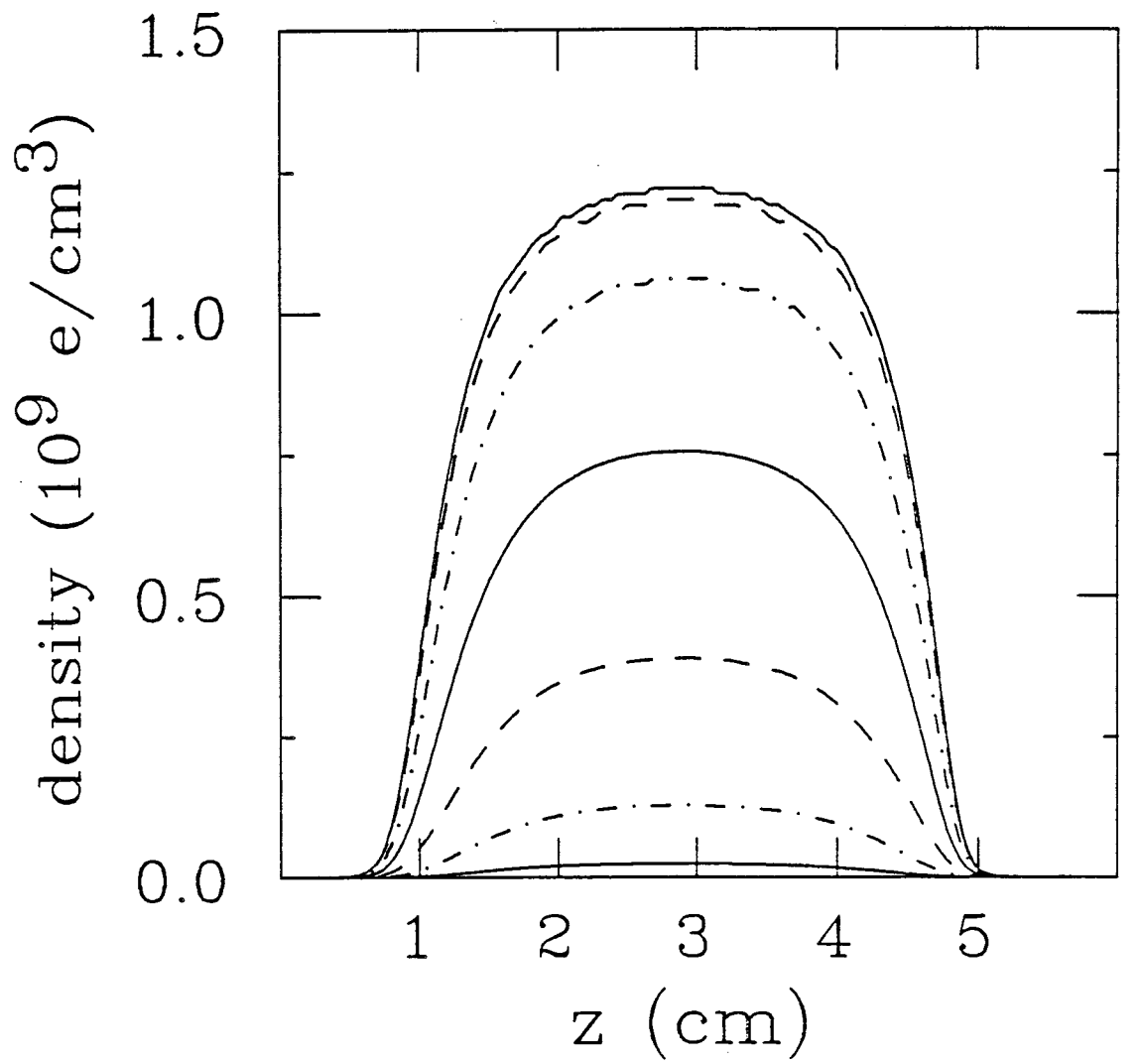


**Figure 3.6:** $n(r, z)$ versus $z$ for various radii with $T = 10^4$ K. The highest curve is for $r = 0$ and each succeedingly lesser curve is an additional 1/80 cm out in radius.

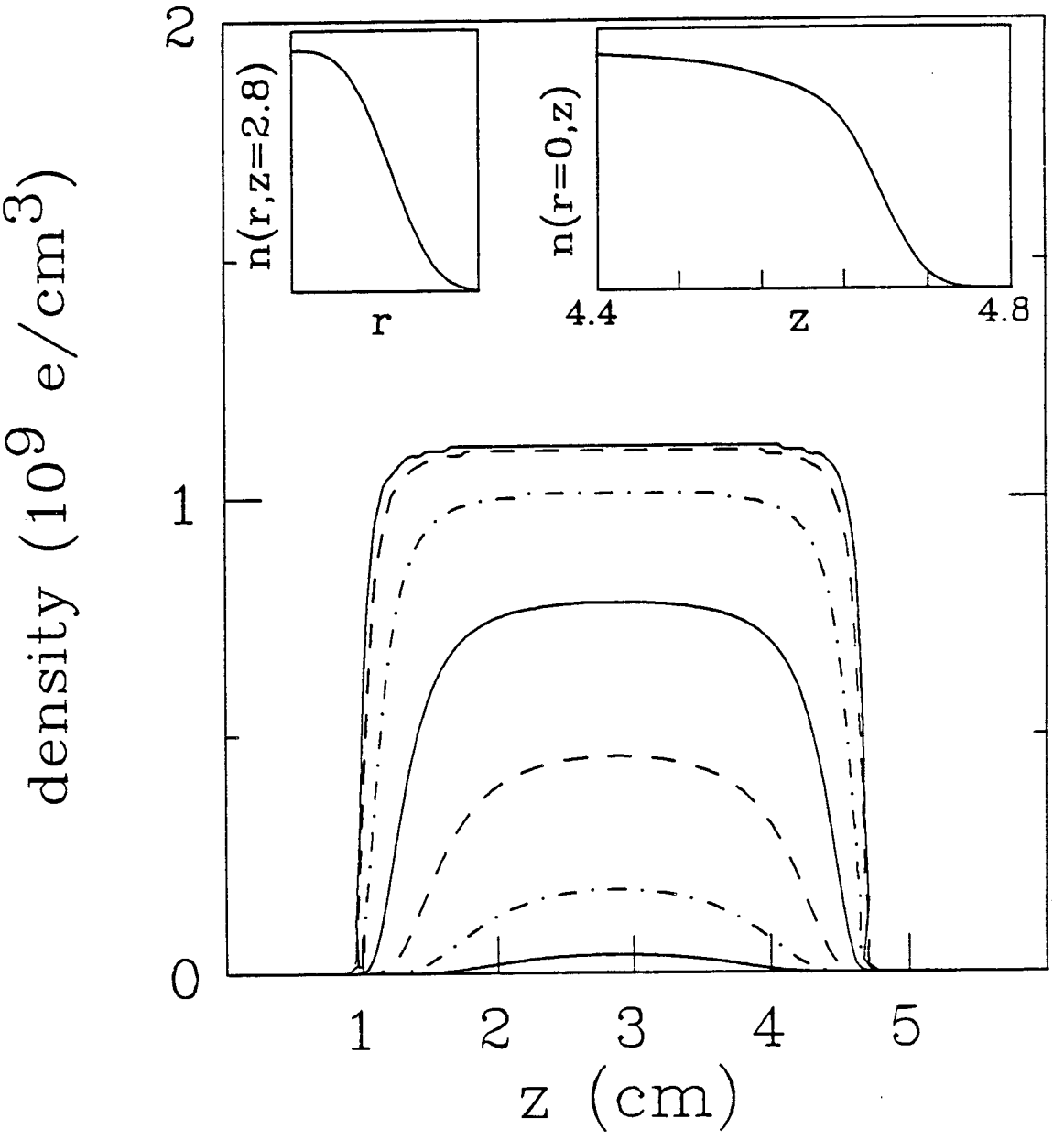


**Figure 3.7:** $n(r, z)$ versus $z$ for various radii with $T = 10^3$ K. The highest curve is for $r = 0$ and each succeedingly lesser curve is an additional 1/80 cm out in radius.

### 3.7.1 Plasma Length

We define the plasma length at a radius $r$ as

$$l_{\rm p}(r) = \frac{1}{n_{\rm m}(r)} \int n(r,z)\, dz \tag{3.18}$$

where $n_{\rm m}(r)$ is the maximum density at the radius $r$. Using this definitions as the plasma length for the data in Figs. 3.5 and 3.6, we find that the plasma length varies by about a factor of two, and for $r < r_1$ this variation is about 20%. However, a more important issue relating to the relaxation measurement has to do with the fractional length change of the plasma when the voltage on one of the confinement gates is changed slightly. More precisely, if the length change due to changing a gate potential is $\delta l(r)$, how does $\epsilon(r) \equiv \delta l(r)/l(r)$ vary with radius? Numerically one finds that, although $l(r)$ may vary by about a factor of two over the plasma radius, the variation in $\epsilon(r)$ is much less. This will be important to consider when the compressional heating model is presented in section 5.2. The amount of heating depends on $\epsilon^2(r)$, which implies that certain radial regions of the plasma may be heated more than other radial regions.

We can interpret $l_{\rm p}(r)$ as the average axial bounce length for the electrons at radius $r$. Of course, about 1/2 the electrons will have a bounce length that is longer than $l_{\rm p}(r)$ and the rest will have a bounce length that is shorter than $l_{\rm p}(r)$, with the actual bounce length depending on an electron's velocity.

As an electron moves axially is feels a potential near the ends of the plasma which slow the electron down and reflect it. However, there is a region in the center of the plasma where an electron's velocity is essentially independent of axial position. In this region the potential is essentially constant along an axial line (i.e. the axial electric field is essentially zero). From Eq. 3.17 we see that in the region where the potential is independent of $z$, the density will be uniform along $z$. The region near the end of the plasma where the potential is varying is called the end sheath. The

size of the end sheaths depend on the plasma temperature. This can be seen in Figs. 3.6 and 3.7 by observing the decease in plasma density as one moves axially away from the center of the plasma. In Fig. 3.6 the density gradually decreases as one moves axially from the plasma center, and in Fig. 3.7 the density is essential uniform along $z$ and then falls off rapidly at the ends.

We can write an electron's bounce length as $l_b(r, v_0)$ to explicitly show that it is a function of radius and velocity. Here $v_0$ is the electron's axial velocity at the axial center of the plasma (or, if the plasma is not symmetrical, the maximum axial velocity of the electron). (We will ignore the dependence of $l_b$ on radius since we discussed it in the beginning of this section). When we heat the plasma to measure the relaxation rate, we modulate the potential on one of the confining gates, and this varies $l_b(r, v_0)$ to $l'_b(r, v_0)$ (it also varies $v_0$). However, we are more interested in the quantity $\epsilon(r, v_0) = (l'_b(r, v_0) - l_b(r, v_0))/l_b(r, v_0)$, which is also a function of the electron's velocity. In the heating model (see section 5.2) we assume that $\epsilon(r, v_0)$ is independent of radius and $v_0$ (see Eq. 5.3). We have checked this assumption and find that $\epsilon(r, v_0)$ is essentially independent of $v_0$ for temperature $T_{||} \ll 10^4\,\mathrm{K}$. For $T_{||} \gtrsim 10^4\,\mathrm{K}$ this effect may cause some error in the measured relaxation rates.

# Chapter 4

# Plasma Temperature and Temperature Measurement

## 4.1 Introduction

The plasma temperature measurement is without a doubt the most useful measurement presently on CV. With it we have been able to measure temperatures from about 30 K to about 2,000,000 K. It is the main measurement for determining the relaxation rate, as single relaxation rate measurement can require 400 or more temperature measurements. In this chapter we will describe how we are able to vary and measure the plasma temperature.

To measure the plasma temperature we slowly ramp the potential on $G_8$, $V_d$, to ground[1] (see Fig. 3.1) and count the number of electrons, $N_e$, that escape past $G_8$ as a function of the potential on $G_8$. From conservation of energy we know that any electron with velocity $v_{||}$ such that

$$\frac{mv_{||}^2}{2} - e\phi > -eV_b \tag{4.1}$$

will escape past $G_8$. Here, $-eV_b$ is the minimum energy needed by an electron to escape past the $G_8$ gate. Since $G_8$ is of finite length, $-eV_b$ is less than $-eV_d$. Note

[1]Here we assume that $G_8$ is the gate which confines the plasma from escaping towards the end collector. In general, this could be almost any gate. The gate which confine the electrons from escaping toward the end collector is called the dump gate, hence the symbol $V_d$.

that $\phi$ is a function of axial position, hence $v_{||}$ is also a function of axial position. However, the left-hand side of Eq. 4.1 can be evaluated at any axial position, and it is simplest to evaluate it at the axial center of the plasma. (The space charge potential is the major contributor to $\phi$ ($> 95\%$) at the axial center of a typical CV plasma when $l_p \gtrsim 3.5\,\mathrm{cm}$.)

Assume for the moment that $\phi$ does not change as the potential on $G_8$ is raised to ground. In this case, measuring $N_e$ as a function of $V_b$ will give information about the parallel velocity distribution, $f(v_{||})$. Assuming a Maxwellian for $f(v_{||})$ we fit the measured $N_e$ versus $V_b$ to a model to determine the plasma temperature.

This simple explanation of how we measure the plasma temperature works quite well at temperatures above about 1000 K, as long as we allow only about 1% of the electrons to escape and the plasma length is greater than about 3 wall radii. For a Maxwellian this means that we use only the energetic tail (i.e. $v_{||} > 2v_T$, where $v_T$ is the thermal velocity) to measure the temperature. At low temperatures it becomes important to include changes in the space charge potential due to the electrons that have escaped.

For temperatures above about 200 K, we believe that the temperature measurement is accurate to approximately 10%. There are several tests that verify this claim. Section 4.3.2 describes a method for heating the plasma to a temperature that can be estimated, and we find reasonable agreement between this estimate and the measured temperature. We also know that the plasma cools via cyclotron radiation (see section 4.2). Comparing the plasma temperature versus time to that calculated from radiation theory we find good agreement (see Fig. 4.1). Another test of the $T_{||}$ measurement was done by Hyatt [25] on a different pure electron trap (see column OTHER in Table 3.1), where $T_\perp$ can be measured to about 5% accuracy. For plasmas that should be in thermal equilibrium Hyatt measured both $T_{||}$ and $T_\perp$ and

finds agreement to about 10%.

For a plasma temperature of 50 K we believe that the measurement is accurate to approximately 30%, and at 20 K the temperature measurement is, at its present state, probably not believable. There are many possible explanations for why the present measurement is limited to about 30 K. For a while the lowest temperature we could measure was proportional to the number of electrons that we could measure. This, in turn, is proportional to the noise on the front stage amplifier used to measure the electrons. Great effort was made to build a quiet amplifier, and each time we had reduced the amplifier noise we were able to measure lower temperatures. Presently, microphonic noise limits the minimum number of electrons which we can to measure, and this may still be a problem at the lowest temperature. Second, 30 K is equivalent to about 3 mV, whereas the plasma has about 20 volts of space charge potential. This means that to measure a temperature of 30 K we must include the changes in the space charge potential due to the escaped electrons and from rearrangement of the plasma caused by raising the potential on $G_8$ (see section 4.4) to better than 1 part in $10^4$ of the original space charge potential. We must also know the potential change on $G_8$ to better than 1 part in $10^4$.

During the temperature measurement phase we assume that no electrons are transported radially. As long as the density profile is a monotonically decreasing function of radius we believe that this is a valid assumption. However, work done on other pure electron traps at the University of California, San Diego [11, 12] indicates that rapid radial transport can occur when the density profile is no longer a monotonically decreasing function of radius.

At low temperatures the temperature measurement may create a density profile which is a non-monotonically decreasing function of radius. This can occur since the first electrons to escape come from on or near the radial axis (i.e. $r \approx 0$),

where the space charge potential is the most negative.

To measure the temperature we have constructed a model to predict the number of electrons that will escape past $G_8$ as the potential on $G_8$ is slowly raised to ground. In the model assume we that there are no collisions which can increase an electron's velocity to the point that it would be able to escape. This assumption may break down at low temperatures since the three particle collision rate, $\nu_3$, may become large (see Appendix A.6). For example, at 20 K, $\nu_3$ may be as high as $10^6$ Hz, and it takes about 50 $\mu$sec to measure $T_{\|}$. Finally, misalignment of the plasma and all the gates may be enough to give a poor temperature reading. The difference in plasma potential from the plasma center to two Debye lengths out in radius is equivalent to the plasma temperature. At best the experimental apparatus is machined to about one mil (i.e. $2.54 \times 10^{-3}$ cm), which corresponds to one Debye length for a temperature of 100 K and a density of $10^9$ e/cm$^3$. Of course there may be other reasons which limit the present temperature measurement to about 30 K.

There is also a limit on how high a temperature one can measure using the method described in this chapter. This failure reflects the fact that the temperature measurement assumes that the parallel velocity distribution is a Maxwellian, and measures the tail of the Maxwellian to get $T_{\|}$. It will be shown in the next section that the plasma is cooling via cyclotron radiation. In order for the parallel velocity distribution to stay a Maxwellian, the cyclotron cooling rate must be much less than the relaxation rate. This sets an upper limit for a meaningful temperature of

$$T \approx 2 \times 10^6 \, n^{2/3}/B^{4/3} \text{ K}. \tag{4.2}$$

We have measured value of the plasma temperature to about 30 K but have reason to believe that it is actually cooling to about 6 K at times. This value is obtained by estimating the heating power from radial expansion, Joule heating (see section 4.3.1), and balancing this with the radiation power (see section 4.2).

This chapter is arranged as follows. In section 4.2 cyclotron cooling is calculated and compared to the observed cooling. In section 4.3 different methods for heating the plasma are presented. A simple, low power heating process is presented in section 4.3.3. We assume that this heating process keeps the velocity distribution essentially Maxwellian, and is essential for measuring the relaxation rate.

In section 4.4.1 the temperature measurement models are presented. First the assumptions built into the the models are given and their relevance to a CV plasma are analyzed. Next the high and low temperature models are described along with how we apply these models to measure the temperature. In section 4.4.6 the errors in the measured temperature due to $dT/dr \neq 0$ are analyzed. Finally, in section 4.5 an upper bound to the radial energy transport time is estimated.

## 4.2 Cyclotron Radiation and Plasma Temperature

When a plasma is initially created in CV it typically has a temperature of about $10,000\,\mathrm{K}$. Within seconds the plasma cools to near $30\,\mathrm{K}$ via cyclotron radiation, provided there is no heating of the plasma. In this section the cyclotron cooling rate is calculated. It will be shown that cyclotron cooling causes the plasma temperature to decrease in time as

$$T(t) = T(0)\exp(-t/\tau_{\mathrm{r}}) \tag{4.3}$$

where $\tau_{\mathrm{r}} \simeq 4 \times 10^8 / B^2$ sec. To derive Eq. 4.3 one assumes that the plasma is not being heated, that the relaxation rate is much greater than $\tau_{\mathrm{r}}^{-1}$, and $k_{\mathrm{B}}T \gg \hbar\Omega$ (i.e. quantum effects are ignored).

Consider a single electron in free space (no background radiation) with a magnetic field $\mathbf{B} = B\hat{z}$. The motion of the electron is simple, $v_{||} \equiv v_{\mathrm{z}} = \text{const}$, $v_{\mathrm{x}} = v_{\perp}\sin(\Omega t)$ and $v_{\mathrm{y}} = v_{\perp}\cos(\Omega t)$ where $\Omega = eB/mc$ is the cyclotron frequency.

This motion has an acceleration $a_\perp = v_\perp \Omega$ and it is well known that an accelerating charge radiates. The power radiated by circular motion is given by the Larmor formula as

$$\frac{dE_\perp}{dt} = \frac{2e^2}{3c^3} a_\perp^2 = \frac{4e^2\Omega^2}{3mc^3} E_\perp, \tag{4.4}$$

where $E_\perp = mv_\perp^2/2$.

For a pure electron plasma with a Maxwellian distribution in $v_\perp$, Eq. 4.4 becomes (see Appendix A.2)

$$\frac{1}{k_B}\left\langle \frac{dE_\perp}{dt} \right\rangle = \frac{dT_\perp}{dt} = -\frac{4e^2\Omega^2}{3mc^3} T_\perp. \tag{4.5}$$

Here the brackets mean a average over the distribution function.

### 4.2.1 Plasma Cooling Rate

The cyclotron radiation rate can be determined for many plasmas in CV. However, we do not directly measure $T_\perp$ to obtain the radiation rate. Instead, we rely on the fact that the relaxation rate is much larger than $(\tau')^{-1}$ so that $T_\parallel \simeq T_\perp$, and we measure $T_\parallel$.

When the total kinetic energy of the plasma is conserved, the time evolution of $T_\parallel$ and $T_\perp$ can be written as

$$\frac{dT_\parallel}{dt} = -2\nu(T_\parallel - T_\perp) \tag{4.6}$$

$$\frac{dT_\perp}{dt} = \nu(T_\parallel - T_\perp) \tag{4.7}$$

Here, one assumes that $T_\parallel \simeq T_\perp$ (as is the case for most plasmas confined in CV) and that the distribution of parallel and perpendicular velocity components are described by a Maxwellian. (See reference [7] for an expression which gives $dT_\perp/dt$ and $dT_\parallel/dt$ when $T_\parallel \not\simeq T_\perp$.)

It is straightforward to show that together Eq. 4.6 and Eq. 4.7 conserve the total kinetic energy of the plasma. This is achieved by adding Eq. 4.6 to twice Eq. 4.7

(there is one degree of freedom in the parallel coordinate and two degrees of freedom in the perpendicular coordinate), from which one obtains $d(T_{||} + 2T_{\perp})/dt = 0$.

It is also instructive to subtract Eq. 4.7 from Eq. 4.6, which yields

$$\frac{d(T_{||} - T_{\perp})}{dt} = -3\nu(T_{||} - T_{\perp}). \tag{4.8}$$

Thus, $T_{||} - T_{\perp}$ relaxes to zero at an e-folding rate of $3\nu$. In section 5.2 a plasma heating model will be presented. In the model we assume that the plasma length is modulated sinusoidally at a frequency $f$. One conclusion we draw from the model is that maximum heating per cycle occurs when $2\pi f = \omega = 3\nu$. The factor of 3 in the equation $\omega = 3\nu$ is a result of the 3 appearing in Eq. 4.8, and is due to the definition of $\nu$ used in Eq. 4.7 (or Eq. 4.6).

When the total plasma kinetic energy is not conserved, the time evolution of $T_{||}$ and $T_{\perp}$ are no longer given by Eq. 4.6 and Eq. 4.7 respectively. However, as long as the distribution of parallel and perpendicular velocity components are described by a Maxwellian and $T_{||} \simeq T_{\perp}$, one can write the time evolution of $T_{||}$ and $T_{\perp}$ as

$$\frac{1}{2}\frac{dT_{||}}{dt} = -\nu(T_{||} - T_{\perp}) + \frac{1}{k_B}\left\langle \frac{dE_{||}}{dt} \right\rangle \tag{4.9}$$

and

$$\frac{dT_{\perp}}{dt} = \nu(T_{||} - T_{\perp}) + \frac{1}{k_B}\left\langle \frac{dE_{\perp}}{dt} \right\rangle. \tag{4.10}$$

Here $dE_{||}/dt$ ($dE_{\perp}/dt$) is the rate of change of parallel (perpendicular) energy for an electron with parallel (perpendicular) energy $E_{||}$ ($E_{\perp}$), excluding collisional rearrangement of the plasma energy. The brackets imply an average over the distribution function. In other words, the rate of change of the kinetic energy per electron is given by

$$\frac{k_B}{2}\frac{d(T_{||} + 2T_{\perp})}{dt} = \left\langle \frac{dE_{||}}{dt} \right\rangle + \left\langle \frac{dE_{\perp}}{dt} \right\rangle. \tag{4.11}$$

When $T_{||} \simeq T_{\perp}$, it is suitable to consider a single plasma temperature, $T$,

given by $3T = T_{||} + 2T_{\perp}$, and where

$$T_{\perp} \simeq T_{||} \simeq T \tag{4.12}$$

and

$$\frac{dT_{\perp}}{dt} \simeq \frac{dT_{||}}{dt} \simeq \frac{dT}{dt}. \tag{4.13}$$

Futhermore, when $\langle dE_{||}/dt \rangle = 0$ and $\langle dE_{\perp}/dt \rangle$ is solely a result of cyclotron radiation (i.e. Eq. 4.5), then (from Eq. 4.11) one obtains

$$\frac{dT}{dt} = -\frac{T}{\tau_{\mathrm{r}}}, \tag{4.14}$$

which yields Eq. 4.3. Here,

$$\frac{2}{3}\tau_{\mathrm{r}} = \frac{3mc^3}{4e^2\Omega^2} = \frac{3m^3c^5}{4e^4B^2} \tag{4.15}$$

where the term on the right hand side of Eq. 4.15 is the radiation rate for $T_{\perp}$ when $T_{\perp}$ and $T_{||}$ are decoupled. When $T_{\perp}$ and $T_{||}$ are decoupled, cyclotron radiation dissipates energy from the 2 perpendicular degrees of freedom. However, when $T_{\perp}$ and $T_{||}$ are coupled, (i.e. $\tau_{\mathrm{r}} \gg \nu^{-1}$), cyclotron radiation must dissipate the energy from the 3-degrees of freedom, hence the factor of 2/3 in the left hand side of Eq. 4.15.

### 4.2.2 Corrections to Calculated Cyclotron Radiation Rate for Low Temperatures

Obviously, Eq. 4.3 cannot be correct for large times (i.e. $t/\tau_{\mathrm{r}} \gg 1$) since it would predict a plasma temperature that is lower than the apparatus temperature, $T_{\mathrm{w}} = 4.2\,\mathrm{K}$. In fact, one expects the plasma temperature to come into thermal equilibrium with the apparatus wall when the plasma is not heated. (This is one of the reasons why the apparatus is submersed in liquid helium.) There are several other reasons why Eq. 4.3 fails when the plasma temperature is about 50 K or less.

At low temperature one must also include quantum effects (i.e. quantized cyclotron orbits, also called Landau levels: see page 456 in reference [32]). The energy difference between adjacent Landau levels is

$$\hbar\Omega/k_{\rm B} = 8.04\, B/(60\,{\rm kG})\,{\rm K}. \tag{4.16}$$

At low temperatures (i.e. $k_{\rm B}T \sim \hbar\Omega$) a good fraction of the electrons are in the lowest Landau level, and are no longer able to radiate. This reduces the total power radiated. Calculating $\langle dE_\perp/dt\rangle$ including finite apparatus temperature and the quantized cyclotron orbits, one finds that (see Appendix A.1)

$$\frac{dT}{dt} = -\frac{T}{\tau_{\rm r}} R\Big(\frac{\hbar\Omega}{T}, \frac{\hbar\Omega}{T_{\rm w}}\Big) \tag{4.17}$$

where

$$R(x,y) = x\,\frac{\exp(y)-\exp(x)}{(\exp(y)-1)(\exp(x)-1)}. \tag{4.18}$$

Finally, there are heating terms in Eq. 4.9 and Eq. 4.10 which have been ignored. One source of plasma heating is due to the radial expansion of the plasma. This effect will be discussed in section 4.3. A second source of heating is due to potential fluctuations, noise, on the confining gates. Heating due to noise on the confining gates has been observed in CV. However, it is believed that this latter heating process is ignorable when the potentials on the confining gates are properly filtered. There may also be other sources of plasma heating which we have not considered.

### 4.2.3 Experimentally Measured Plasma Temperature

Figure 4.1 shows a comparison of a measured plasma temperature (square points) and that predicted by Eq. 4.17 (dashed curve) as a function of time for $B =$ 61.3 kG. For almost three decades in temperature the plasma cools exponentially as predicted by Eq. 4.17; however, the radiation time, $\tau_{\rm r} = 0.147$ sec, is about 30%

larger than the calculated radiation time. At about 50 K the measured temperature deviates from an exponential decay, but still continues to cool to about 20 K. At present we are not sure if the decrease in the cooling rate for temperatures less than about 50 K is a real effect and if so what is causing it, or if the $T_{||}$ measurement is failing.

Figure 4.2 is a plot of the measured radiation time, $\tau_r$, versus magnetic field. The solid line is a plot of $\tau_r$ as given by Eq. 4.15. Note that for large magnetic fields the experimentally measured radiation time is close to the predicted radiation time. However, at low fields there is about a factor of 2.5 difference between theory and experiment.

To calculate $\tau_r$ we have ignored the fact that the electrons are confined in a conducting vessel. Such a vessel may act as a waveguide or, possibly, a resonant cavity (note the vessel in this case is most likely the cylindrical gates $G_3$ to $G_8$ and the end collectors). Although at the large magnetic fields the fact that the plasma is contained in a conducting vessel seems to have little effect on the radiation time. It is not *a priori* obvious that the radiation time and the calculated time should agree so well since the wave guide cutoff frequency is equal to the cyclotron frequency of an electron in a magnetic field of 3.2 kG.

We have also assumed, indirectly by calculating $\tau_r$ for a single electron, that an electron does not reabsorb photons emitted by the other electrons (although, the calculation in Appendix A.1 does include absorption by photons produced by a black body radiator). We have estimated the opacity of the plasma, and concluded that it probably does not significantly alter the calculated radiation time.

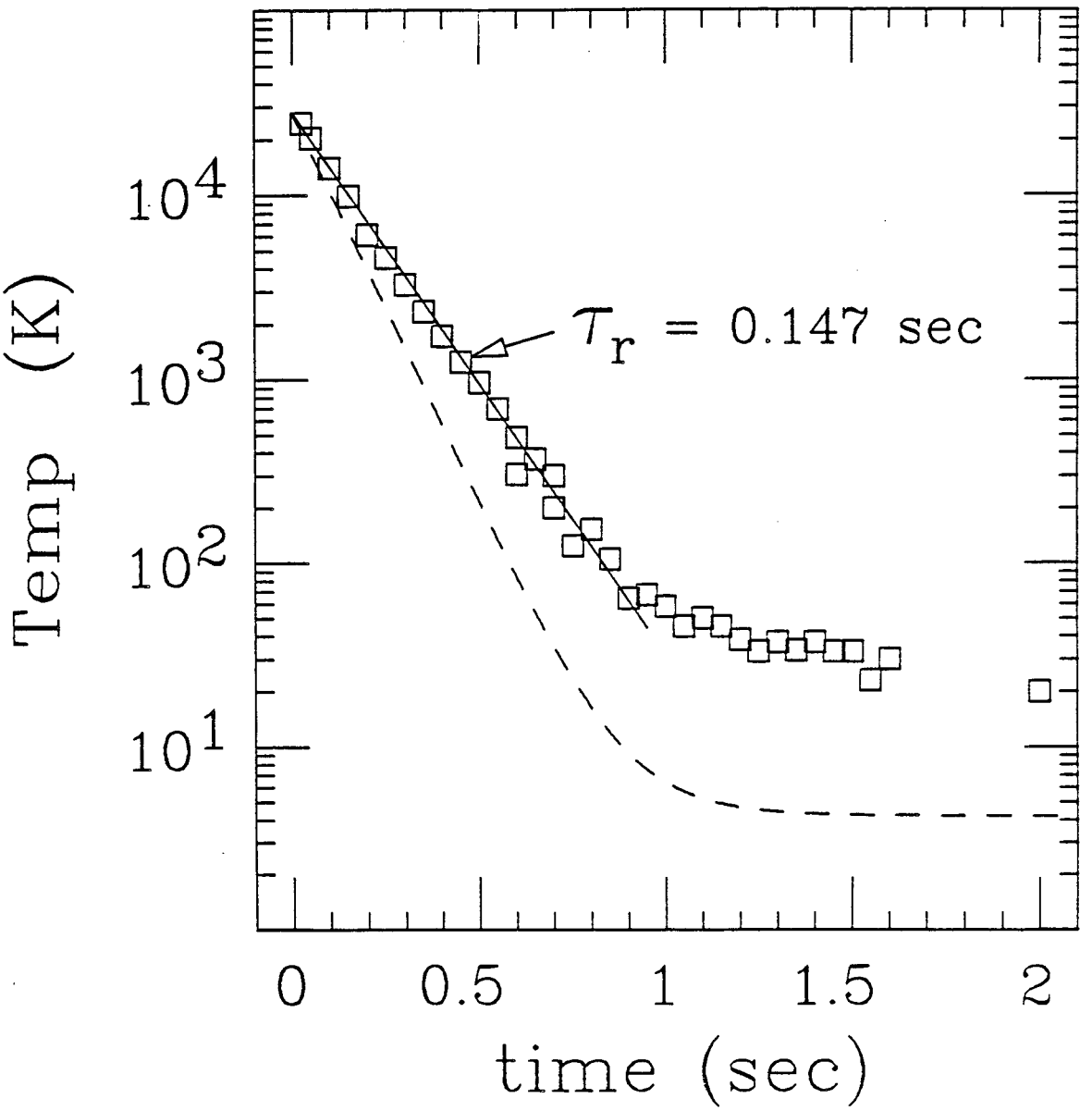


**Figure 4.1:** Temperature versus time for $B = 61.3$ kG. The dashed curve is a plot of the temperature calculated using Eq. 4.17. The measured radiation time $\tau_r$ is about 30% higher than the predicted time.

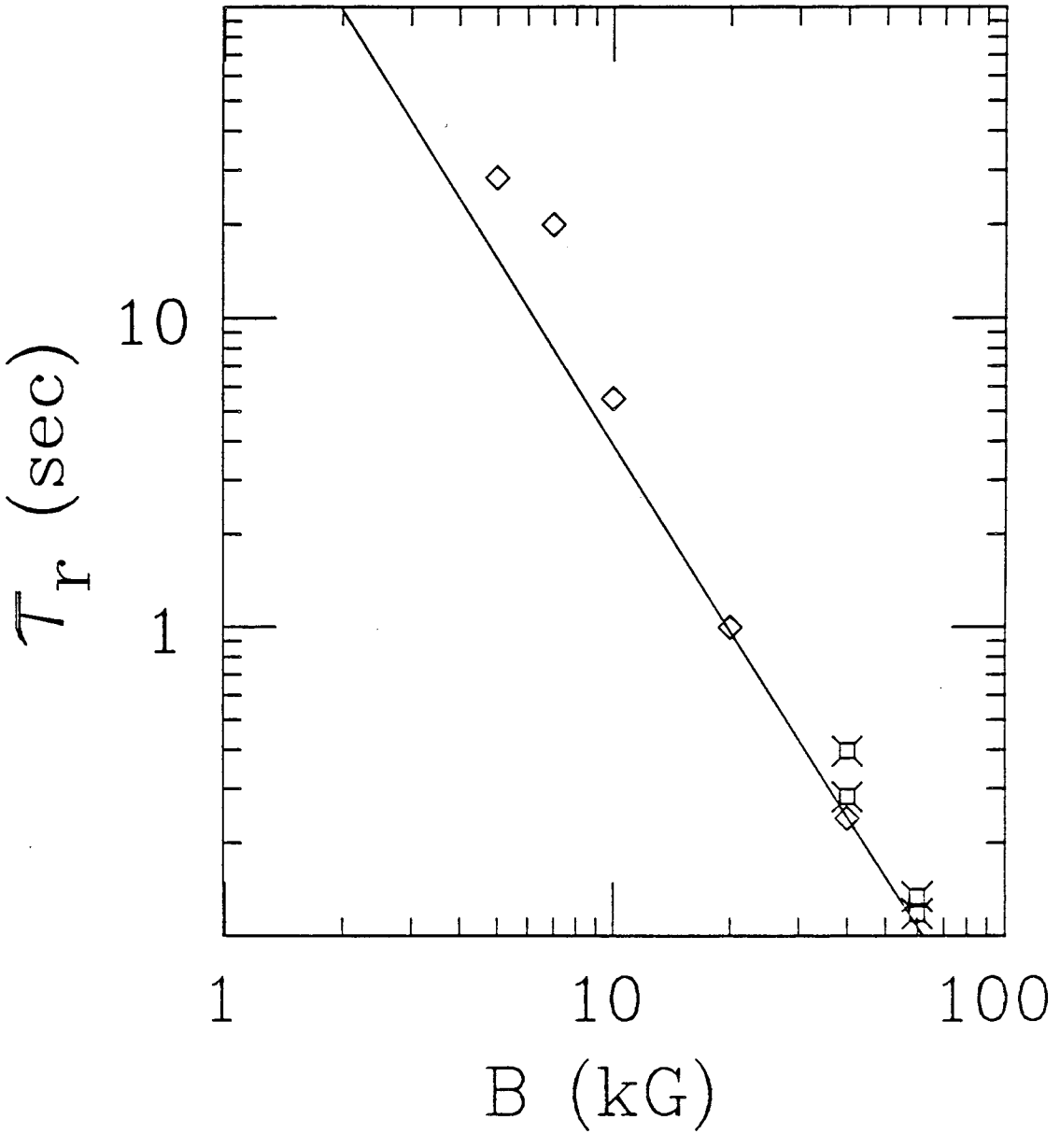


**Figure 4.2:** $\tau_r$ versus magnetic field. The solid line is a plot of Eq. 4.15. The diamond points are from several years ago when the filament and the gates were all situated in the constant field region of the magnetic.

## 4.3 Plasma Heating

In order to measure the relaxation rate with reasonable accuracy, we need a method for heating the plasma that leaves the distribution of parallel and perpendicular velocity components essentially Maxwellian with $T_{\|} \simeq T_{\perp}$. We also occasionally want a plasma that is hot ($T \gg 10,000\,\mathrm{K}$). There are several ways to heat the plasma. One method heats the plasma a lot but makes the parallel velocity distribution non-Maxwellian. The other method can be used to heat the plasma a little while, we believe, keeping the distribution of parallel and perpendicular velocity components essentially Maxwellian with $T_{\|} \simeq T_{\perp}$. The plasma can also be heated by the electrostatic energy released as the plasma expands radially (Joule heating). Joule heating is undesirable, and we must therefore insure that this effect is small.

### 4.3.1 Joule Heating

To estimate the maximum heating possible from radial expansion (Joule heating) we assume that the plasma is infinitely long, constant in density $n$ out to a radius $r_{\mathrm{p}}$, and inside a grounded, perfectly conducting cylinder of radius $R_{\mathrm{w}}$. If the plasma expands radially then the total potential energy per unit length, $PE$, decreases, and we assume that this energy goes into heating the plasma. We also assume that the radial energy transport time scale (see section 4.5) is much shorter than $\tau_{\mathrm{r}}$ and $n(dn/dt)^{-1}$. The potential energy per unit length is

$$PE = e^2 N_{\mathrm{p}}^2 \left( \log\left(\frac{R_{\mathrm{w}}}{r_{\mathrm{p}}}\right) + \frac{1}{4} \right) \tag{4.19}$$

where $N_{\mathrm{p}}$ is the number of electrons per unit length. Differentiating $PE$ with respect to time yields[2]

$$\frac{d(PE)}{dt} = \frac{e^2 N_{\mathrm{p}}^2}{2} \left(\frac{1}{n}\frac{dn}{dt}\right) \tag{4.20}$$

[2]In general, if $n(r,t) = n(r/x(t))/x^2(t)$ where $x(0) = 1$, then $d(PE)/dt = -e^2 N_{\mathrm{p}}^2 (dx/dt)/x$ (see Appendix A.7). This is a more general form for a change in density and gives the same result for $d(PE)/dt$ as Eq. 4.20 if one evaluate $n^{-1}\, dn/dt$ at the origin.

where $nr_p^2 = N_p$ and $dN_p/dt = 0$. Dividing this by $N_p$ to get the energy per electron and subtracting from the right side of Eq. 4.17 one obtains

$$\frac{dT}{dt} = -\frac{TR}{\tau_r} - 8.4 \times 10^{-4} N_p \left(\frac{1}{n}\frac{dn}{dt}\right). \tag{4.21}$$

Here we have converted $d(PE)/dt$ from erg/sec to K/sec and $R$ is defined by Eq. 4.18. Setting $dT/dt$ to zero gives an equilibrium temperature of

$$T_{eq} = -\frac{8.4 \times 10^{-4} N_p \tau_r}{R}\left(\frac{1}{n}\frac{dn}{dt}\right) K. \tag{4.22}$$

Equation 4.22 is easily checked by creating a plasma that expands sufficiently fast that $T_{eq}$ is measurable with the temperature measurement. For example, the higher the average density, for fixed plasma length and fixed plasma radius, the larger, in general, the radial expansion rate, $n^{-1}(dn/dt)$. Note that increasing the density also increases $T_{eq}$ since $N_p$ also increased. Figure 4.3 shows a plot of the actual central plasma temperature versus time for a plasma with a large expansion rate. Also plotted in Fig. 4.3 is the temperature calculated from Eq. 4.22 where $dn/dt$ is estimated from the electrons collected on $R_1$. Note that $T_{eq}$ is a function of time (this is due to the fact that the experimentally estimated expansion rate varies with time). Figure 4.3 shows that Eq. 4.22 is good to within a factor of two for a fast radially expanding plasma.

As was pointed out earlier we try to generate a plasma that we believe cools to about 6 K. This value is calculated from Eq. 4.22 and the estimated plasma expansion rate, and assumes that all other heating processes are ignorable.

### 4.3.2 Heating: Dropping Electrons into a Potential Well

The simplest way to heat a non-neutral plasma is to push it over a potential energy hill. As the electrons fall down the potential energy hill their average kinetic energy ($KE$) is increased by $-e\langle V\rangle$ where $\langle V\rangle$ is the average electrostatic potential

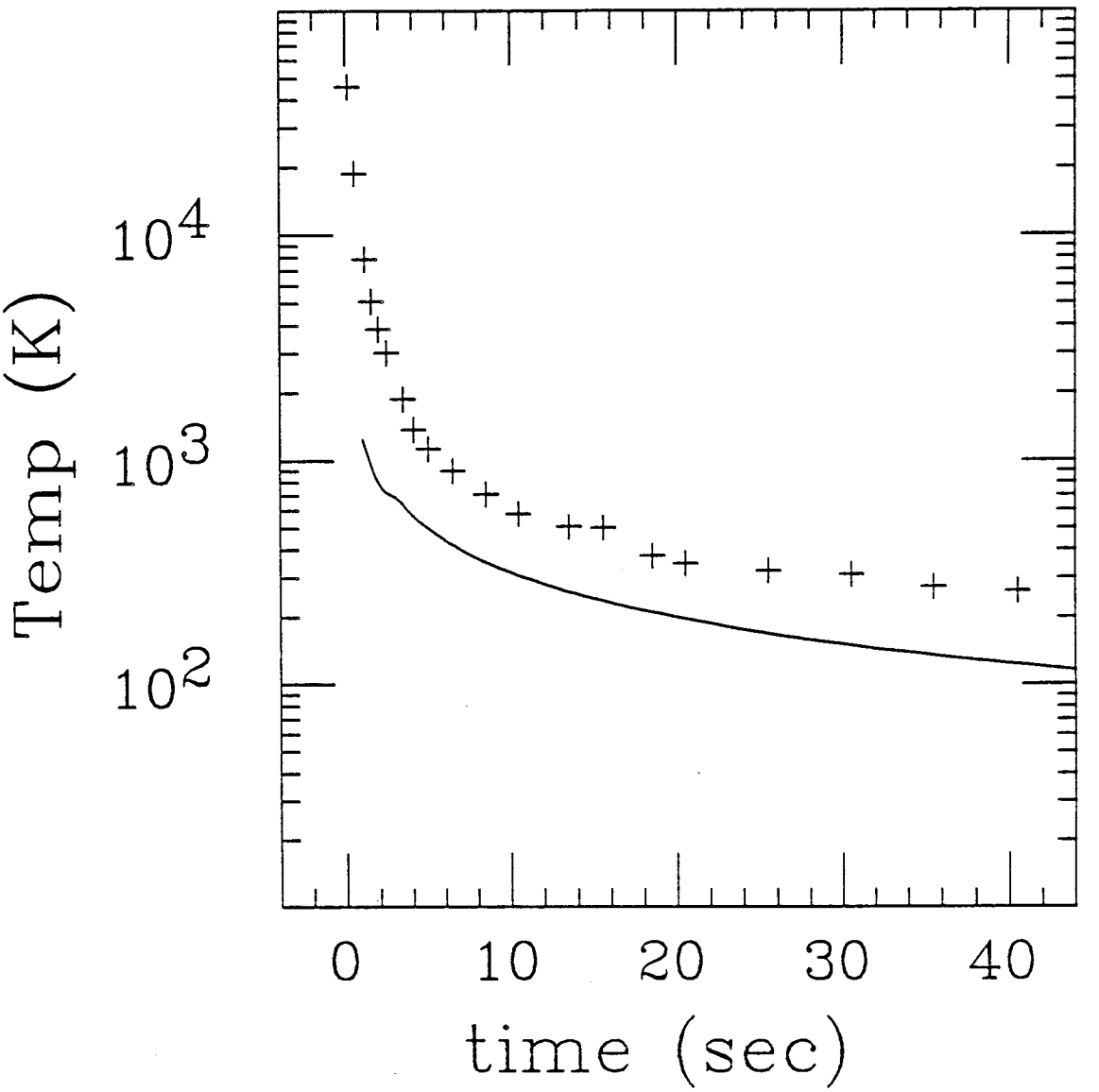


**Figure 4.3:** Temperature versus time for different expansion rates ($dn/dt$). The solid curve is a plot of Eq. 4.22 with $dn/dt$ estimated from the signal on $R_1$.

change per electron. After pushing the electrons over the hill and allowing collisions to redistribute their energy the plasma temperature is increased by $-e\langle V\rangle/3$ (the 3 comes from converting 1 degree of freedom into 3 degrees of freedom).

Although a hot plasma may be created by making $V_{\text{bias}}$, the electron source, very negative, this method is not employed since the reproducibility of a plasma is poor under these conditions. It is better to first capture a reproducible plasma and then heat it. Figure 4.4 shows how this is done (also refer to Fig. 3.3). First, a stable, reproducible plasma is captured in $G_2$. At time $t_1$ the potential on $G_2$ is lowered to $-V$, pushing the plasma past $G_3$ and trapping it into $G_4 + G_5 + G_6 + G_7$ and possibly $G_3$. Finally, at time $t_2$ the potential on $G_3$ is made more negative, trapping the electrons into $G_4 + G_5 + G_6 + G_7$. To insure entrapment of the plasma during this process $-eV_1$ and $-eV_8$ must be much greater than $-e(V_3/3 + \phi)$ where $\phi$ is the potential in the center of the plasma. A good estimate of $\langle V\rangle$ is

$$\langle V\rangle \approx V_3 - \phi/2. \tag{4.23}$$

This calculation underestimates the heating since the plasma is also compressed when $G_2$ and $G_3$ are lowered.

This method provides a fast simple procedure for heating the plasma. However, one drawback of this type of heating is that it drastically alters the distribution function and makes it non-Maxwellian. Of course, in time collisions will evolve the velocity distribution to a Maxwellian.

### 4.3.3 Heating (and Cooling): Longitudinal Invariant and $T_{\|}$

Another method of heating the plasma is to change the plasma length slowly compared to an electron's bounce time, $t_b = v_{\|}/(2l)$. If the electron sustains no collisions with other electrons, then the bounce invariant predicts that to good ap-

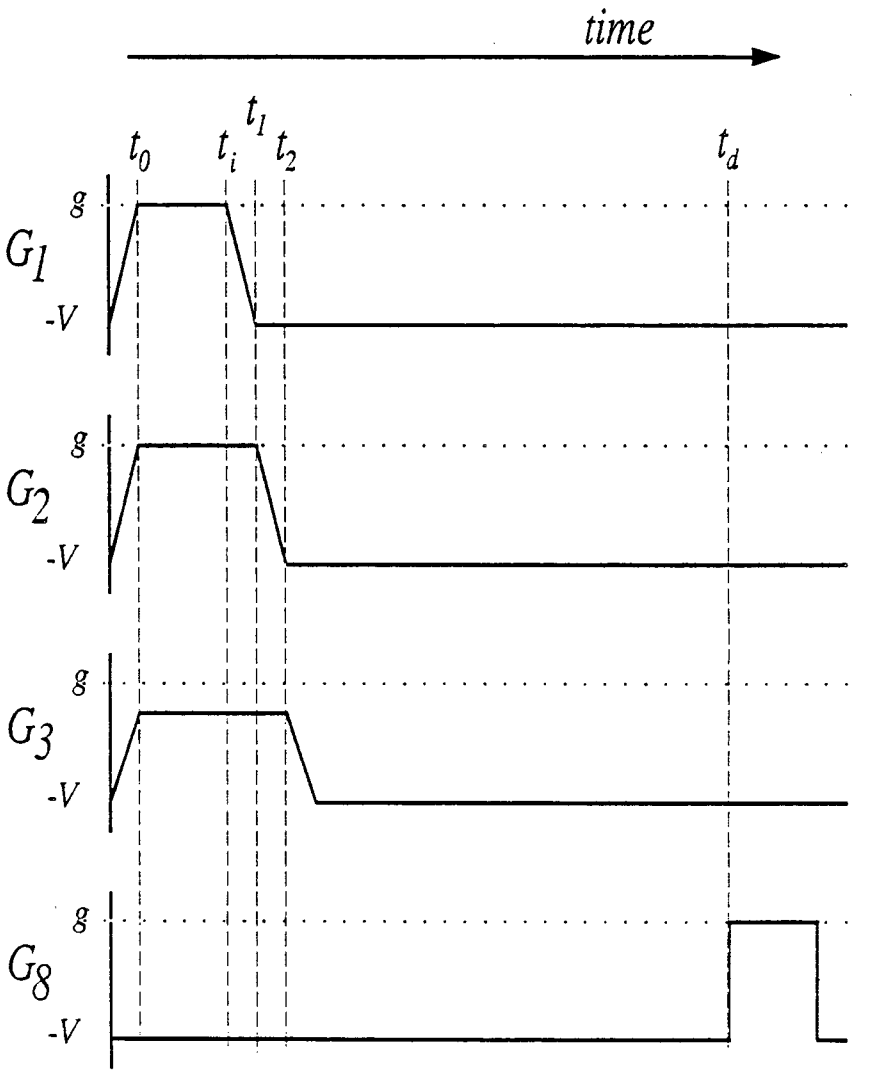


$g$ = *ground*

$$G_4 + G_5 + G_6 + G_7 = g$$

**Figure 4.4:** Timing chain to create a hot stable plasma.

proximation $v_{||}(t) = v_{||}(0)\, l(0)/l(t)$. Thus the average parallel energy of the plasma can be varied.

This method of heating the plasma has several advantages over the method described in section 4.3.2. First, it can also be used to cool the plasma; in fact, this method can either increase or decrease $v_{||}$ for each electron. Second, it keeps the distribution of parallel velocity essentially Maxwellian as long as $\{l(t) - l(0)\}/l(0)$ is small. Finally, it can be used to change $T_{||}$ by a small amount (less than 1%)[3]. All of these points are crucial for measuring the relaxation rate in CV.

Consider a particle with velocity $v$ in a 1-dimensional box of length $l(t)$. If $l$ is changed slowly compared to the bounce frequency, $\omega_b = v/(2l)$, of the particle, then it is well known that $vl$ is an adiabatic invariant, which we will take to be a constant (i.e. $vl$ = const). This can be written in terms of the particle's kinetic energy, ($E = mv^2/2$), as $El^2$ = const, so that

$$\frac{dE}{dt} = -2\frac{E}{l}\frac{dl}{dt} \tag{4.24}$$

For a collection of particles described by a Maxwellian with temperature $T$, Eq. 4.24 becomes (see Appendix A.2)

$$\frac{1}{2}\frac{dT}{dt} = \frac{1}{k_B}\frac{d\langle E\rangle}{dt} = -\frac{T}{l}\frac{dl}{dt} \tag{4.25}$$

or

$$T_f = T_i \left(\frac{l_i}{l_f}\right)^2 \tag{4.26}$$

where $i$ and $f$ are the initial and final values.

For a plasma in CV we take $l$ as the plasma length, so that $T$ is $T_{||}$. In going from $El^2$ = const to Eq. 4.26, $dl/l$ is assumed to be the same for all electrons. For a plasma in CV $l$ is a function of an electron's velocity (see section 3.7.1). It is easy

[3]In principle, the other method can also be used to heat the plasma by small amounts, but in practice it may be impossible to implement.

to estimate this correction for a plasma of average length $\langle l \rangle$ with a difference in length between low velocity electrons and high velocity electrons of $\delta l$. Let $\Delta E$ be the difference in energy an electron gets from expansion if its length is $\langle l \rangle - \delta l/2$ versus $\langle l \rangle + \delta l/2$. One finds that

$$\frac{\Delta E}{E} \approx 2\frac{\delta l}{\langle l \rangle}. \tag{4.27}$$

For the data in this thesis, we estimate that $(\delta l/\langle l \rangle)_{\max} \approx 5\%$ so that $(\Delta E/E)_{\max} \approx 10\%$. There is also the problem that electrons at different radii expand by different amounts. We estimate this effect to give $(\Delta E/E)_{\max} \approx 10\%$.

Although this method of varying $T_{||}$ leaves the parallel velocity distribution essentially a Maxwellian, it is not true that this Maxwellian will persist when collisions start mixing $T_{||}$ and $T_{\perp}$. We believe that as long as $|(T_{||} - T_{\perp})|/T_{||} \ll 1$ a Maxwellian describes $v_{||}$ and $v_{\perp}$ quite well. We have estimated $(|(T_{||} - T_{\perp})|/T_{||})_{\max}$ to be about 0.1 for the relaxation rate data present in this thesis.

## 4.4 Temperature Measurement

Unfortunately, low temperature measurements require more sophisticated analysis than high temperatures, though the same basic ideas are employed in both. The high temperature measurement technique is simple to employ, and a single temperature can be analyzed in seconds on the small computer connected to the experiment. On the other hand, the low temperature measurement, which can actually be used to measure any temperature, has taken considerable time to develop, and the data for each temperature must be transferred to a larger computer for analysis. Furthermore, it takes several minutes to analyze a single temperature.

### 4.4.1 Temperature Measurement Assumptions

The temperature measurement only works for a subset of the CV plasmas. Below is a list of assumptions that are built into the temperature measurement and under what plasma conditions these assumptions are met.

- The parallel velocity distribution is Maxwellian.
- All particles with $v_{||}$ such that $mv_{||}^2/2 - e\phi(r) > -eV_b$ escape over the potential energy barrier, $-eV_b$, and are collected on the end collectors. Here $\phi(r)$ is calculated from the electrons which are still confined by $V_b$. This implies that the remaining parallel velocity distribution is

$$f(v_{||}) = \begin{cases} \text{const} \times \exp(-mv_{||}^2/2T), & \text{if } v_{||} < \sqrt{-2e(V_b - \phi)/m}; \\ 0, & \text{otherwise.} \end{cases} \tag{4.28}$$

- Finite length effects are unimportant.
- $V_b$ and $T$ are independent of radius, $r$.
- The density is a constant out to a radius of five Debye lengths (low temperature assumption).
- $\phi(r)$ is independent of $V_b$ (required only for the high temperature analysis).

Further, we assume that only electrons which are on or near the axis escape over the potential energy barrier, $-eV_b$. In particular, we assume that only those electrons which are at a radius, $r$, such that $r < 5\lambda_D$, escape. At low temperatures about 99% of the electrons that are used to measure the plasma temperature come from a radius such that $r < 5\,\lambda_D$. To understand why this is so, consider an infinitely long column of plasma with constant density, $n_0$. If no electrons have escaped then

$$\phi(r) = \phi(0) - \left(\frac{r}{2\lambda_D}\right)^2 \left(\frac{k_B T}{e}\right). \tag{4.29}$$

As the potential energy barrier is slowly lowered (i.e. as $V_d$ is raised to ground), electrons begin to escape, and this changes the plasma density. We write the new plasma density as $n(r,t)$ and assume that $\delta n(r,t) = n_0 - n(r,t) \ll n_0$. One can then estimate the number of electrons that make it over the potential barrier, $-eV_b$, at $r = \lambda_D$ and at $r = 5\lambda_D$. At $r = \lambda_D$ only electrons with $m\,v_{||}^2/2 > -e(V_b - \phi(0)) + (1/2)^2\,k_B T$ escape; whereas, for $r = 5\lambda_D$ only electrons with $m\,v_{||}^2/2 > -e(V_b - \phi(0)) + (5/2)^2\,k_B T$ escape. For a Maxwellian the ratio of the number of electrons that escape near $r = 5\lambda_D$ to those near $r = \lambda_D$ is

$$\frac{N(r = 5\lambda_D)}{N(r = \lambda_D)} \approx \frac{5\,\exp(e(V_b - \phi(0))/k_B T - (5/2)^2)}{\exp(e(V_b - \phi(0))/k_B T - (1/2)^2)} \approx 10^{-2}. \qquad (4.30)$$

For $r = 8\lambda_D$ this number is about $10^{-7}$.

This calculation uses the $\phi$ calculated from $n_0$ (i.e. very few electrons have escaped). Computer modelling of how the electrons escape (see section 4.4.3) shows that this argument is good until $\delta n(r = 0, t) \approx n_0/2$. Note that $\delta n(r,t)$ is the largest at $r = 0$. Thus, most of the electrons used to measure the plasma temperature come from $r < 5\lambda_D$ as long as $\delta n(r = 0, t) \lesssim n_0/2$.

### Isotropic Temperature and Maxwellian Distribution

One of the basic assumptions we make in measuring the plasma temperature is that the plasma is Maxwellian in $v_{||}$ and $v_\perp$ and that $T_{||} = T_\perp$. This assumption breaks up into two parts. First, the plasma must be a Maxwellian just prior to the start of the temperature measurement phase. Second, it must remain essentially Maxwellian during the temperature measurement phase. The first assumption is related to how fast the plasma evolves compared to $\nu^{-1}$. The fastest evolution time for a CV plasma is the cyclotron radiation time which has a minimum time scale of 0.1 sec (at a magnetic field of 60 kG), or a rate of about 10 Hz. For temperatures greater than about 25 K and densities greater than about $10^9 e/cm^3$, the minimum

relaxation rate is about 1kHz. Therefore we believe that the plasma is described quite well by a Maxwellian immediately prior to the start of the temperature measurement phase.

It is also true that at times we perturb the plasma, and this may change $f(v_{||}, v_{\perp})$. After such perturbations we hold the plasma an additional time which is long compared to $\nu^{-1}$ before measuring the plasma temperature. This should allow the parallel velocity distribution to relax to a Maxwellian.

During the temperature measurement phase the potential on $G_8$, $V_d$, is ramped to ground which causes the plasma to expand axially. In order for the plasma to remain a Maxwellian during this expansion the bounce time of the electrons must be much faster than the rate at which $V_b$ is changing (see derivation for Eq. 4.26). This condition can be written as $-e(dV_b/dt) \ll (k_B T)v_T/l_p$ (see condition 1 on page 78).

Finally, in the actual procedure for measuring $T_{||}$ we least squares fit over a range of $v_{||}$ to determine the temperature. By using least squares fitting to measure $T_{||}$, small random fluctuations in the parallel velocity distribution which deviate from a Maxwellian are essentially averaged to zero.

### All particles with $mv_{||}^2/2 - e\phi(r) > -eV_b$ escape past the confining gate $G_8$

The condition that an electron escapes over a potential $V_b$ is given by Eq. 4.1. If $V_b$ is a function of time then $\phi(r)$ can be a complicated function which may depend on time and $z$. To good approximation the time and $z$ dependence of $\phi$ can be ignored if the following conditions are met:

1. $-e(dV_b/dt) \ll (k_B T)v_T/l_p$ where $v_T$ is the thermal velocity and $l_p$ is the plasma length ($2l_p/v_T$ is a thermal electron's bounce time).

2. $|(dV_d/dt)/V_d| \ll \overline{\omega}_p \simeq \omega_p k r_p/\chi_{0,1} \approx 7.4 \times 10^4 \sqrt{n}\, r_p/l_p$ where $\overline{\omega}_p$ is the lowest plasma mode frequency [9], $\omega_p$ is the plasma frequency, $k = \pi/l_p$, and $\chi_{0,1} \approx 2.4$ and is the first root of $J_0(\chi_{0,k}) = 0$.

Condition 1 essentially insures that $f(v_{||}, v_\perp) = 0$ for $v_{||} > \sqrt{-2e(V_b - \phi)/m}$. The necessity for condition 1 can be understood from the following argument. Suppose at $t = 0$ the confining voltage, $V_b$, goes quickly, compared to the electron bounce time, from some large value that confines all the electrons to a new value that lets some of the electrons escape. For such a rapid change in $V_b$, the electrons near $G_8$ see a $\phi(r) = \phi(r, t = 0)$, and all of these electron which are traveling towards[4] the end collector with a $v_{||}$ such that

$$\frac{m v_{||}^2}{2} - e\phi > -eV_b \tag{4.31}$$

will escape. As these electrons escape they change $\phi$ until the last electron escapes with $\phi(r, t = \infty)$. A calculation of $\phi(r, t)$ is very complicated, making it difficult to find the number of electrons that escape versus $V_b$. To make this problem calculable we assume that only and all electrons with $v_{||} > v_e = \sqrt{-2e(V_b - \phi)/m}$ escape so that the distribution function of remaining electrons is

$$f_r = \text{const} \times \exp(-m v_{||}^2/2T) \tag{4.32}$$

for $v_{||} < v_e$ and is zero otherwise.

In order that Eq. 4.32 describe to good approximation the actual plasma in CV while the potential on $G_8$ is being ramped, condition 1 above must be satisfied. Assume that Eq. 4.32 with $v_e = v_1$ describes the parallel velocity distribution when $V_b = V$. If $V$ is now lowered by $\delta V$ in a time $\delta t = l_p/v_1$, then only electrons with velocities greater than $v_2$, where $m v_2^2/2 - e\phi > -e(V - \delta V)$, have a chance of escaping. If $(v_1 - v_2)/v_1 \ll 1$ then Eq. 4.32 will still be a good approximation. Note

[4]Those going in the opposite direction may not escape until a time $2l_p/v_{||}$ later.

that $(v_1 - v_2)/v_1 \approx -e\delta V/mv_1^2$. Dividing $-e\delta V/mv_1^2 \ll 1$ by $\delta t = l_p/v_1$ and using as a lower limit for $v_1$ the thermal velocity one obtains $-e(\delta V/\delta t)/(k_B T) \ll v_T/l_p$, which is condition 1.

A second problem with changing the potential on $G_8$ quickly is that it creates electrostatic waves in the plasma. This effect has been seen on other pure electron traps studied by Malmberg et al., and is avoided as long as condition 2 is satisfied.

### Finite length effects are not important

Raising the potential on $G_8$ toward ground will cause the plasma length to increase, and this will cool the plasma. It typically takes many relaxation times from the time we start ramping the potential on $G_8$ until the plasma begins to escape past $G_8$. At this point it takes a time of about $\nu^{-1}$ or less to measure the temperature. Since the plasma length increases slowly compared to $\nu^{-1}$ we expect the plasma to cool as $T_m = T_0(l_0/l_f)^{2/3}$ (i.e. 3-D expansion) where $T_0$ and $l_0$ are the plasma temperature and length just prior to ramping the potential on $G_8$, $l_f$ is the plasma length when electrons start escaping past $G_8$, and $T_m$ is the measured temperature. Computer simulations give $(l_0/l_f \approx 0.909)$ so that $T_m/T_0 \approx 0.94$.

In general, the $\phi$ in Eq. 4.1 is the sum of the gate potentials and the space charge potential. Suppose that for small changes in $V_b$ one can write $\phi = \phi_p + fV_b$, where $\phi_p$ is the space charge potential and $f < 1$. Then Eq. 4.1 becomes

$$\frac{mv_\parallel^2}{2} - e\phi_p > -eV_b(1 - f). \tag{4.33}$$

This says that small changes in $V_b$ are seen as even smaller changes by the plasma so that not as many electrons escape past $G_8$ as one might expect. Note that this simply means that changing all the potentials seen by a plasma by the same amount does nothing. To make the effect ignorable $f$ must be much less than 1. In section 3.7 it is argued that $\phi$ is essentially a constant along $z$ inside a CV plasma (at least

for temperatures below 1000 K). This allows one to evaluate $\phi$ at any $z$ position inside the plasma. In the center of a long plasma the contribution to $\phi$ from the gate potential is small. Even for a plasma 3 cm long in a cylinder of radius 1 cm, the gate potential in the center of the plasma is only about 5% of $\phi$. Moreover, the radial dependence of the gate potential is much less than 5% of $\phi$ in the center of the plasma. Therefore, as long as the plasma is longer than about 3 cm, finite length effects should not be important.

### $T$ and $V_b$ are independent of $r$

The radial dependence of the vacuum potential in the center of $G_8$, $V_d(r,z)$, can be estimated from Laplace's equation[5],

$$\frac{1}{r}\frac{\partial}{\partial r}\left(r\frac{\partial}{\partial r}V_d\right)+\frac{\partial^2}{\partial z^2}V_d=0, \tag{4.34}$$

to be

$$\Delta V_d = V_d(r)-V_d(0)\approx -\left.\frac{\partial^2}{\partial z^2}V_d\right|_{r=0}\left(\frac{r}{2R_w}\right)^2. \tag{4.35}$$

Since we are only interested in $r$ out to a maximum of five Debye lengths one finds that $(\Delta V_d/(k_BT))_{max}\approx 6\%$. For temperatures above 2000 K this error is much less than 6% since the radial size on the electron collector ($R_1$ in Fig. 3.1) is less than five Debye lengths. For low temperatures, one is more interested in an average of $\Delta V_d/(k_BT)$ out to about five Debye lengths. We estimate this average to be less than 2%.

A discussion of the temperature measurement when the temperature is a function of radius (i.e. $dT/dr\neq 0$) is given in section 4.4.6.

[5]To good approximation the radial dependence of $V_b$ is the same as the radial dependence of $V_d$.

**The density is a constant out to five Debye lengths**

The high temperature measurement is insensitive to the radial dependence of the plasma density (see end of section 4.4.2); to make the low temperature measurement calculable we have assumed that the plasma density is constant out to a radius of five Debye lengths. Using the density data (see section 3.7), we estimate that for a plasma temperature of 400 K and a plasma density of $10^9 e/cm^3$ there is about a 10% variation in the plasma density out to five Debye lengths. This will give an error of about 10% to the low temperature measurement.

**$\phi(r)$ is independent of $V_b$**

For the high temperature measurement we assume that the number of electrons that have escaped is small so that the change in $\phi$ compared to the temperature is ignorable. This means that we are able to measure only the tail of the Maxwellian to get the plasma temperature. This is also the main reason why the high temperature analysis fails for low temperatures. For low temperatures the change in $\phi(r)$ due to the electrons which have escaped over the potential energy barrier can be of order $k_B T$. To include this change in $\phi(r)$ we calculate $\phi(r)$ using the density of electrons which are still confined by the barrier $-eV_b$.

### 4.4.2 High Temperature Measurement Model

Using the assumptions in section 4.4.1 one can calculate the number of electrons that escape past $G_8$, $N_e$, as a function of the barrier energy, $-eV_b$, and show that, to within 5%,

$$\frac{1}{e}\frac{d}{dV_b}\log(N_e) \simeq \frac{1.05}{k_B T}. \tag{4.36}$$

If the constant 1.05 in Eq. 4.36 were 1, then the right hand side of Eq. 4.36 contains the first term of an asymptotic expansion. The second term in the asymptotic

expansion results in corrections which vary from 0% to about 10%. We have chosen an average value for the second term by multiplying the first term by 1.05.

The number of electrons that escape between $r$ and $r + dr$, $dN_e$, is obtained by integrating a Maxwellian from $v_{||} = \sqrt{-2e(V_b - \phi)/m}$ to infinity and multiplying by $2\pi l_p\, n(r)\, r\, dr$,

$$\begin{aligned} dN_e &= 2\pi l_p\, n(r)\, r\, dr \int_{\sqrt{-2e(V_b-\phi)/m}}^{\infty} \text{const} \times \exp(-mv_{||}^2/(2k_B T))\, dv_{||} \\ &= 2\pi l_p\, n(r)\, r\, dr\, \text{erfc}\left(\sqrt{-e(V_b - \phi)/(k_B T)}\right), \end{aligned} \tag{4.37}$$

where $\text{erfc}(x)$ is the complementary error function of $x$. Integrating Eq. 4.37 over the radius of the central end collector $R_1$ gives the total number of electrons $N_1$ that escape past $G_8$ and hit the collector $R_1$,

$$N_1 = 2\pi l_p \int_0^{r_1} n(r)\, \text{erfc}\left(\sqrt{-e(V_b - \phi)/(k_B T)}\right) r\, dr. \tag{4.38}$$

Next, calculating Eq. 4.36 with the assumption that $d\phi/dV_b = 0$ and letting $y = \sqrt{-e(V_b - \phi)/(k_B T)}$ one obtains

$$\frac{k_B}{e}\frac{d}{dV_b}\log(N_1) = \frac{\int_0^{r_1} n(r)\, \exp(-y^2)/(T\sqrt{\pi}\, y)\, r\, dr}{\int_0^{r_1} n(r)\, \text{erfc}(y)\, r\, dr}. \tag{4.39}$$

Here we have dropped a term containing $d\phi/dV_b$.

For large $y$ (i.e. $v_{||} >> v_T$) one can approximate $e^{-y^2}/(\sqrt{\pi}\, y)$ as

$$\frac{\exp(-y^2)}{\sqrt{\pi}\, y} = \text{erfc}(y)\left(1 + \frac{1}{2y^2} - \frac{1}{2y^4} + \vartheta\left(\frac{1}{y^6}\right)\right). \tag{4.40}$$

This gives

$$\frac{k_B}{e}\frac{d}{dV_b}\log(N_1) = \left\langle\frac{1}{T}\right\rangle + \left\langle\frac{1}{2y^2\, T}\right\rangle - \left\langle\frac{1}{2y^4\, T}\right\rangle + \vartheta\left\langle\frac{1}{y^6 T}\right\rangle, \tag{4.41}$$

where

$$\langle A\rangle \equiv \frac{\int_0^{r_1} A\, n(r)\, \text{erfc}(y)\, r\, dr}{\int_0^{r_1} n(r)\, \text{erfc}(y)\, r\, dr}. \tag{4.42}$$

Since we are dealing with values of $y$ that are greater than 2, we have

$$0 < \frac{\langle 1/(2y^2\,T)\rangle}{\langle 1/T\rangle} \lesssim .12. \tag{4.43}$$

Thus Eq. 4.36 is good to about 5% as long as $y$ is greater than about 2.

Note that when $dT/dr = 0$, $\langle 1/T\rangle$ is independent of $n(r)$ (i.e. $\langle 1/T\rangle = 1/T$). This is due to the fact that to lowest order in $1/y$, $d(\mathrm{erfc}(y))/dy = \mathrm{erfc}(y)$. In other words, we have kept only the first term in the right hand side of Eq. 4.40, and the left hand side is $d(\mathrm{erfc}(y))/dy$.

### 4.4.3 Low Temperature Measurement Model

To model how electrons escape for low temperatures it is simpler and more instructive to calculate the density of the escaped electrons, $n_e$, as a function of $V_b$. By escaped density we mean $n_e = n_0 - n$ where $n_0$ is the density just prior to any electrons escaping over the potential barrier, $-eV_b$, and $n$ is the density of the electrons still confined by $-eV_b$. For a density which is initially uniform one finds that $n_e$ is a monotonically decreasing function of radius and for $r > 5\lambda_D$, $n_e$ is approximately zero as long as $n_e(r=0) \lesssim n_0/2$. This is due to the space charge potential which makes the potential barrier, $-eV_b$, smallest at $r = 0$. For $r = 5\lambda_D$ the barrier is about 2.5 thermal velocities higher than at $r = 0$ and allows a much smaller fraction of the electrons to escape.

The change in the space charge potential due to the escaped electrons, $\phi_e$, depends only on $n_e$, and can be calculated from Poisson's equation,

$$\nabla^2\phi_e(r) = 4\pi\, e\, n_e(r). \tag{4.44}$$

Integrating a Maxwellian for $v_\parallel < \sqrt{-2e(V_b - \phi)/m}$ and using $n_e = n_0 - n$, Eq. 4.44 becomes

$$\nabla^2\phi_e(r) = 4\pi\, e\, n_0\ \mathrm{erfc}\left(\sqrt{\frac{-e(V' + \phi_e)}{k_B T} + \left(\frac{r}{2\lambda_D}\right)^2}\right) \tag{4.45}$$

where $V' = V_b - \phi_0(0)$ and $\phi_0(0)$ is calculated from $n_0$. If there is no radial dependence to either $T$ or $V_b$, then Eq. 4.45 can be written as

$$\nabla_x^2 \psi = -\mathrm{erfc}\left(\sqrt{(\psi + (x/2)^2)}\right) \tag{4.46}$$

where $\psi = -e(V' + \phi_e)/(k_B T)$, $x = r/\lambda_D$ and

$$\nabla_x^2 = \frac{1}{x}\frac{d}{dx}x\frac{d}{dx}. \tag{4.47}$$

Equation 4.46 can be numerically integrated to yield $\psi(x, \psi(0))$. The dependence of $\psi$ on $V_b$ comes from the choice of $\psi(0)$, and gives the fraction of electrons at $r = 0$ that have escaped as $n_e(r = 0)/n_0 = \mathrm{erfc}\sqrt{\psi(0)}$. Once $\psi$ is known the total number of electrons that escape onto $R_1$ is calculated as

$$N_e = 2\pi\, l_p \int_0^{r_1} n_e\, r\, dr = 2\pi\, l_p \lambda_D^2\, n_0 \int_0^{r_1/\lambda_D} \mathrm{erfc}\left(\sqrt{\psi + (x/2)^2}\right)\, x\, dx. \tag{4.48}$$

For $r_1/\lambda_D > 5$ one makes less than a 1% error to $N_e$ by letting $r_1/\lambda_D \to \infty$. To this approximation $N_e$ is only a function of $\psi(0)$, and can be written as

$$N_e = 2\pi\, l_p \lambda_D^2\, n_0\, \aleph(\psi(0)) \tag{4.49}$$

where

$$\aleph(\psi(0)) = \int_0^{\infty} \mathrm{erfc}\left(\sqrt{\psi + (x/2)^2}\right)\, x\, dx. \tag{4.50}$$

Writing

$$\psi(0) = \frac{-e(V_b - \phi_0)}{k_B T} - \frac{e\phi_e(0)}{k_B T}, \tag{4.51}$$

we next calculate $e\phi_e(0)/(k_B T)$. From Eq. 4.44, and assuming that no electrons escape for $r > 5\,\lambda_D$, $e\phi_e(0)/(k_B T)$ becomes

$$\frac{e\phi_e(0)}{k_B T} = \psi(x = 5) + \aleph \log\left(\frac{R_w}{5\lambda_D}\right). \tag{4.52}$$

From Eqs. 4.49 and 4.52 one finds that if $\psi(5)$ and $\aleph$ are known as a function of $\psi(0)$, then $N_e$ can be computed versus $V_b$ for given $T$, $l_p$, $\phi_0$ and $n_0$. Note that the

dependence on $n_0$ is logarithmic, and therefore uncertainties in the density of order 10% are ignorable as long as $R_w/(5\,\lambda_D) \gg 1$.

Experimentally this method may fail when $n_e(0) \approx n_0/2$. Letting $n_e(0) = n_0/2$ fixes $\psi(0)$, which in turn fixes $\aleph$. From Eq. 4.49 one see that for fixed $\aleph$ the number of electrons that escape depend only on $l_p$ and $T$ ($\lambda_D^2\, n \propto T$). For fixed $l_p$ the lowest temperature one can measure will then depend on the number of electrons that can be measured.

### 4.4.4 Differences Between the Temperature Measurement Models

In the beginning of section 4.4 we state that "measuring the plasma temperature *requires* two different analyses". Here we have underline the word "requires" because we need to explain its meaning. Also, we will explain the essential difference between the two temperature models.

If the plasma density profile is known to reasonable accuracy, the low temperature analysis could be used to measure all temperatures. However, using the low temperature analysis to measure all temperatures would greatly decrease the rate of data collection. From a practical stand point, it is better to use the high temperature analysis whenever possible, especially since for high temperatures the two analyses yield temperatures which agree to within the accuracy of the models (i.e. to about 10%).

Although, the high and low temperature models have been derived differently, there are only three differences between these model: 1) the low temperature model assumes a uniform density profile; 2) and the high temperature model does not include changes to $\phi$ as electrons escape; and 3) the high temperature model assumes that $y \gtrsim 2$. Aside from these difference, these models are identical.

The failure of the high temperature analysis at low temperatures is due to

microphonic noise from the lead which connects the end collector $R_1$ to the first stage amplifier. This noise is equivalent to about $10^3$ electrons. That is, the minimum number of electrons presently detectable is about $10^3$. However, in order to obtain a reasonable determination of the temperature we need to measure at least ten times the noise limit, or about the first $10^4$ electrons which escape. If, for a typical CV plasma, $10^4$ electrons are removed from the region around the axis, then the space charge potential changes by about 5 mV. Let this change be $\delta\phi$. If $-e\delta\phi/(k_B T) \ll 1$ we can neglect this small change in the temperature analysis. In the high temperature analysis we assume that $-e\delta\phi/(k_B T) \ll 1$ (in Eq. 4.39 we dropped a term containing $d\phi/dV_b$). When $-e\delta\phi/(k_B T)$ becomes of order 0.1 the high temperature analysis fails, and this typically occurs when $T \approx 500$ K.

There is an additional assumption built into the high temperature analysis which also fails when $-e\delta\phi/(k_B T) \sim 1$. One can show that when $-e\delta\phi/(k_B T) \sim 1$, $y = \sqrt{-e(V_b - \phi)/k_B T} \approx 1$ for the electrons near the axis which just have enough energy to escape. When $y \approx 1$ it is no long appropriate to keep only the first term in the asymptotic expansion of $\exp(y^2)/y$ (see Eq. 4.40).

For temperatures in the range $500\,\mathrm{K} \lesssim T \lesssim 2000\,\mathrm{K}$ and for a central density $n \approx 10^9 \mathrm{e/cm}^3$, the two temperature analyses agree to within 10%. Below about 500 K the high temperature analysis is no long valid. In the low temperature analysis we assume that all the initially escaping electrons hit $R_1$. However, when $T \gtrsim 2000\,\mathrm{K}$ there are a significant number of electrons which hit $R_2$ and are not counted as escaped electrons.

### 4.4.5 Temperature Measurement: Experimental Method

Experimentally the temperature is measured by simultaneously digitizing the signal on $R_1$ and the potential $V_d$ while $V_d$ is being ramped to ground. The digitizers are controlled by the same clock and can digitize up to a rate of 1 MHz with about

10 bits of resolution full scale.

The signal on $R_1$ is connected to an inhouse-built, low noise amplifier which has a noise floor of about $10^{-9}\,\mathrm{V}/\sqrt{\mathrm{Hz}}$ and a gain of either 14.6 or 1460. Presently, the minimum number of electrons that can be measured on $R_1$ is limited by microphonic noise from the lead that connects $R_1$ to the amplifier, and not by noise from the first stage amplifier. From the first amplifier the signal goes through a second amplifier/filter and then into the digitizer.

The power source controlling the potential $V_\mathrm{d}$ is an inhouse-built $-150\,\mathrm{V}$ to $+150\,\mathrm{V}$ amplifier that is linearly ramped to ground during the time the electrons used to measure the plasma temperature are escaping over the hill $V_\mathrm{d}$. At low temperatures the deviation of the varying potential $V_\mathrm{d}$ from a linear ramp (due to noise from the power source) is enough that it becomes impossible to measure the temperature. To overcome this problem a 1-pole lowpass RC filter with a 3-db point at 100 Hz is added to the power source. The potential $V_\mathrm{d}$ is monitored by an offset/amplifier circuit after the filtering. The offset/amplifier circuit allows one to offset and amplify $V_\mathrm{d}$ so that it is within the voltage range of the digitizer when the electrons just begin to escape over the barrier $-eV_\mathrm{b}$.

Both digitized signals are then read by a small computer. If the temperature is high enough, Eq. 4.36 is used to determine the plasma temperature. Enough data is acquired before the electrons begin to escape so that any offset in the signal from $R_1$ can be subtracted out. Once this is done the logarithm[6] of $N_1$ is taken and a line is fitted to the linear portion of $\log(N_1)$. A line is also fitted to $V_\mathrm{d}$. The slope of each line gives an average of $d(\log(N_1))$ and $dV_\mathrm{d}$ which is then put into Eq. 4.36 to determine $T$. Figure 4.5 shows a plot of $N_1$ and $\log_{10}(N_1)$ versus $V_\mathrm{b}$ for a high temperature plasma. In general, the straight line region for $\log_{10}(N_1)$ goes from about one decade in $N_1$ at a temperature of 1000 K to about three decades in $N_1$ at

[6]Care is taken to insure that $N_1$ is never less than or equal to zero.

much higher temperature.

For low temperatures the approximates that $y = \sqrt{-e(V_b - \phi)/(k_B T)} > 2$ and that $\phi$ is independent of $V_b$ brake down, and the high temperature analysis fails. In this case the data is transferred to a larger computer where a more sophisticated program uses Eqs. 4.50, 4.51 and 4.52 to determine $T$. The program varies $T$, $l_p$, and $\phi_0$ ($n_0$ is known to sufficient accuracy experimentally) until the sum

$$\sum (N_1(V_b) - C_0 \aleph(g(V_b)) + C_1)^2 \tag{4.53}$$

is minimized. The sum is over a window in the $N_1$ data chosen by the experimentalist. $C_1$ removes any offset in the data, and for perfect data $C_0 = 2\pi l_p \lambda_D^2 n_0$. Comparing $l_p$ as calculated from $C_0$ to an $l_p$ as estimated from section 3.7 gives a check of the fit. The function $g(V_b)$ gives $\psi(0)$ for a given $V_b$, $T$ and $\phi_0$. Once the parameters have been determined, $N_1$ and $N_e$ are plotted versus $V_b$ so that the experimentalist can determine if the fit is satisfactory. Figure 4.6 shows a plot of $N_1$ and $N_e$ versus $V_b$ for a low temperature plasma.

### 4.4.6 Temperature Measurement Error When $dT/dr \neq 0$

From Eq. 4.39 and 4.42 one sees that if $dT/dr = 0$ then $\langle 1/T \rangle = 1/T$, independent of $n(r)$. Also, for $y(r = 0) > 2$, Eq. 4.43 overestimates the error when $y$ is set to 2. Note that if $l_p$ is also a function of radius, the same arguments hold. This can be seen by letting $N_l(r) = l_p(r)\, n(r)$ in Eq. 4.37 and repeating the calculation with $N_l(r)$. For low temperatures only the electrons near the axis are important. Here it is believed that $l_p(r)\, n(r)$ varies by less than 10% (see section 3.7) so that little error is made by setting $l_p(r)\, n(r)$ to a constant.

If $dT/dr \neq 0$, the analysis is a little more complicated. We still ignore radial variations in $T(r)$ for the low temperature measurement, arguing that we are only measuring the temperature over a small region near the axis.

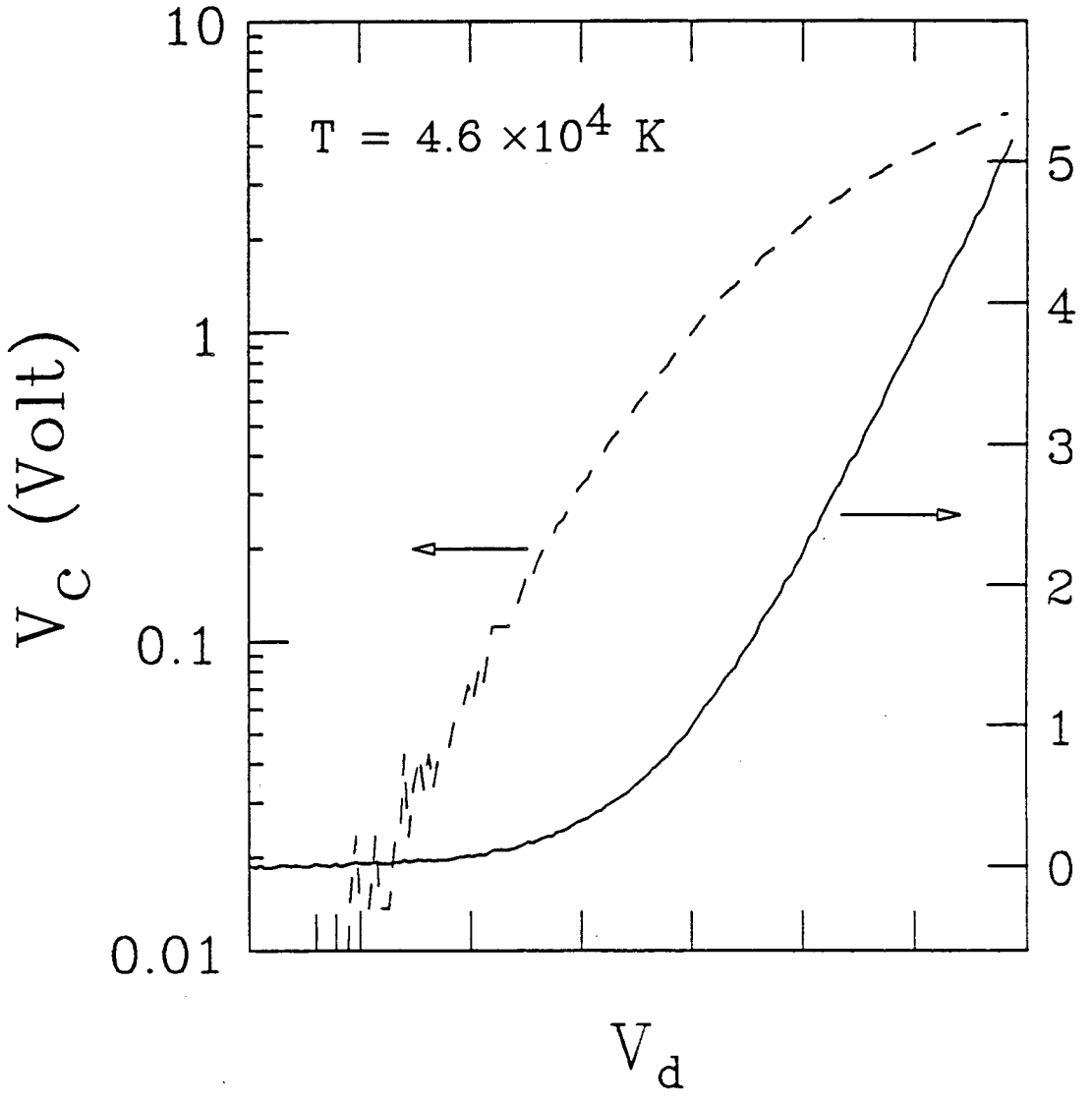


**Figure 4.5:** $N_1$ and $\log_{10}(N_1)$ versus $V_b$ for high temperature measurement. The solid curve is $N_1$ and the dashed curve is $\log_{10}(N_1)$. The temperature is determined from the straight line region of the $\log_{10}$ plot.

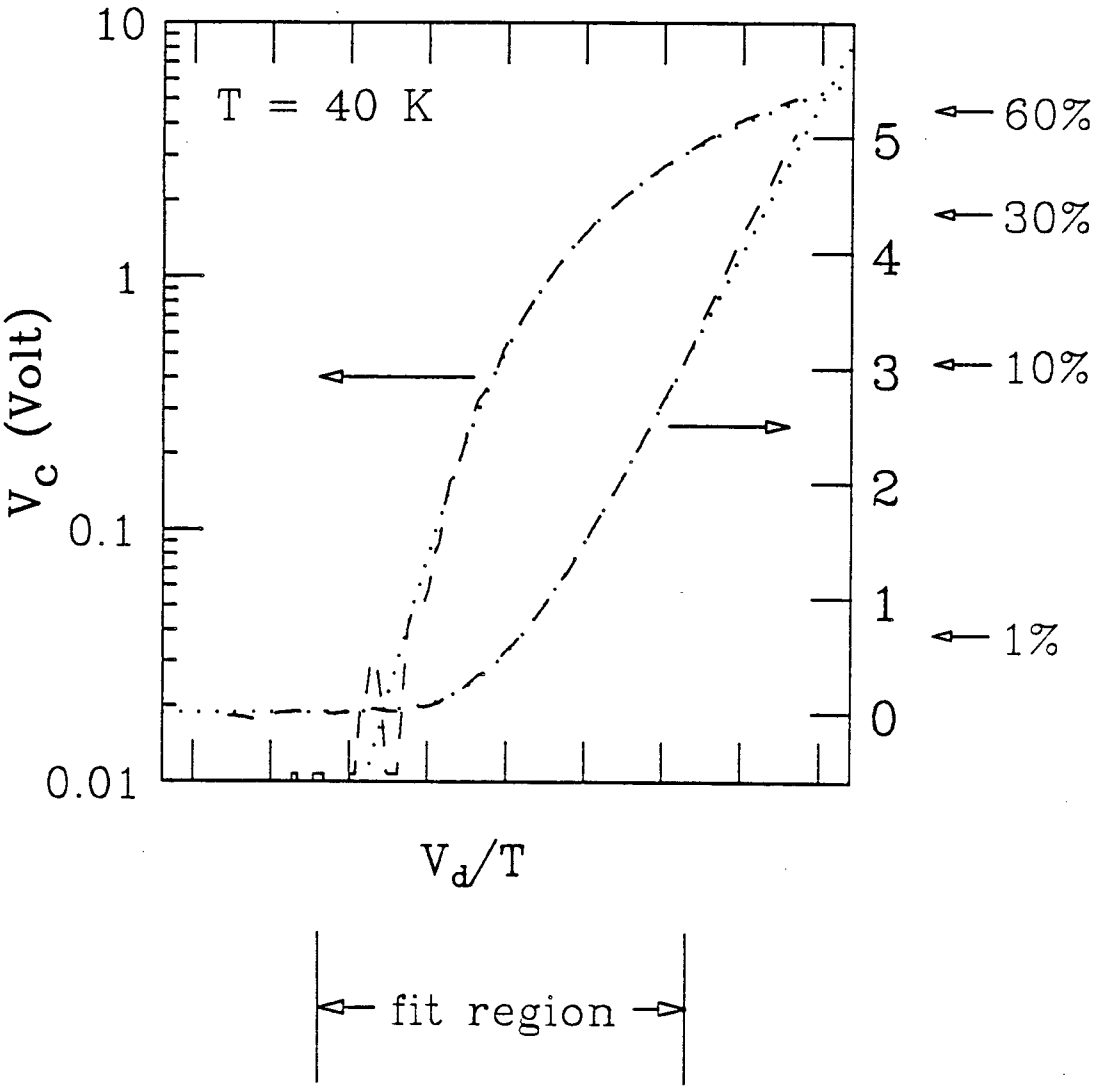


**Figure 4.6:** $N_1$ and $N_e$ versus $V_b$ for the low temperature measurement. Both $N_1$ and $\log_{10}(N_1)$ are shown. The dashed curves are the experimental $N_1$, and the dotted curves show the fit. The percentages on the right mark the fraction of central density that has escaped for the log plot.

We believe that the radial variation in the plasma temperature is less than about a factor of two. Note that even the high temperature measurement does not measure $\langle 1/T \rangle$ over the whole plasma. The signal that hits $R_1$ is about 1/2 the total plasma. At times we have observed the signals on $R_1$ and $R_2$. The following is what one would expect to happen if $|(dT/dr)|/T < 1/r_1$. At very high temperatures, where the space charge potential across the plasma is small compared to the plasma temperature (i.e. $r_1 \ll \lambda_D$), one expects[7] $N_1$ and $N_2$ as a function of $V_d$ to be about the same. This is because the total number of electrons collected on $R_1$ and $R_2$ are the same when $V_d$ is quickly raised to ground. As the temperature reaches about 1000 K (i.e. $5\lambda_D \approx r_1$ for $n = 10^9 \mathrm{e/cm^3}$) one expects most of the electrons with $r < r_1$ to escape past $G_8$ before those electrons with $r > r_1$. This, in fact, is what is experimentally observed and leads one to believe that $T(0)$ and $T(r \simeq r_1)$ are within about a factor of two of each other.

To estimate the effect of the radial dependence on the temperature we will take $T(r)$ to be

$$T(r) = \frac{T_0}{1 + \delta(r/r_1)^2}. \tag{4.54}$$

One can show from Eq. 4.41 that for small $\delta$,

$$\left\langle \frac{T_0}{T} \right\rangle - 1 < \frac{\delta}{2}. \tag{4.55}$$

Numerical integration of $\langle T_0/T \rangle$ for various density profiles shows this to be a good approximation for the range $-0.4 < \delta < 1$, which covers a factor of two variation in $T(r)$ for $r < r_1$. Note that it is important to compare $\langle 1/T \rangle$ to $1/T_0$ since the low temperature measurement essentially measures $T_0$ for any reasonable $\delta$.

[7]The following argument is equivalent to setting $dy/dr = 0$ in Eq. 4.39.

## 4.5 Plasma Energy Transport

As long as the energy transport time (thermal conductivity) between any two points in a plasma is much less than the radiation time and $\nu^{-1}$ is also much less than the radiation time, the plasma will be isothermal[8]. In this section we assume that the relaxation time, $\nu^{-1}$, is much less than the radiation time, which is the case for all the experimental data presented in this thesis.

Consider the energy transport time for the three coordinates $(r, \theta, z)$. For the $z$ coordinate the energy transport time is simply the time it takes an electron to traverse the length of the plasma. This time has a maximum of about 1 $\mu$sec. Therefore, the rate at which the plasma comes into thermal equilibrium along a magnetic field line will be the larger of relaxation rate and the three-body collision rate (see Appendix A.6).

We believe that the plasma temperature is constant along $\theta$ at each radius. The rotation rate of the plasma about the axis of symmetry is not uniform (i.e. $\partial\omega_R/\partial r \neq 0$). This will cause $\partial T/\partial\theta$ to relax to zero provided there is radial diffusion of the electrons. If electrons at a radius $r_\alpha$ diffuse a radial distance $\delta r$ in a time $t_1$, then $\partial T/\partial\theta$ will relax to zero on a time scale $t_\theta$, where $t_\theta|(\partial\omega_R/\partial r)\delta r| \sim 2\pi$ provided $t_\theta > t_1$. We estimate $\partial\omega_R/\partial r$ from the density data in Fig. 3.7 (see Eq. 3.9) and we calculate $t_1$ from Eq. 4.59, and estimate that $t_\theta \lesssim 0.01$ sec.

The radial thermal transport time for a CV plasma is more difficult to calculate. Presently there is no direct experimental data on the radial energy transport time. However, it is possible to estimate a lower bound to the radial energy

[8]Here it is assumed that the plasma's temperature at each point is varying on the time scale of a cyclotron radiation time. To measure the relaxation rate, the plasma is heated by modulating the plasma length at a frequency near the relaxation rate, $\nu$, (see chapter 5). The time scale for heating may seem to be much less than the radiation time since $\tau_r \gg \nu^{-1}$. However, since the heating power is essentially balanced with the radiation power, the heating is effectively varying the plasma temperature at the radiation time scale.

transport time. This is done by assuming that the density and temperature of the plasma depend only on radius, $r$, and also assuming that the particle flux is zero (i.e. $\partial n/\partial t = 0$). Finally, assuming that energy is transported radially by collisions, one obtains (see Eq. 32 in reference [47])

$$\frac{\partial}{\partial t}\left(\frac{3}{2}nT\right) \sim \frac{1}{r}\frac{\partial}{\partial r}r\left(\nu_{ee}r_c^2\, n\frac{\partial T}{\partial r}\right) \tag{4.56}$$

where $\nu_{ee}$ is the electron-electron collision rate.

From Eq. 4.56 one can estimate an upper limit to the time that it takes for two radial points, $(r_a, r_b)$, to come into thermal equilibrium as

$$t_{eq} \approx \frac{1}{\nu_{ee}}\left(\frac{r_b - r_a}{r_c}\right)^2. \tag{4.57}$$

For the temperature measurement we want $r_a = 0$ and $r_b$ to be the smaller of $5\lambda_D$ and $r_1$. For the data in this thesis, this estimate gives $20\,\text{sec} \lesssim t_{eq} \lesssim 1000\,\text{sec}$, depending on the plasma temperature.

Of course, other transport processes may produce a smaller $t_{eq}$. For example, O'Neil [46] recently introduced a theory of cross-magnetic-field transport due to like-particle collisions. In Eq. 4.56 an electron steps a distance $r_c$ in a time $\nu_{ee}^{-1}$. For low plasma temperature this step size is very small. However, for sufficiently small $r_c$ one may employ guiding center drift theory to calculate an electron's motion.

During an electron-electron collision each electron's guiding center experiences an $\mathbf{E} \times \mathbf{B}$ drift, and the time integral of the drift velocity over the duration of the collision yields a step in the guiding center position. For a collision with impact parameter $p$ and relative velocity $\mathbf{u}$, each guiding center will step a distance $\delta x \approx ce/(Bu_{\|}p)$. Integrating over possible impact distances yields an estimate of the diffusion coefficient, $D$,

$$D \sim \int_{p_{min}}^{p_{max}} (\delta x)^2 n u_{\|} 2\pi p\, dp = \frac{2\pi n c^2 e^2}{u_{\|}B^2}\log(p_{max}/p_{min}). \tag{4.58}$$

This will result in a radial thermal relaxation time of

$$t_{\rm eq} \sim \frac{(\delta r)^2}{D}. \tag{4.59}$$

For $\delta r = 0.05\,\mathrm{cm}$ (i.e. average plasma radius) and $B = 60\,\mathrm{kG}$ this yields $3\,\mathrm{sec} \lesssim t_{\rm eq} \lesssim 30\,\mathrm{sec}$ for temperatures between $10^2\,\mathrm{K}$ to $10^4\,\mathrm{K}$. Here we have used $v_{\rm T}$ for an average $u_{||}$. For $B = 30\,\mathrm{kG}$ one obtains $0.8\,\mathrm{sec} \lesssim t_{\rm eq} \lesssim 8\,\mathrm{sec}$.

In this section we have considered the energy transport time along the three coordinates $(r, \theta, z)$. We have argued that energy transport along $\theta$ and $z$ is much shorter than the radiation time, and have concluded that the plasma temperature is independent of $\theta$ and $z$.

For the radial coordinate, a conclusion is not so obvious. We have considered two radial energy transport mechanisms. The first mechanism yields a radial energy transport time which is much longer than the radiation time. This mechanism also yields a transport time which is long compared to 10 sec. (The relaxation rate data was obtained by heating the plasma for about 10 sec.) The second mechanism yields transport times which are on a 1 sec to 10 sec time scale, A time scale of 1 sec may be short enough to keep the plasma temperature essentially independent of radius.

In order to understand why a time scale of 1 sec may be short enough to keep the plasma temperature almost independent of radius, consider what happens during a typical relaxation rate measurement. After some effort, we find a modulation frequency $f$ for which compressional heating balances radiation cooling. The modulation amplitude has been adjusted so that other frequencies near $f$ produce less heating, and the plasma cools for these frequencies. However, for frequencies near $f$, the heating almost balances radiation cooling, so that the effective cooling time is many radiation times. For example, if the effective cooling time is 10 times the radiation time, then the effective cooling time is about 1.4 sec for $B = 60\,\mathrm{kG}$ and is about 5 sec for $B = 30\,\mathrm{kG}$.

Nevertheless, a better calculation for the radial energy transport time is needed before one can say with reasonable certainty whether or not the temperature is independent of radius.

# Chapter 5

# Relaxation Rate Measurement and Data

## 5.1 Introduction

The relaxation rate is measured by sinusoidally modulating the plasma length at various frequencies and determining that frequency which produces the most heating per cycle. By modulating the plasma length, work is done on the plasma through the component of the total plasma pressure which is parallel to the length change. The total pressure is the sum of pressure due to kinetic motion and the pressure due to the potential energy. The potential pressure is much larger then the kinetic pressure; however, as long as an expansion of the plasma is done quasistatically, the potential pressure does not directly effect the kinetic energy of the plasma [16]. The potential pressure indirectly affects the entropy through the self-consistent balance of forces which determines the plasma volume. Here we are mainly interested in the change in the kinetic energy of the plasma as the plasma length is altered quasistatically, and we therefore ignore the potential pressure (except to calculate the volume change during a modulation of the plasma).

Since the length change is parallel to the magnetic field, it is the plasma kinetic energy parallel to the magnetic field which is directly altered by the modulation. Collisions then transfer some of this energy to the perpendicular energy. This

causes the parallel pressure as a function of length to be lower during the expansion part of a cycle than during the compression part of a cycle so that a net heating of the plasma occurs. In other words, the process is irreversible, implying that entropy is added to the system which causes the plasma to heat. A model for this heating process, which we call compressional heating, predicts that maximum heating per cycle occurs for an oscillating angular frequency $\omega = 3\nu$ where $\omega = 2\pi f$ and $\nu$ is the relaxation rate. Thus, by measuring the heating as a function of $\omega$, and determining which $\omega$ produces the most heating per cycle, we are able to measure the relaxation rate.

In section 5.2 the compressional heating model is presented. The assumptions built into the model are first presented and their relevance to a CV plasma are analyzed. It will be shown that the amount of heating per cycle depends on the amplitude of the oscillator and on the parameter $\beta = \omega/(3\nu)$.

Since the relaxation rate is a function of temperature, one would like to heat the plasma as little as possible so that corrections to the relaxation rate due to the temperature changing are small. Unfortunately, the resonance in the peak heating versus frequency is broad, and the temperature measurement has a relatively large uncertainty at low temperatures. Together, these make a small peak difficult to measure. To circumvent is problem we adjust the amplitude of the oscillator so that the heating power balances the cyclotron cooling power when the frequency is adjusted to produce maximum heating. For all other frequencies the cooling dominates. When this is done, small differences between the heating and cooling powers lead to large temperature drops when the heating is applied for many radiation times. These large temperature drops are easily measured. In section 5.3 the procedure of balancing the cyclotron cooling with compressional heating is presented.

In section 5.4 the experimental data of the relaxation rate are presented and

compared to theory. Finally, in section 5.5 the major uncertainty in the measurement of the relaxation rate is analyzed. This uncertainty is due to lack of knowledge of the radial energy transport time and to the fact that the plasma density and length depend on radius. This leads to uncertainties in the measured relaxation rate and the corresponding temperature of about ±20%.

## 5.2 Relaxation Rate Measurement Model

To calculate the amount of compressional heating produced by modulating the plasma length one uses Eq. 4.9 with $\langle dE_{||}/dt\rangle = -k_B T_{||}(dl/dt)/l$. Here, we will first treat the case where $\langle dE_{\perp}/dt\rangle = 0$ (e.g. no cyclotron radiation). The term $-2T_{||}(dl/dt)/l$ was derived in section 4.3.3 using the bounce invariant (i.e. $v_{||}l = \text{const}$). A second way of deriving this expression, which is more in line with statistical mechanics, is to consider the work $W$ done on an ideal gas by a small change in its volume $V$. (Recall (see section 5.1) that the pressure resulting from the potential energy of the plasma can not alter the plasma kinetic energy as long as the plasma is expanded quasistatically.) For a plasma $W$ is the work performed on the kinetic pressure, and not the total work performed on the plasma. Changes in the gas's volume are assumed to be along one axis (i.e. along the magnetic field for the electrons in CV), and end effects are assumed small, so that $dV = A\,dl$ where $dl$ is a small length change, and $A$ is the area of the gas perpendicular to the length change. For an ideal gas $dW = -P_{||}\,dV$ and $P_{||} = nk_B T_{||}$ where $n$ is the density of the gas. If no external heat is added to the gas then $dW = dE$ where $E = k_B(T_{||} + 2T_{\perp})N/2$. Dividing $dW$ by $dt$ one obtains

$$\frac{dW}{dt} = k_B \frac{d(T_{||} + 2T_{\perp})}{dt}\frac{N}{2} = -n\,A\,k_B T_{||}\,\frac{dl}{dt}. \tag{5.1}$$

Dividing this by $N/2$ and substituting $nA/N = 1/l$ gives

$$\frac{d(T_{||} + 2T_{\perp})}{dt} = -2\,T_{||}\,\frac{1}{l}\frac{dl}{dt}. \tag{5.2}$$

Equation 5.2 is equivalent to adding twice Eq. 4.10 to Eq. 4.9 with $\langle dE_{||}/dt \rangle = -k_B T_{||}(dl/dt)/l$ and $\langle dE_{\perp}/dt \rangle = 0$. The connection between these two derivations comes from the assumption that the bounce time of a particle (electrons for CV) is much faster than the time scale for the volume change. This insures that the pressure $P_{||}$ is uniform throughout the volume (see page 45 in reference [34]).

### 5.2.1 Relaxation Rate Measurement Assumptions

Below is a list of assumptions that are built into the relaxation rate measurement. The plasma conditions for which these assumptions are relevant are explained in this section.

- The plasma length is modulated as

$$l = l_0 [\, 1 + \epsilon \sin(\omega t) \,] \tag{5.3}$$

  where $\epsilon \ll 1$, when the voltage on one of the confinement gates is modulated as

$$V(t) = V_0 + \delta V \sin(\omega t). \tag{5.4}$$

- $f(v_{||}, v_{\perp})$ is a bi-Maxwellian with $T_{||} \approx T_{\perp}$ at all times.

- The dominant heating process is compressional heating (i.e. the plasma is expanded quasistatically).

- The relaxation rate is a constant (i.e. changes in the relaxation rate due to changes in the plasma temperature and the plasma density during one modulation cycle are ignored).

- $T_{||}(t) = T_{||}(0) \exp(\alpha t) [\, 1 + |\Delta'| \sin(\omega t + \theta') \,]$ when the plasma length is modulated sinusoidally at angular frequency $\omega$. Collisions cause the modulations to be irreversible, producing a net heating per modulation which we include with the factor $\exp(\alpha t)$. We assume that $\alpha \omega^{-1} \ll 1$ and $|\Delta'| \ll 1$.

- $T$ and $n$ do not depend on radius, the plasma lifetime is very long, and all electrons have the same $\epsilon$.
- The plasma is treated as an ideal gas.

### The plasma length is modulated sinusoidally

To modulate the plasma length the voltage on one of the confining gates is modulated as

$$V(t) = V_0 + \delta V \sin(\omega t). \tag{5.5}$$

In general, a sinusoidal modulation of one of the end gates does not produce a purely sinusoidal modulation of the plasma length. However, the plasma length can be written as a Fourier series with lowest non-zero frequency $\omega$,

$$l(t) = l_0 [\, 1 + \sum_n B_n \sin(n\omega t + \theta_n) \,] \tag{5.6}$$

where $n = 1, 2, 3, ..., \infty$, $B_1 \equiv \epsilon$ and the $B_n$'s are determined from the gate potentials and the plasma density (see section 3.7). To analytically estimate the $B_n$'s, we will write the length as a function of confinement gate voltage $V$ and Taylor expand for small changes in the voltage $\Delta V$,

$$l(V) = l(V_0) + \left.\frac{dl}{dV}\right|_{V=V_0} \Delta V + \frac{1}{2} \left.\frac{d^2 l}{dV^2}\right|_{V=V_0} (\Delta V)^2 + \vartheta((\Delta V)^3). \tag{5.7}$$

From Eq. 5.5 we have that $\Delta V = \delta V \sin(\omega t)$. In Appendix A.3, $B_1$ and $B_2$ are analytically estimated for a well confined plasma (one in which the confining gate potentials are much greater than the plasma space charge potential). For this case,

we find that[1]

$$B_1 \approx \frac{-R_w}{l_0 \chi_{0,1}(1 + 2R_w/(l_0\chi_{0,1})} \frac{\delta V}{V_0}, \tag{5.8}$$

and

$$B_2 \approx \frac{R_w}{4l_0(1 + 2R_w/(l_0\chi_{0,1}))} \left(\frac{\delta V}{V_0}\right)^2 \approx -\frac{B_1}{4}\left(\frac{\delta V}{V_0}\right) \tag{5.9}$$

where $R_w$ is the wall radius and $\chi_{0,1}$ is the first root of $J_0(\chi_{0,k}) = 0$. In general, to lowest order in $\delta V/V_0$ one can show that

$$B_n \propto \epsilon^n. \tag{5.10}$$

For the plasmas studied in this thesis $R_w/(l_0\chi_{0,1}) \approx 1/6.6$. For $\delta V/V_0 = 1/2$, worst case, $B_1 \approx 1/17$ and $B_2 \approx -B_1/8$. For $\delta V/V_0 = 1/5$, a typical case, $B_1 \approx 1/43$ and $B_2 \approx -B_1/20$. These values of $B_1$ agree to within a factor of two with those estimated in Appendix A.8. In Appendix A.8, $\epsilon$ is estimated by experimentally determining the heating per cycle and comparing it to Eq. 5.39. For most (94%) of the data in this thesis $\epsilon < 0.06$ so that $B_2$ is estimated to be less than $B_1/14$. Therefore, the harmonics in Eq. 5.6 are ignored and Eq. 5.3 is used for the modulated plasma length.

Also, for finite $B_2$ the peak in the heating does not occur at $\omega = 3\nu$. For $B_2 = -B_1/10$ we have estimated this error to be about 1%, and for $B_2 = -B_1/5$ the error is about 4% (see Appendix A.4). This error is smaller than those estimated from other uncertainties and will be ignored.

[1] A more accurate expression for $B_n$ is

$$B_n = \left(\frac{\delta V}{V_0}\right)^n \sum_{k=0}^{\infty} A_{k,n} \left(\frac{\delta V}{V_0}\right)^{2k}.$$

For $\delta V/V_0 = 1/2$, the worst case, we estimate $|B_1 - A_{0,1}| \lesssim 0.05\, B_1$.

**$f(v_{||}, v_{\perp})$ is a Maxwellian and $T_{||} \simeq T_{\perp}$.**

Although $f(v_{||}, v_{\perp})$ is never measured, we believe it is, to a good approximation, described by a Maxwellian during the entire heating process. First, it most likely starts out as a Maxwellian at the beginning of the heating phase since the plasma is trapped by static fields for time which is long compare to $\nu^{-1}$ prior to the heating phase, and the plasma evolves on a time scale which is slow compared to $\nu^{-1}$. Second, the potential used to heat the plasma (i.e. $\delta V$ in Eq. 5.5) is added to an existing static field, and all other fields are unchanged. Third, to measure the relaxation rate, $v_{||}$ and $v_{\perp}$ are varied by small amounts (order $\epsilon$) at a rate near the relaxation rate, which is the minimum rate at which the distribution function is relaxing to a Maxwellian. This is also the rate at which collisions equilibrate $T_{||}$ and $T_{\perp}$. Finally, although more than $10^4$ cycles are applied to a given plasma to measure the relaxation rate, these cycles are not applied in one long set. Instead, the cycles are applied in sets of 8 to 138 cycles, and the sets are separated by a time which is much longer than $\nu^{-1}$. This time between sets when there is no heating should give the plasma ample time to return to a Maxwellian at the start of each set.

As was mentioned in section 2.3.1, for $r_c/b > 1$ it is the low velocity electrons, compared to $v_T$, which contribute the most to the relaxation rate. For a Maxwellian this is the bulk of the electrons. On the other hand, for $r_c/b < 1$ it is the electrons with parallel velocities greater than about $v_T(2.34(b/r_c)^{1/5} - 1)$ which contribute the most to the relaxation rate (see Appendix A.5). For $r_c/b \ll 1$, this implies that electrons in the tail of a Maxwellian contribute the most to the relaxation rate, which may constitute a small fraction of the electrons. If, for some reason, the heating process creates a plasma with a distribution function which has no electron with $v_{||} \geq v_T(2.34(b/r_c)^{1/5} - 1)$, then the measured relaxation rate would be lower than $\nu_M$, where $\nu_M$ is the relaxation rate for a plasma with the same average kinetic

energy per electron and the same plasma density but with a velocity distribution which is Maxwellian. We believe that this is does not happen.

### The dominant heating comes from compressional heating

Of course, a sinusoidal modulation of the plasma length at an frequency $f$ may launch plasma waves which may heat the plasma through Landau damping [31], or the plasma may be heated by some other unknown process. We call these non-compressional heating processes. We feel that Figs. 5.1 and 5.2 demonstrate that compression heating is the dominant heating process over the frequency range $1\,\mathrm{kHz} \lesssim f \lesssim 1\,\mathrm{MHz}$. We have many experimental curves similar to that in Fig. 5.1 for different values of $T_0$ (see Eq. 5.39), and all yield maximum heating when the modulated frequency is near the estimated relaxation rate.

### Relaxation rate is a constant

The following derivation for the amount of compressional heating per cycle assumes that the relaxation rate is a constant even though the temperature and density are changing due to the changing plasma length. This adds little error to the results since the changes in the temperature and density are of order $\epsilon$. For example, during one heating cycle the maximum change in $T_{||}$ will occur when $\omega \gg \nu$ ( one-dimensional compression). If $\epsilon = 0.02$, the most common value, there will be approximately a 4% ($2\,\epsilon$) uncertainty in the measurement of $T_{||}$ associated with the relaxation rate. In other words, instead of adding this uncertainty to the relaxation rate uncertainty, we add it to the uncertainty in $T_{||}$. Note that for 90% of the data in this thesis, this effect is less than the 10% uncertainty in the temperature measurement. The fractional density change is $\epsilon$, which gives an uncertainty to the relaxation rate of about 5% or less in most cases.

### Time dependence of $T_{||}$ due to compressional heating

To calculate the amount of heating caused by sinusoidally modulating the plasma length, we assume that

$$T_{||}(t) = T_{||}(0)\,\exp(\alpha t)\,[\,1 + |\Delta'|\sin(\omega t + \theta')\,] \tag{5.11}$$

where $|\Delta'| \ll 1$, $\alpha\omega^{-1} \ll 1$ and use Eqs. 5.2 and 4.7 to solve for $\alpha$. The procedure is to expand $T_{||}$ and $T_{\perp}$ in terms of $\epsilon$, keeping terms only to order $\epsilon^2$, and then solving for $\alpha$, $\theta'$ and $|\Delta'|$. To order $\epsilon$, one finds that $T_{||}$ and $T_{\perp}$ vary only sinusoidally in time. One therefore expects $\Delta'$ to be of order $\epsilon$ and $\alpha$ of order $\epsilon^2$. Expanding $\exp(\alpha t)$ for $\alpha t \ll 1$, one finds from Eq. 5.11 that

$$\frac{dT_{||}}{dt} = T_{||}(0)\,[\,\omega|\Delta'|\cos(\omega t + \theta') + \alpha + \vartheta(\epsilon^3)\,]. \tag{5.12}$$

Averaging this over one cycle gives

$$\left\langle \frac{dT_{||}}{dt} \right\rangle_{\text{cycle}} = \alpha T_{||}(0). \tag{5.13}$$

From this one concludes that $|\Delta'|$ and $\alpha\omega^{-1}$ are small as long as $\epsilon$ is small. Later (see section 5.2.2), we will estimate $dT_{||}/dt$ and average over a cycle to obtain $\alpha$.

### $T$ and $n$ do not depend on radius, $T$ and $n$ are repeatable from shot to shot, the plasma lifetime is long, and all electrons have the same $\epsilon$

When modelling how the relaxation rate measurement works, we will assume that the temperature and density are independent of radius. In the actual experiment it is known that the density is a function of radius (see section 3.7). The temperature's radial dependence is not known and depends on the radial energy transport time of the plasma which is also unknown, experimentally or theoretically.

Lack of knowledge of the radial energy transport time contributes the largest uncertainty to the measured relaxation rates. In section 5.5 we analyze the relaxation rate measurement, using density profile similar to that in Fig. 3.7, for two cases: zero radial energy transport and infinitely fast radial energy transport. We argue that this should put a lower and upper limit on the relaxation rate uncertainty.

It takes many shots to measure the relaxation rate. During each shot, only the temperature or density of the plasma can be measured. This means that the temperature and density must be repeatable from shot to shot in order for the relaxation rate measurement to work. The repeatability of the temperatures and densities for the plasmas studied in this thesis was about 97%. This adds about 3% uncertainty to the measured relaxation rates.

To measure the relaxation rate, the compressional heating is applied to the plasma for about 10 sec. During this time the plasma density is changing by at most 3% due to transport process. This density change adds an uncertainty of about 3% to the measured relaxation rate.

There is also a correction to the heating due to the fact that each electron has a different $\epsilon$ (see Eq. 5.3). There are two reasons why $\epsilon$ is not the same for each electron: 1) the plasma length and the amount of length change due to the modulated voltage is different for different radii, and 2) the length and the amount of length change due to the modulated voltage depend on an electron's velocity for a given radius. The latter condition is caused by the end sheaths, and will most likely be a problem only at high temperatures (i.e. $T \gtrsim 10^3$ K). Note that when $\epsilon$ is a function of an electron's velocity, the distribution function in $v_{||}$ is no longer a Maxwellian during a modulation cycle.

### The plasma is treated as an ideal gas

The derivation of Eq. 5.2 assumes that the electrons are uncorrelated (i.e. $\Gamma \ll 1$ where $\Gamma = (e^2/k_B T)(4\pi n/3)^{1/3}$), and the ideal gas equation of state is used, $p = nk_B T$. For most of the data presented here, this is a valid assumption; however, a few of the points were taken with a $\Gamma \approx 0.1$. One might wonder if correlations contribute much to the equation of state when $\Gamma \approx 0.1$. To estimate the correction to the equation of state, we will follow along the lines of Dubin and O'Neil [16].

Here we will treat the case in which the expansion is one-dimensional and the plasma is assumed to be thermally isolated so that the plasma entropy is conserved. This is equivalent to setting $dT_\perp/dt = 0$ in Eq. 5.2 and allowing no other forms of external heating. However, external work applied to the plasma can change the kinetic energy of the plasma (see page 44 in reference [34]). Conservation of entropy can be written as

$$\log\left(Y^{5/3}\,\Gamma/\Gamma_0\right) = 2\int_{\Gamma_0}^{\Gamma} \frac{C_{\rm ocp}(\Gamma')}{\Gamma'} d\Gamma', \tag{5.14}$$

where $C_{\rm ocp}$ is the specific heat at constant density for a classical one component plasma (OCP). An OCP is a system of like-point charges embedded in a rigid neutralizing background charge and has been shown to be equivalent to pure electron plasmas trapped in a CV (or similar) trap [38]. If $C_{\rm ocp} = 0$, uncorrelated plasma, then for the plasma parameters in CV, $Y \approx V/V_0$, and conservation of entropy, Eq. 5.14, gives

$$\left(\frac{V}{V_0}\right)^{5/3}\left(\frac{\Gamma_0}{\Gamma}\right) = \left(\frac{V}{V_0}\right)^{2}\left(\frac{T}{T_0}\right) = 1. \tag{5.15}$$

This is Eq. 5.2 with $\nu = 0$ and $T = T_{||}$.

For $\Gamma \ll 1$, $C_{\rm ocp} \approx (\sqrt{3}/4)\,\Gamma^{3/2}$ so that conservation of entropy gives

$$\left(\frac{V}{V_0}\right)^{2}\left(\frac{T}{T_0}\right) = 1 + \frac{5}{2\sqrt{3}}\,\Gamma_0^{3/2}\,\epsilon^{\pm}, \tag{5.16}$$

where $\epsilon^{\pm} = (V - V_0)/V_0$. Letting $\Gamma = 0.1$ and $|\epsilon^{\pm}| = 0.1$, one finds that this correction

is indeed small ($\approx .3\%$) and thus will be ignored in further calculations. That is, we will use $p = nk_{\rm B}T$ as the equation of state for a plasma in CV.

### 5.2.2 Compressional Heating Model

Writing $T_{\|}(t)$ as given by Eq. 5.11 and using the assumptions in section 5.2.1, we solve for the average heating rate per cycle $\alpha$. We start with the following equations,

$$\frac{dT_{\perp}}{dt} = \nu\,(\,T_{\|} - T_{\perp}\,) \tag{5.17}$$

and

$$\frac{d(T_{\|} + 2\,T_{\perp})}{dt} = -2\,T_{\|}\,\frac{dl/dt}{l}. \tag{5.18}$$

Next we write $l$ as

$$l = l_0[\,1 + \epsilon\sin(\omega t)\,] = l_0\left[1 + \epsilon\left(\frac{e^{i\omega t} - C.C.}{2\,i}\right)\right], \tag{5.19}$$

where C.C. means complex conjugate. To order $\epsilon^2$ one then obtains

$$\frac{dl/dt}{l} = \epsilon\,\omega\left(\frac{e^{i\omega t} + C.C.}{2}\right)\left[1 - \epsilon\left(\frac{e^{i\omega t} - C.C.}{2i}\right)\right]. \tag{5.20}$$

Writing $T_{\|}$ and $T_{\perp}$ as an expansion in $\epsilon$,

$$T_{\|} = T_{\|}^{(0)} + \epsilon T_{\|}^{(1)} + \epsilon^2 T_{\|}^{(2)} + \vartheta(\epsilon^3) \tag{5.21-a}$$

and

$$T_{\perp} = T_{\perp}^{(0)} + \epsilon T_{\perp}^{(1)} + \epsilon^2 T_{\perp}^{(2)} + \vartheta(\epsilon^3) \tag{5.21-b}$$

one finds that, to order $\epsilon^0$ in Eq. 5.17 and Eq. 5.18,

$$\frac{dT_{\perp}^{(0)}}{dt} = \nu\,(\,T_{\|}^{(0)} - T_{\perp}^{(0)}\,) \tag{5.22}$$

and

$$\frac{d(T_{\|}^{(0)} + 2T_{\perp}^{(0)})}{dt} = 0. \tag{5.23}$$

Since we take $T_{\|}(t=0) = T_{\perp}(t=0)$, this has the trivial solution,

$$T_{\|}^{(0)} = T_{\perp}^{(0)} = T^{(0)} \tag{5.24}$$

To order $\epsilon^1$ one gets

$$\frac{dT_{\perp}^{(1)}}{dt} = \nu\,(\,T_{\|}^{(1)} - T_{\perp}^{(1)}\,) \tag{5.25}$$

and

$$\frac{d(T_{\|}^{(1)} + 2T_{\perp}^{(1)})}{dt} = -2\,\omega\,T^{(0)}\left(\frac{e^{i\omega t} + C.C.}{2}\right). \tag{5.26}$$

Integrating Eq. 5.26 gives

$$T_{\|}^{(1)} + 2\,T_{\perp}^{(1)} = -2\,T^{(0)}\left(\frac{e^{i\omega t} - C.C.}{2i}\right). \tag{5.27}$$

Solving for $T_{\|}^{(1)}$ and substituting into Eq. 5.17 gives

$$\frac{dT_{\perp}^{(1)}}{dt} = -3\,\nu\,T_{\perp}^{(1)} - 2\,\nu\,T^{(0)}\left(\frac{e^{i\omega t} - C.C.}{2i}\right). \tag{5.28}$$

Letting

$$T_{\perp}^{(1)} = T^{(0)}\left(\frac{\Delta\; e^{i\omega t} - C.C.}{2i}\right) \tag{5.29}$$

and writing $\Delta = |\Delta|\;\; e^{i\theta}$ one finds that

$$\tan(\theta) = -\frac{\omega}{3\,\nu} = -\beta \tag{5.30}$$

and

$$|\Delta| = \frac{2}{3}\frac{1}{\sqrt{1+\beta^2}}. \tag{5.31}$$

One can now solve for $T_{\|}^{(1)}$,

$$T_{\|}^{(1)} = T^{(0)}\left[\frac{\omega}{\nu}\left(\frac{\Delta\; e^{i\omega t} + C.C.}{2}\right) + \left(\frac{\Delta\; e^{i\omega t} - C.C.}{2i}\right)\right] \tag{5.32}$$

To order $\epsilon^2$ one gets

$$\frac{dT_{\perp}^{(2)}}{dt} = \nu\,(\,T_{\|}^{(2)} - T_{\perp}^{(2)}\,) \tag{5.33}$$

and

$$\frac{d(T_{\|}^{(2)} + 2T_{\perp}^{(2)})}{dt} = -2\omega \left[ T_{\|}^{(1)} - T_{\|}^{(0)} \left( \frac{e^{i\omega t} - C.C.}{2i} \right) \right] \left( \frac{e^{i\omega t} + C.C.}{2} \right). \quad (5.34)$$

Substituting Eq. 5.32 into Eq. 5.34 and time averaging over one oscillation period yields

$$\left\langle \frac{d(T_{\|}^{(2)} + 2T_{\perp}^{(2)})}{dt} \right\rangle_{\text{cycle}} = \frac{4\,\nu\,\beta^2}{1+\beta^2} T_{\|}^{(0)}. \quad (5.35)$$

Using the approximation that

$$\left\langle \frac{dT_{\|}^{(2)}}{dt} \right\rangle_{\text{cycle}} = \left\langle \frac{dT_{\perp}^{(2)}}{dt} \right\rangle_{\text{cycle}}, \quad (5.36)$$

one finally obtains

$$\left\langle \frac{dT_{\|}^{(2)}}{dt} \right\rangle_{\text{cycle}} = \frac{4}{3} \frac{\nu\,\beta^2}{(1+\beta^2)} T_{\|}^{(0)}. \quad (5.37)$$

Thus, to order $\epsilon^2$ the resulting solution is

$$\left\langle \frac{dT_{\|}}{dt} \right\rangle_{\text{cycle}} = \frac{4}{3} \frac{\epsilon^2\,\nu\,\beta^2}{(1+\beta^2)} T_{\|}^{(0)}. \quad (5.38)$$

In Appendix A.4, Eq. 5.38 is rederived with $B_2$ included in Eq. 5.6. In this case the maximum heating per cycle is no longer given by $\omega = 3\nu$. However, this error is estimated to be small for the data in this thesis.

Experimentally, we have tested Eq. 5.38 for two different heating methods. In one method, the number of heating cycles is held fixed. Note that the total heating time for this method depends on $\omega$. In the other method, the total heating time is held fixed. A qualitative difference between these two methods can be seen by integrating Eq. 5.38 for a fixed number of cycles which gives

$$T_{\text{f}} = T_0 \left( 1 + \frac{8\pi}{9} \epsilon^2 N_{\text{t}} \left( \frac{\beta}{1+\beta^2} \right) \right) \quad (5.39)$$

where $T_0$ ($T_{\text{f}}$) is the initial (final) temperature and $N_{\text{t}}$ is the number of heating cycles. Recall that the formula for $dT/dt$ is only valid for a time which is less than

$\alpha^{-1} = 3(1+\beta^2)/(4\nu\epsilon^4\beta)$ (see Eq. 5.13). The important feature about this equation is that it peaks when $\beta = 1$ (i.e. $\omega = 3\nu$). On the other hand, if one heats for a fixed time, then Eq. 5.38 integrates to

$$T_f = T_0 \left(1 + \frac{4}{3}\epsilon^2 (\nu t_h) \left(\frac{\beta^2}{1+\beta^2}\right)\right) \tag{5.40}$$

where $t_h$ is the total heating time. Note that this equation peaks for $\beta \to \infty$. Thus, by measuring the peak heating when heating for fixed number of cycles versus $\beta$ (i.e. $\omega$), one can determine $\nu$; whereas, measuring the peak heating when heating for a fixed time gives no information about[2] $\nu$.

Figure 5.1 is a plot of $T_f$ versus frequency (i.e. $f = \omega/(2\pi)$) when the number of heating cycles is held fixed. Figure 5.2 is a plot of $T_f$ versus frequency when the heating time is held fixed. Both figures show qualitative agreement with the heating model (i.e. Eq. 5.39 for Fig. 5.1 and Eq. 5.40 for Fig. 5.2). In both figures, the solid line is a plot of Eq. 5.38 numerically evaluated with the relaxation rate recalculated after each heating cycle from Eqs. 2.11 and 2.12. In other words, the solid lines are plots of Eq. 5.39 and Eq. 5.40 except that the relaxation rate is recalculated after each heating cycle to include the fact that the average temperature is changing, which changes the relaxation rate. Also included in the model for the solid lines is the important effect of cooling from cyclotron radiation.

The experimental parameters for the data in Figs. 5.1 and 5.2 are $n \approx 7 \times 10^8$ e/cm$^3$, $B = 61.3$ kG, $T_0 = 1364$ K. In Fig. 5.1 $N_t = 80$ cycles and in Fig. 5.2 $t_h = 4$ msec. To insure that all the data points get essentially the same amount of energy loss from cyclotron radiation, all $T_f$ were measured 50 msec after the start of

[2]One might guess that letting $\omega \to \infty$ when heating for a fixed time would be the same as letting $\nu = 0$. In fact, this is not the case, as can be seen by writing Eq. 5.40 in terms of $\omega$,

$$T_f = T_0 \left(1 + \frac{4\pi}{3}\epsilon^2 (\nu t_h) \left(\frac{\omega^2}{(3\nu)^2 + \omega^2}\right)\right).$$

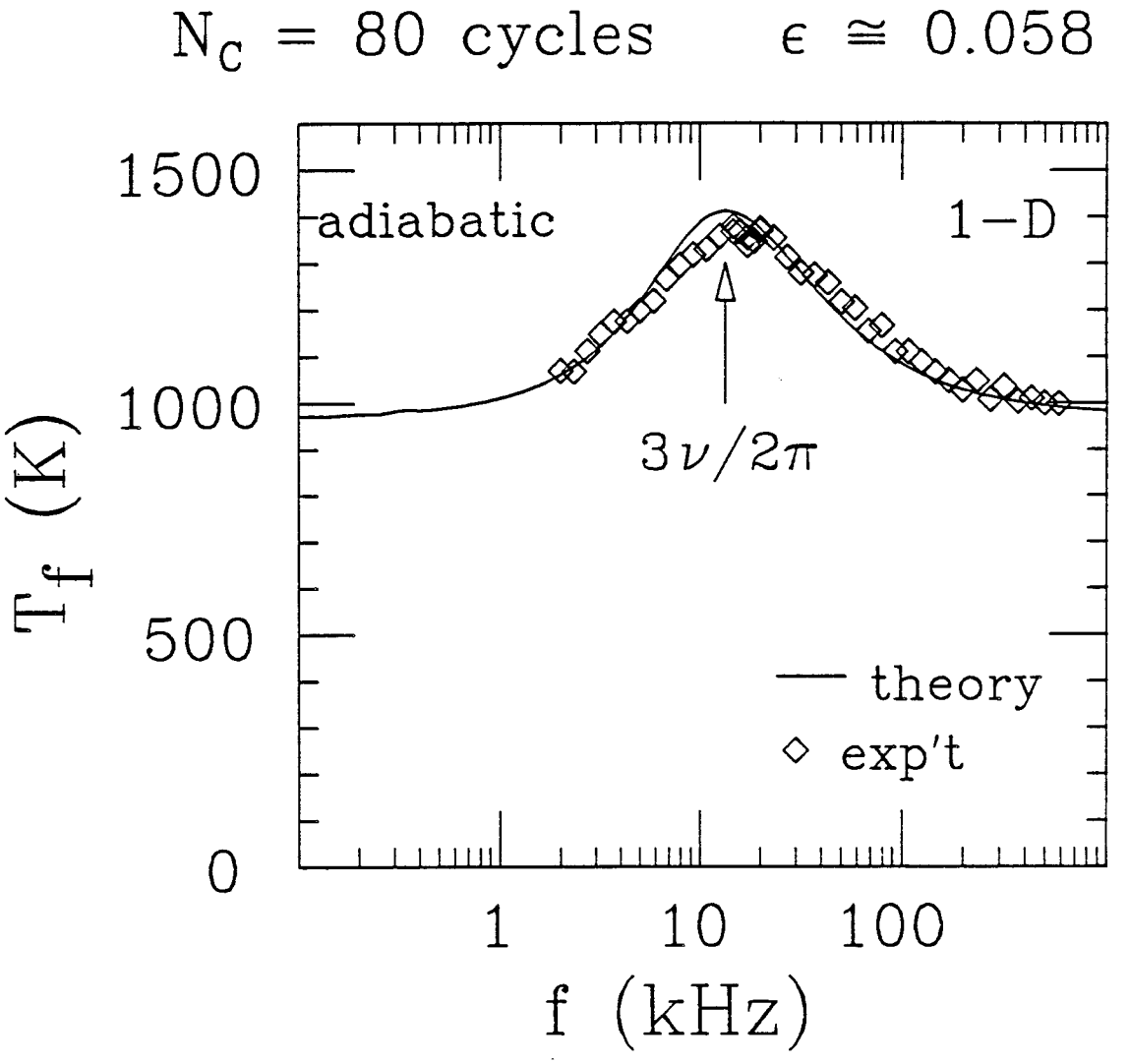


**Figure 5.1:** Final temperature versus frequency of oscillator. Heating fixed number of cycles. The solid line is from theory.

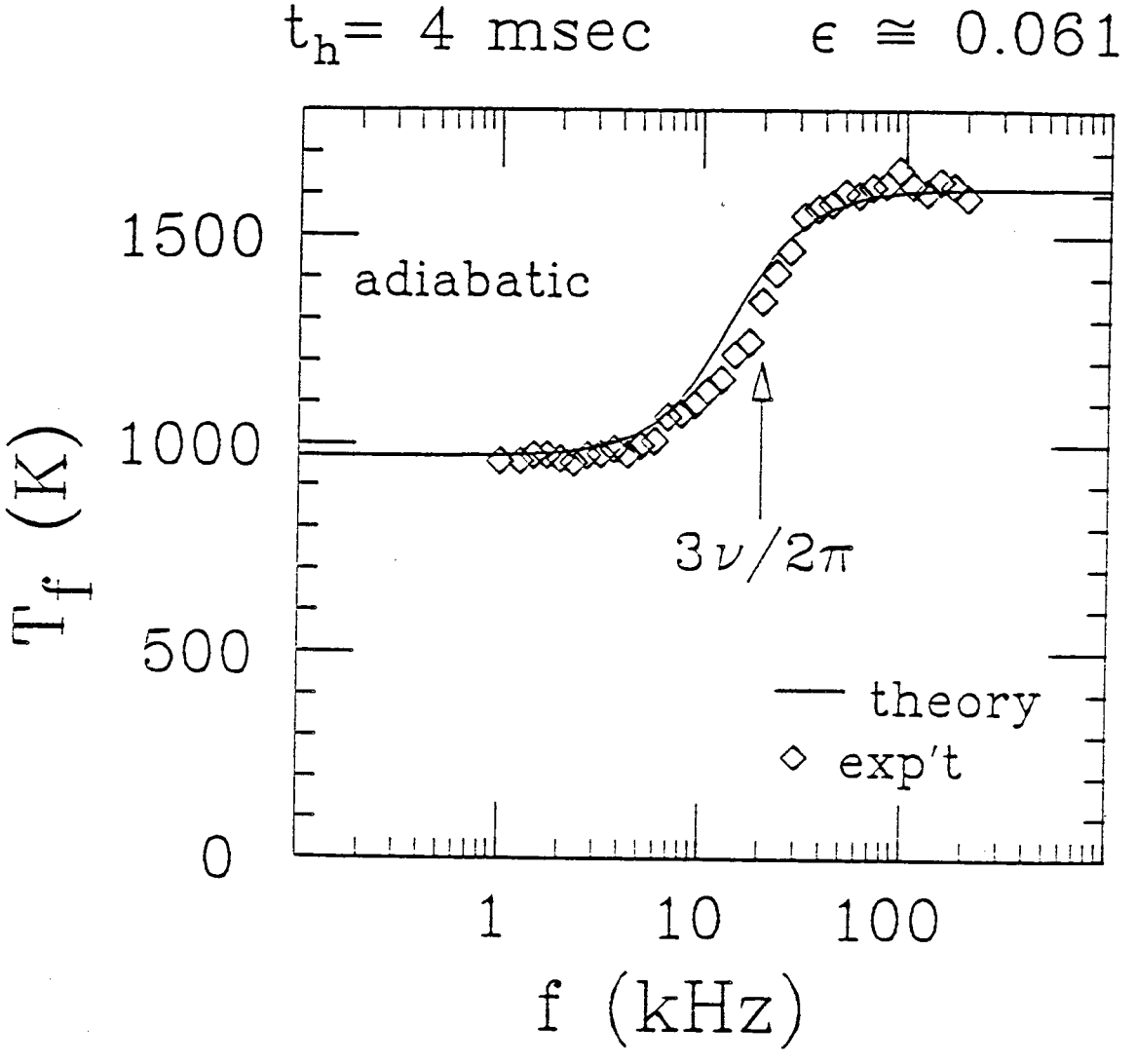


**Figure 5.2:** Final temperature versus frequency of oscillator. Heating for fixed time. The solid line is from theory.

the heating process (independent of $\omega$).

In calculating the relaxation rate there are no free parameters. For Fig. 5.1 the solid line was plotted with $\epsilon = 0.058$ and for Fig. 5.2 an $\epsilon = 0.061$ was used. These values of $\epsilon$ agree well with the value of $\epsilon = 0.056$ obtained from a computer code which determines plasma length given the plasma density and the confinement gate voltages.

## 5.3 Balancing Compressional Heating with Cyclotron Cooling

At this point one could take many experimental points of $T_f$ versus frequency (similar to that in Fig. 5.1) for different $T_0$ and roughly measure $\nu(T)$. We say roughly because $\nu$ is a function of temperature which means that $\nu(T_0)$ may be quite different than $\nu(T_{max})$ ($T_{max}$ is the maximum temperature reached during the heating process). For example, the point in Fig. 5.1 taken at 20 kHz has a $T_f = 1375$ K. Applying 80 cycles at 20 kHz takes 4 msec, so that $T_f$ was not measured until 46 msec after the heating had ceased. Taking into account the radiation cooling, the temperature for the 20 kHz point rises from 1364 K at the start of the heating process to about 1960 K 4 msec later. After another 46 msec, when $T_f$ is measured, the temperature cools to 1375 K. Suppose $\nu \propto T^{-1}$ (from the data we find that $\nu \propto T^{-1}$ for $T \approx 1500$ K), then $\nu(T = 1364\,\mathrm{K})$ will differ by 44% from $\nu(T = 1960\,\mathrm{K})$. Thus, in order to get a good estimate of the relaxation rate from data like that in Fig. 5.1, one must have a reasonable model of $\nu(T)$.

Of course, one could make $T_{max}$ slightly greater than $T_0$ when $\beta = 1$ so that $\nu(T_0) \approx \nu(T_{max})$. However, this makes the peak difficult to measure, especially at low temperatures where the measured temperatures have large uncertainties. In fact, it was the difficulty in determining the relaxation rates at low temperatures which led

us to modify the relaxation rate measurement from merely a simple heating process.

The modified procedure is to allow cyclotron cooling to balance the compressional heating, as given by Eq. 5.39, when $\beta = 1$. Heating for a fixed number of cycles is done because it produces maximal heating when $\beta = 1$. When $\beta \neq 1$, holding all other parameters fixed, cyclotron cooling will dominate the compressional heating, and the plasma temperature will drop. This effect can already be seen in Fig. 5.1, where $T_0 = 1364\,\mathrm{K}$ and most of the points lie below this temperature. To make the effect much more drastic, the total number of heating cycles is increased so that the plasma is heated for many radiation times. This results in a large difference between the final temperature, $T_\mathrm{f}$ and the initial temperature, $T_0$ unless the heating and cooling powers are approximately equal. However, to insure that the cooling time is the same for each $\omega$ while holding the total number of cycles constant, the cycles are produced in sets like those shown in Fig. 5.3[3].

In Fig. 5.3, $N_\mathrm{c}$ is the number of cycles per set and the set repetition rate is $t_\mathrm{s}^{-1}$. To insure that no sets overlap, we keep $N_\mathrm{c}/f_\mathrm{min} < t_\mathrm{s}$, where $f_\mathrm{min}$ is the minimum frequency used. Finally, $t_\mathrm{s}$ is made much smaller than the radiation time. This reduces the error which is due to the fact that the plasma is overheated. The overheating is needed to compensate for the radiation cooling that occurs during $t_\mathrm{r}$ where $t_\mathrm{r}$ is the time during each set when the heating is off, and is a function of $\omega$. For example, in Fig. 5.1 it was pointed out that $T_0 = 1364\mathrm{K}$, and that the plasma was actually heated to about 1960 K for the 20 kHz data point. From Fig. 5.1 one finds that the maximal heating occurs near 20 kHz. Once this is known, $f_\mathrm{min}$ can be set to 10 kHz, $N_\mathrm{c}$ to 40 cycles and $t_\mathrm{s}$ to 4 msec. At 20 kHz it takes 2 msec to apply 40 cycles so that the plasma cools for 2 msec between cycles. If 20 kHz is found to give

[3]One might reason that heating for a large fixed number of continuous cycles, versus applying the cycles in sets, would also work. The problem with this procedure can be demonstrated by letting $\omega \to \infty$ (i.e. $\beta \to \infty$). In this limit Eq. 5.39 predicts no heating. However, holding the number of cycles fixed and allowing $\omega \to \infty$ means that the heating time goes to zero. This, in turn, gives no time for cooling so that $T_\mathrm{f} = T_0$, independent of $\epsilon$ and $N_\mathrm{c}$.

maximal heating, then for $f = 20\,\mathrm{kHz}$ we adjust $\epsilon$ so that the temperature at the start of each cycle is the same. This implies that $T_{\max} \approx T_0 \exp(2\,\mathrm{msec}/\tau_r)$ where $\tau_r$ is the radiation time. For $B = 60\,\mathrm{kG}$, $\tau_r \approx 130\,\mathrm{msec}$, so that the temperature varies by about 2% at 20 kHz. In general, this error is about $(\exp(t'_r/\tau_c) - 1)$ where $\tau_c$ is the cooling time[4], $t'_r = (t_s - N_c/f_{\max})$ and $f_{\max}$ is the frequency that produces maximum heating. In Appendix A.8, $t'_r/\tau_r$ is given for each data point ($\tau_r$ is most likely smaller than $\tau_c$ and will therefore overestimate $T_{\max}$).

Figure 5.4 shows a plot of final temperature, $T_f$, versus frequency when the multiple heating scheme is implemented. If we measure the final temperature a time $t_s$ after the start of the last heating set (see figure 5.3), then the maximum temperature should be $T_0$ (when $\epsilon$ is properly adjusted). However, the actual temperature is measured a time $t_s + t_m$ after the start of the last heating set; consequently, the maximum temperature will be less that $T_0$ and is called the matching temperature, $T_{\mathrm{match}}$. Typically $t_m$ is about 20 msec. For this data, $N_c = 24$, $N_s = 301$ ($N_s$ is the number of sets; the total number of cycles is $N_t = N_c \times N_s = 7224$), $t_s = 5\,\mathrm{msec}$, $n \approx 7 \times 10^8\,\mathrm{e/cm^3}$ and $B = 61.3\,\mathrm{kG}$. Note that the heating phase lasts about 1.5 sec (= 5 msec × 301 *cycles*) and is about 10 radiation times. For the diamond points $T_0 = 1130\,\mathrm{K}$ and for the square points $T_0 = 110\mathrm{K}$. Note that each curve is not symmetrical about its own peak, but instead has a sharp edge at the point we take to be $\omega = 3\,\nu$. The same shape of $T_f$ versus frequency is seen in computer simulations of the heating process where the relaxation rate is calculated from theory. This $T_f$ versus frequency profile gives more information about the relaxation rate than just its value at $T_0$.

To explain the shapes of the curves in Fig. 5.4, we will focus on the data

[4]Note that here we have injected the phrase "cooling time" instead of "cyclotron cooling time". The argument above does not depend on the cooling process being cyclotron cooling. In general, any cooling process (or combination of cooling and heating) will work as long as it does not depend on $\omega$ (and the cooling dominates).

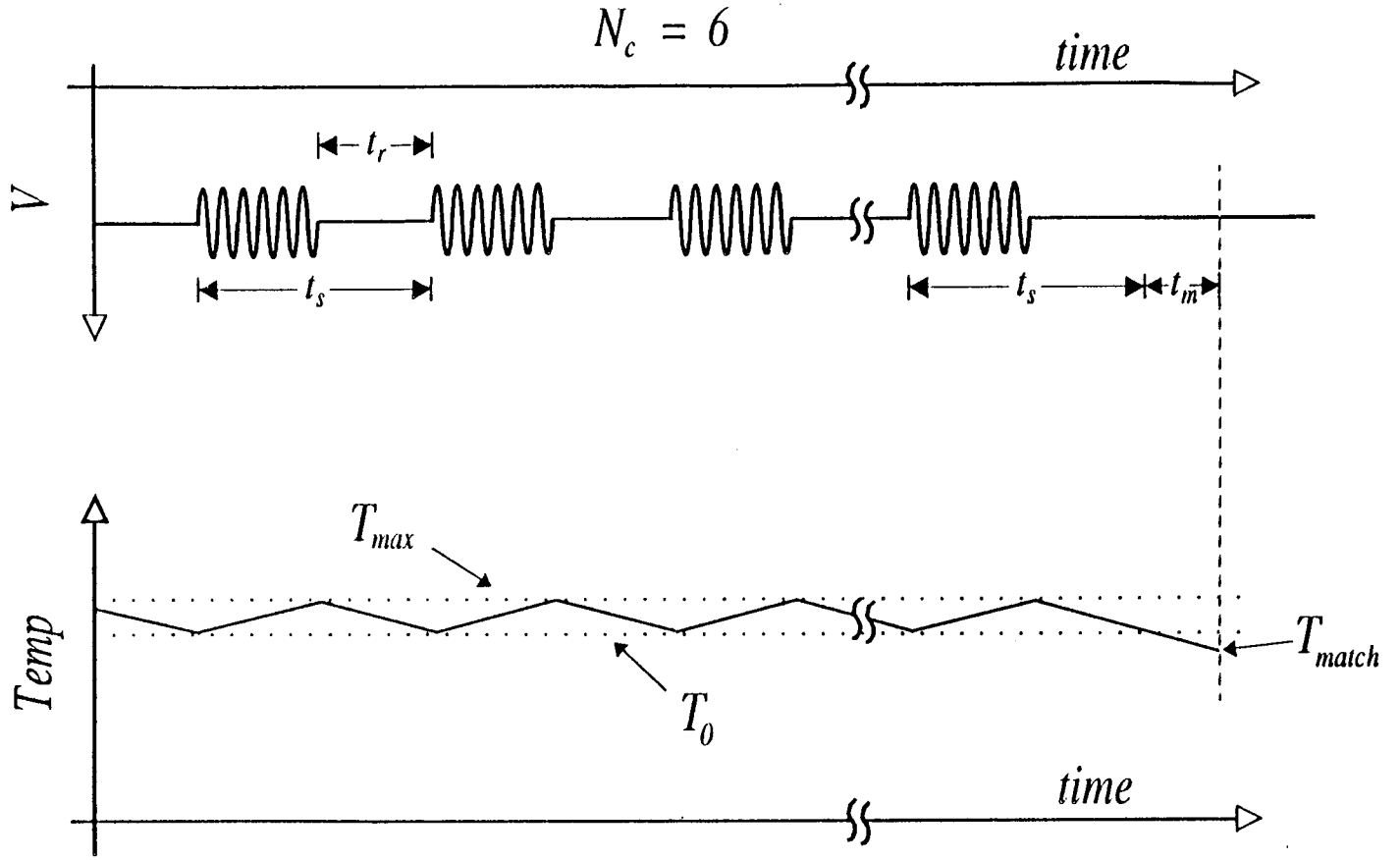


**Figure 5.3:** The top part of the figure is a schematic of the multiple heating scheme. The bottom part of the figure shows the temperature as a function of time when $\beta = 1$.

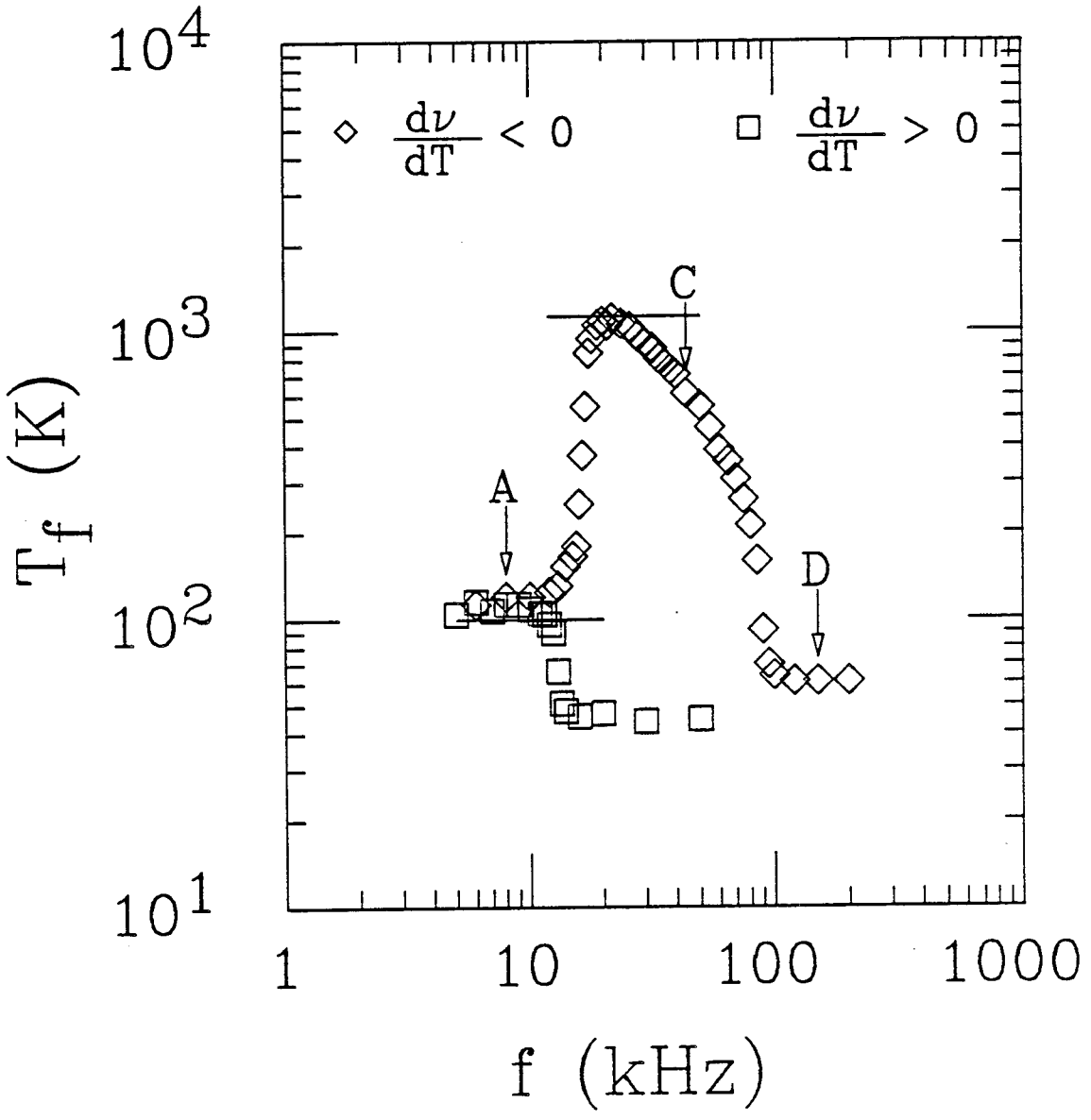


**Figure 5.4:** Final temperature, $T_f$, versus frequency of oscillator. Heating with many sets of fixed numbers of cycles. The diamond points are for $T_0 = 1130$ K and the square points are for $T_0 = 110$ K. The two horizontal lines mark $T_{\text{match}}$

taken with $T_0 = 1130\,\mathrm{K}$. Similar arguments explain the shape of the curve with $T_0 = 110\,\mathrm{K}$. Consider what happens to the point marked $C$. At the beginning of the heating cycle $T = 1130\,\mathrm{K}$. Data point $C$ has $f = 40\,\mathrm{kHz}$ so that at the beginning of the heating phase $\beta \approx 2$ (here we will take $\nu = 42\,\mathrm{kHz}$, or $\beta = 1$ at $20\,\mathrm{kHz}$, which we get from the data). At this $\beta$ cooling dominates heating and the plasma cools ($\epsilon$ has been adjusted so that the heating and cooling balance for $\beta \simeq 1$). As the plasma temperature drops the relaxation rate changes. If $d\nu/dT > 0$ then $\beta$ increases and the plasma cools even faster. If, on the other hand, $d\nu/dT < 0$ then $\beta$ approaches 1 and the cooling rate decreases. If the temperature drops to a value where $\beta \approx 1$, the heating and cooling balance, and the temperature stabilizes. This mechanism prevents the temperature from continuously falling for the points between 20 kHz to 80 kHz, and indicates that $d\nu/dT < 0$ for temperatures near 1000 K.

In general, all points cool until a temperature is reached such that $\beta \approx 1$. However, if the relaxation rate versus temperature has a peak of $\nu_\mathrm{p}$ and one modulates the plasma at angular frequency $\omega > 3\nu_\mathrm{p}$, then $\beta$ is all ways greater than one. For these modulated frequencies the plasma presumably cools to a temperature near 6 K (well below the lowest measurable temperature). For the data in Fig. 5.4 we know that $\nu_\mathrm{p}$ is about 160 kHz, so for points where the modulated frequency is greater than about 80 kHz the plasma should cool to about 6 K. This is presumably what is happening for the point marked $D$; however, the measured temperature is about 60 K which was the limit of the temperature measurement for these data points.

Now consider what happens to the point marked $A$. At the beginning of the heating cycle $T = 1130\,\mathrm{K}$. This point has $f = 8\,\mathrm{kHz}$ so that at the beginning of the heating phase $\beta \approx 0.4$. Again, at this $\beta$ cooling dominates heating, the plasma cools and the relaxation rate changes. Initially, $d\nu/dT < 0$, $\beta$ becomes smaller and the plasma cools even faster. However, at a temperature near 250 K the relaxation

rate peaks, and $\beta$ reaches a minimum value. As the temperature cools further $\beta$ now increases. Finally near 100 K $\beta \simeq 1$, the heating and cooling balance, and the temperature stabilizes.

Arguments similar to the one given above explain the shape of the $T_0 = 110$ K data set. However, note that for the 1130 K data set, the final temperature versus frequency increases sharply to $T_f \simeq 1130$ K, and then falls off slower as the frequency is increased. This is due to the fact that $d\nu/T < 0$ for temperatures near 1130 K. On the other hand, for the 110 K the final temperature versus frequency decreases sharply from $T_f \simeq 110$ K as the frequency is increased past 10 kHz. This is due to the fact that $d\nu/T > 0$ for temperatures near 110 K. Thus, a plot of final temperature versus frequency gives $\nu$, the sign of $d\nu/dT$, and possibly more.

To measure the relaxation rate for a particular temperature, many curves of $T_f$ versus frequency are taken until an $\epsilon$, $\epsilon_{\text{balance}}$, is found such that for a single $T_f$ versus frequency curve, the maximum temperature is approximately $T_{\text{match}}$. To get the relaxation rate to higher accuracy, several curves of $T_f$ versus frequency are taken with slightly different $\epsilon$'s. The $\beta = 1$ point is then determined by estimating where the peak is for each $T_f$ versus frequency curve, drawing a line through the peaks, and measuring the frequency where this line crosses the $T_{\text{match}}$ line. Figure 5.5 shows such a plot for an actual data point with $B = 40.9$ kG and $T_0 = 2700$ K. In Fig. 5.5 two curves of $T_f$ versus frequency are shown; one with a slightly larger $\epsilon$ than is needed to balance the heating with the cooling and one with a slightly smaller[5] $\epsilon$. A curve has been drawn through each set of points to better estimate where the maximums occur. The dashed line in Fig. 5.5 connects the peaks. This line crosses the $T_{\text{match}}$ line at $f \approx 16.5$ kHz with an estimated uncertainty of 5%. In general, the determination of this frequency has an uncertainty of about this amount.

[5] For $d\nu/dT < 0$ a curve of $T_f$ versus frequency with $\epsilon > \epsilon_{\text{balance}}$ underestimates $\nu$ and a curve with $\epsilon < \epsilon_{\text{balance}}$ overestimates $\nu$; for $d\nu/dT > 0$ the inverse occurs.

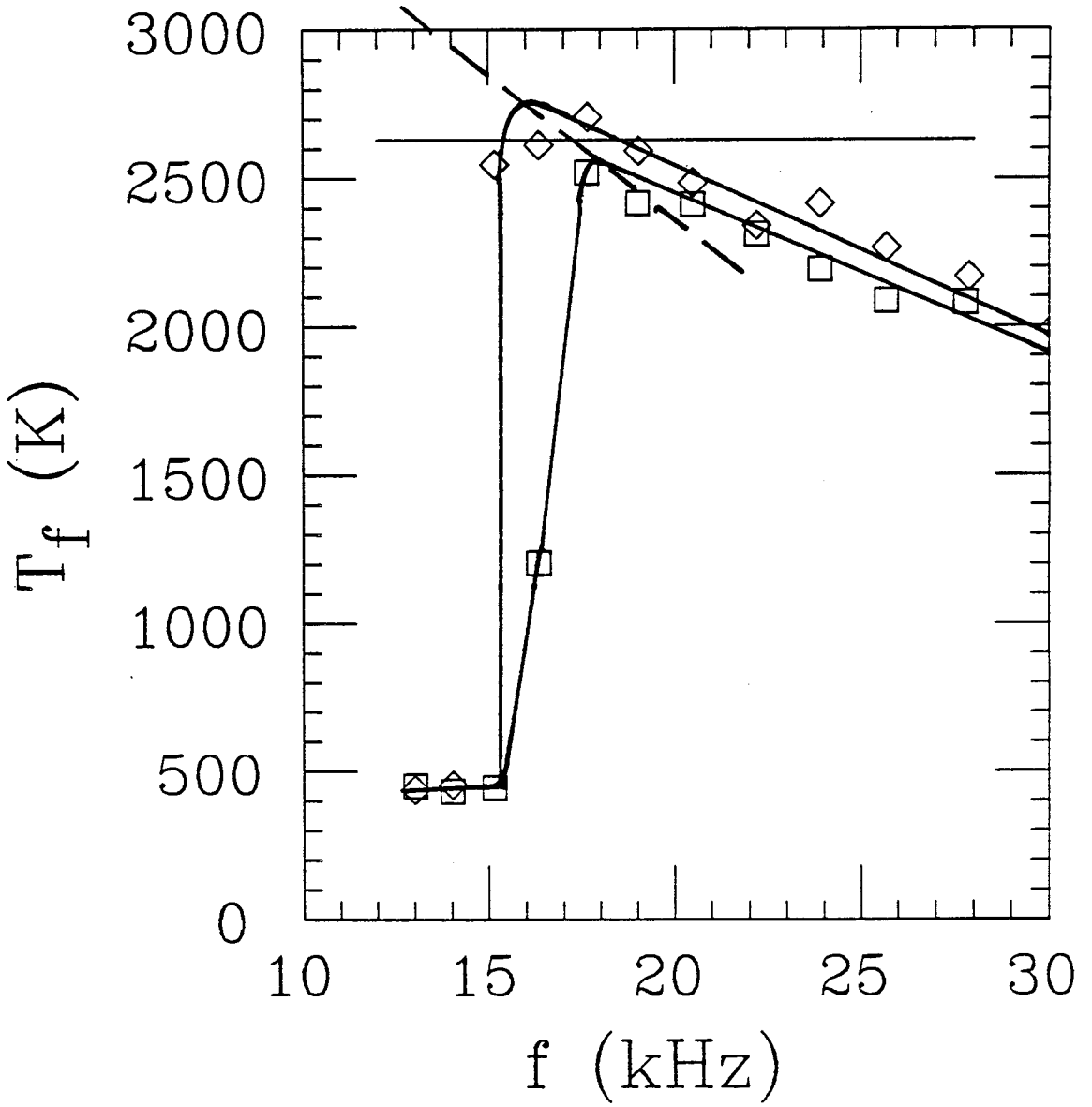


**Figure 5.5:** Final temperature versus frequency of oscillator for two slightly different oscillator amplitudes. The maximum heating frequency is taken to be the frequency where the solid line and the dash line cross.

## 5.4 Experimentally Measured Relaxation Rate

In this section we present plots of the measured relaxation rates and compare these results to theory (see chapter 2). In Appendix A.8, a table of the measured relaxation rates and other relevant data is given, as well as the experimental setup used to take this data.

Figure 5.6 shows experimental points of the relaxation rate versus temperature for three magnetic fields, 30.7, 40.9 and 61.3 kG. For these points the plasma density was[6] $n \approx (8 \pm 1) \times 10^8$ e/cm$^3$. For most of the data in Fig. 5.6 the measured relaxation rate and the associated temperature have errors which are approximately the size of the plotted symbols. However, there are a few points where the measured temperature has a larger error. For these latter points we have added the appropriate error bars.

We find that the relaxation rate peaks near $r_c/b \approx 1$, thus the lower the magnetic field, the lower the temperature at which the peak occurs. Also, for the same density, the lower the magnetic field, the higher the peak in the relaxation rate. In Fig. 5.6 we see that the relaxation rate decreases rapidly as the temperature decreases below the point $r_c/b \sim 1$. This behavior is consistent with a recent theoretical prediction of O'Neil-Hjorth, who argue that the collisional dynamics is constrained by a many electron adiabatic invariant in the regime $r_c/b \ll 1$ (see section 2.3.2).

In Fig. 5.7 we have plotted the data taken at a magnetic field of 61.3 kG. Here we compare the data with several theories. There are no free parameters in the theoretical curves; we use the average density on the plasma inside the radius $r_1$ to calculate the theories. Note that on the bottom abscissa we have plotted the temperature and on the top abscissa we have plotted $r_c/b$. The solid line is a plot of the predicted relaxation rate as calculated by O'Neil-Hjorth where we have used

[6] Average density as measured on the central collector (see section 3.7).

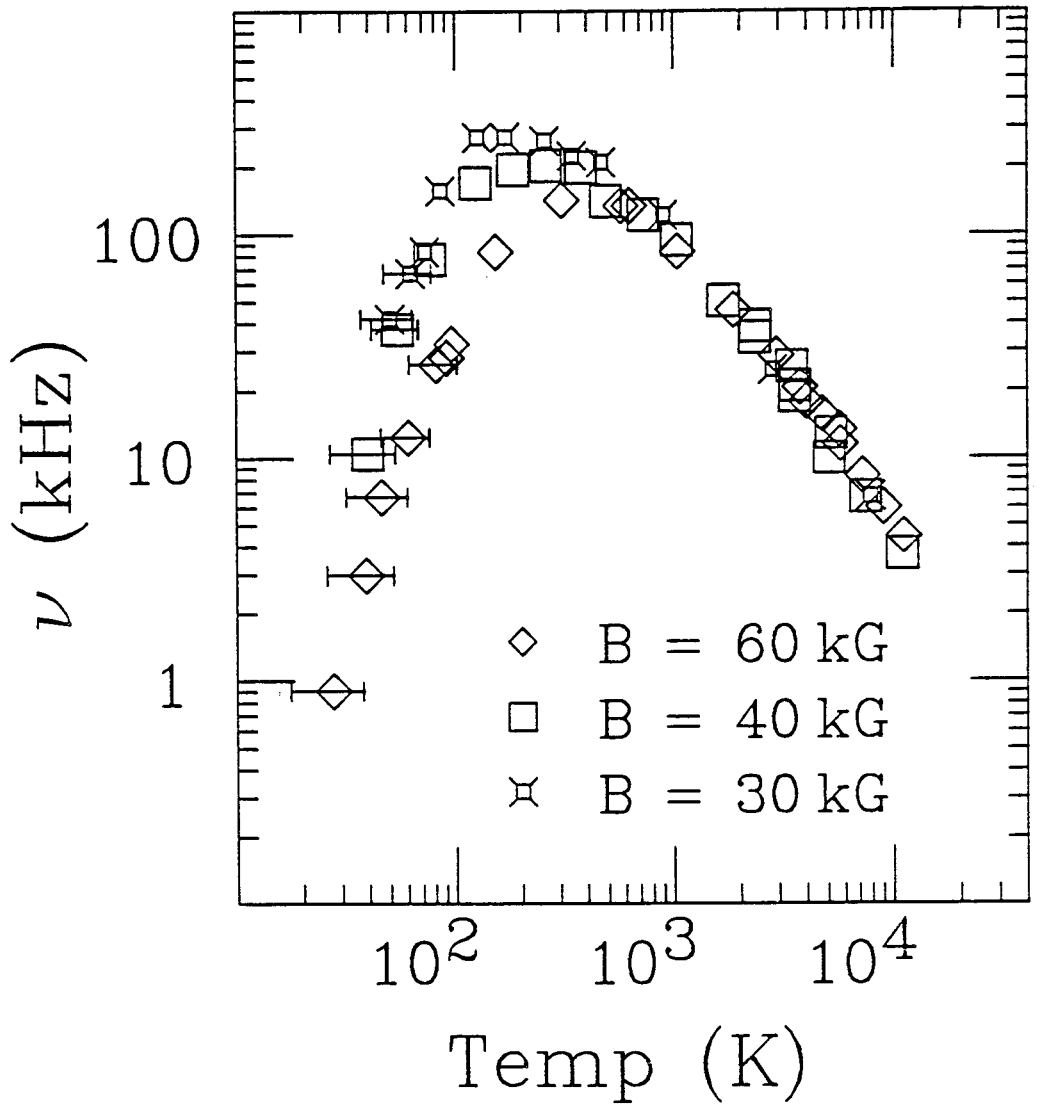


**Figure 5.6:** The measured relaxation rate for three different magnetic fields (61.3 kG, 40.9 kG and 30.7 kG. The central plasma density was about $8 \times 10^8$ e/cm$^3$.

Eq. 2.20 for $\bar{I}$.

The dashed line is a plot of the relaxation rate calculated from a Fokker-Planck equation where $r_c$ is used instead of $\lambda_D$ as the maximum impact distance. That is, Eq. 2.12 is used to calculate $\bar{I}$. In the regime where this theory is expected to be valid we find good agreement between the experimental data and theory. The dash-dotted line is a plot of the Fokker-Planck theory where $\lambda_D$ is used as the maximum impact distance. Note that for this data $\lambda_D/r_c \simeq 600$. Figure 5.7 clearly demonstrates that for mixing of perpendicular and parallel energies, the coulomb interaction is effectively cut off at a distance of about $r_c$ and not $\lambda_D$ when $\lambda_D \gg r_c$.

As was argued in section 2.3, all points of the relaxation rate should lie on a single curve if normalized as $\nu/(nb^2v_T)$ and plotted versus $r_c/b$. Figure 5.8 is a plot of all the experimentally measured relaxation rates normalized by $nb^2v_T$ and plotted versus $r_c/b$. The solid line is a plot of the O'Neil-Hjorth prediction (where $\bar{I}$ is calculated from Eq. 2.20) which is valid for $r_c/b \ll 1$. The dash line is a plot of the Fokker-Planck prediction with $r_c$ as the coulomb cutoff distance (i.e. $\bar{I}$ is calculated from Eq. 2.12). This prediction is valid when $r_c/b \gg 1$. The '$\odot$' points are from numerical simulations done by Hjorth [23, 24]. Hjorth placed 50 electrons in a box of volume $L^3$ (i.e. $-L/2 < (x, y, z) < L/2$) and followed their exact orbits, including their gyromotion. He started the electrons with a bi-Maxwellian distribution, that is $T_\perp/T_{||} = 0.2$, and computed the subsequent relaxation rate.

## 5.5 Error Analysis for the Relaxation Rate

In this section we will estimate the errors in the measured relaxation rate. The main error is believed to be due to the radial variations in the density. If the density is not constant, we must determine which density is appropriate (i.e. average density, central density, etc.). There is an added error if $\epsilon$ is a function of radius (i.e.

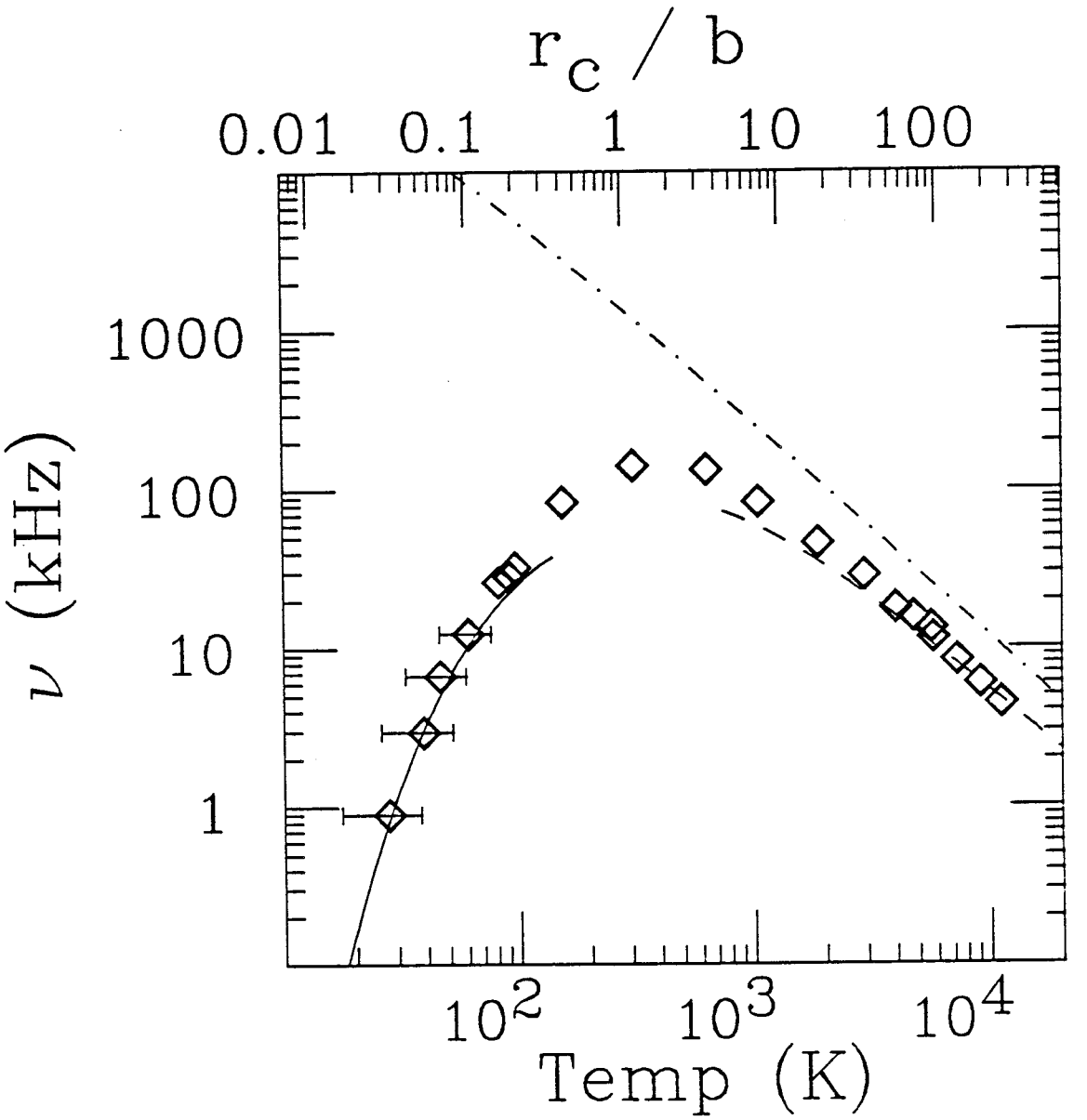


**Figure 5.7:** The measured relaxation rate taken at 61.3 kG compared with several theories. The solid curve is the O'Neil-Hjorth prediction valid for $r_c/b \ll 1$. The dash curve is a Fokker-Planck prediction with $r_c$ as the cutoff distance. The dot-dash curve is the Fokker-Planck prediction with $\lambda_D$ as the cutoff distance.

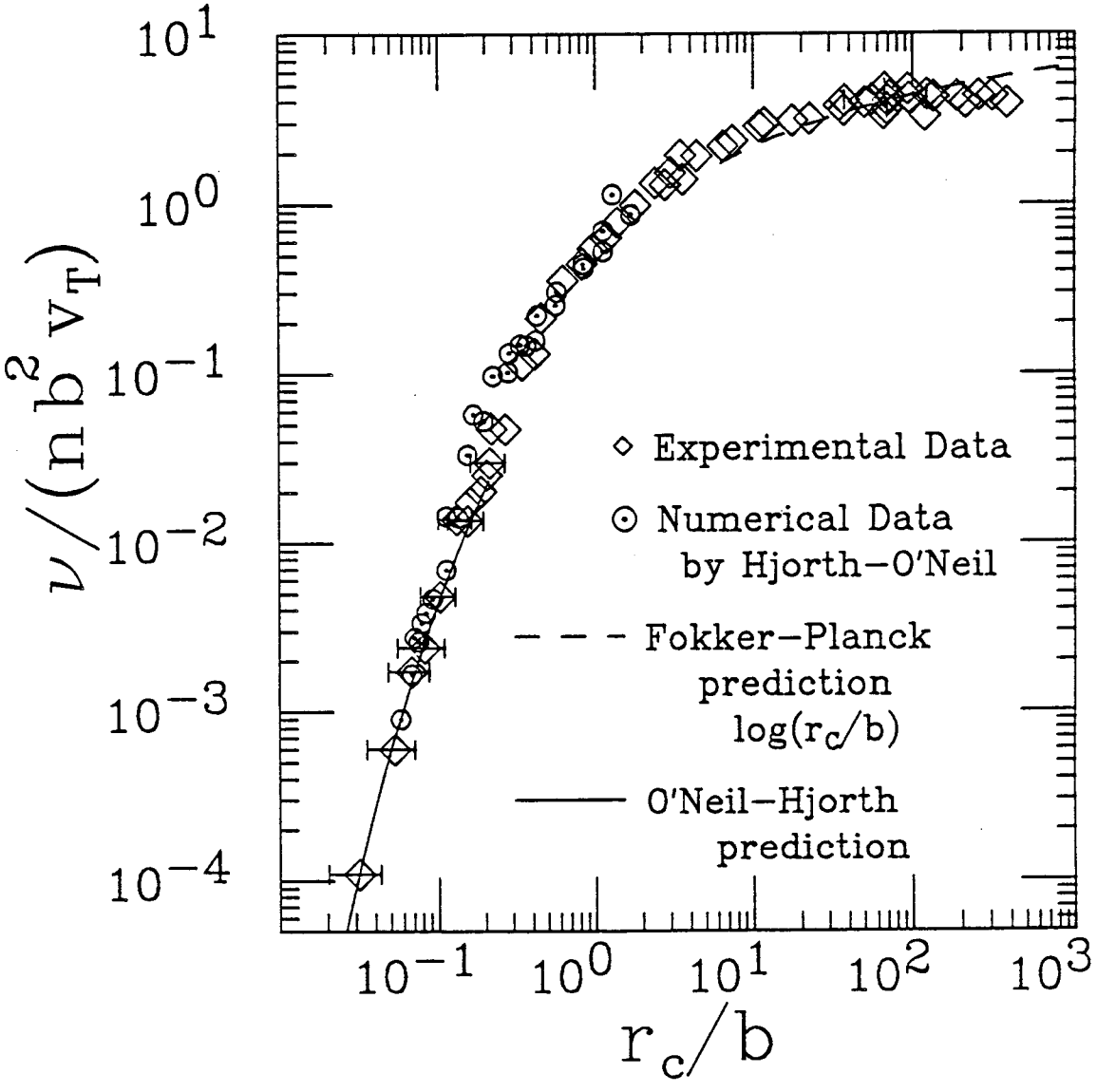


**Figure 5.8:** All the experimental relaxation rate data normalized by $n\,b^2\,v_T$ and plotted versus $r_c/b$. The solid curve is the O'Neil-Hjorth prediction valid for $r_c/b \ll 1$. The dash curve is a Fokker-Planck prediction with $r_c$ as the cutoff distance. The '⊙' points are the relaxation rates determined by Hjorth from numerical simulations.

some radii will do more heating than other radii). For temperatures near $10^4$K, there is the added problem that an electron's bounce length will depend on its velocity. This may cause $\epsilon$ to be a function of electron velocity.

All of this is complicated by the radial energy transport time, which is unknown (see section 4.5). In particular, if electrons at a particular radius are heated more than other electrons, is the energy transport times short so that the whole plasma is at the same temperature, or is a hot spot created in the plasma which will give an error to the measured temperature (see section 4.4.2). A general analysis of this problem is too complicated. We will therefore restrict the analysis to two cases which are easier to analyze and hope that the real answer lies somewhere between them. The two cases are 1) a very slow radial energy transport time and 2) a very fast radial energy transport time. The conclusion of this analysis is that the density we use in comparing our experimental results to theory generally has an uncertainty of about 20%. At low temperatures the measured temperatures have uncertainties of about 30%.

Until now we have ignored the $z$ variations in the density. From Figs. 3.6 and 3.7, one finds that the density depends on $z$, especially at high temperatures and at large radii. For a given radius, the relaxation rate measurement measures the average relaxation rate is given by

$$\langle \nu(r) \rangle = \int \nu(r,z) n(r,z)\, dz / \int n(r,z)\, dz. \tag{5.41}$$

This average is straightforward to calculate since $\nu$ can be written as $\nu(r,z) = n(r,z)g(T)$ where $g(T)$ is the temperature dependent part of the relaxation rate.[7] This gives

$$\langle \nu(r) \rangle = g(T) \int n^2(r,z)\, dz / \int n(r,z)\, dz = g(T)\, \langle n(r) \rangle, \tag{5.42}$$

[7]In general, $g(T)$ may depend on other quantities (e.g. magnetic field), but not on the plasma density. For simplicity, we show explicitly only the temperature dependence.

where $\langle n(r) \rangle$ is the average density at radius $r$.

Note the subtlety of this simple result. As an electron travels along $z$, it enters the sheath at the ends. In the sheaths, the total potential is changing in such a way that it slows the electron down (i.e. $v_{\|}$ is decreasing). Since the velocity scattering rate for a single electron depends on $v_{\|}$, the actual amount of scattering that a single electron does may be very complicated. This is especially true at high temperatures, where the sheaths are long. Since we assume that the plasma is in thermal equilibrium along a field line with temperature $T$, the distribution in $v_{\|}$ is independent of $z$ except for a normalization factor (i.e. the density) and results in this simple expression for $\langle \nu(r) \rangle$.

Analyzing the data in Figs. 3.6 and 3.7, we find that $\langle n(r) \rangle$ is essentially independent of temperature, except at large radii. Note that at large radii there are very few electrons.

To understand what the relaxation rate measurement measures for very slow radial energy transport times, it is first instructive to consider the low temperature limit. For low temperatures, the temperature measurement uses only the electrons near the axis to determine the temperature (see section 4.4.3). We expect the heating, and thus the temperature, to be fairly constant near the axis. For this case then, the relaxation rate is measured for those electrons near the axis. These electrons have a density about 20% greater than the average density measured using end collector $R_1$.

On the other hand, for high temperatures the measured temperature is the average temperature over $R_1$. Crude numerical calculations indicate that $\epsilon$ is fairly constant over $r_1$, and then increases by about 50% out to $2r_1$. Since we are only measuring the temperature for electrons inside $r_1$ (and we assume that there is no radial energy transport), we will let $\epsilon$ be a constant and assume that the density

variation contributes the largest error. In this case one finds that the heating depends only on $\beta = \omega/(3\nu)$ (see Eq. 5.39).

Suppose at some radius $r_0$ ($0 < r_0 < r_1$), $\beta = 1$ and the cooling and heating balance. For high temperatures $d\nu/dT < 0$. This together with $dn/dr < 0$ implies that for $r < r_0$, $\beta$ is less than 1 and that part of the plasma inside of $r = r_0$ cools (similar to point A in Fig. 5.4 (see section 5.3)). For $r > r_0$, $\beta$ is greater than 1 and the plasma at each radius greater than $r_0$ will cool until $\beta \approx 1$ (similar to point C in Fig. 5.4). Now one must ask, for what value of $r_0$ is the highest temperature measured (this is similar to asking what $\beta$ gives the most heating since we determine the heating by measuring the final temperature). Note that for $r > r_0$ the plasma cools until $\omega/3 = \nu$ and since $\omega$ is the same for each radius we conclude that $\nu(r_0) = \nu(r) = n(r_0)g(T(r_0)) = n(r)g(T(r))$. This implies that if we know $n(r)$, $g(T)$ and $T(r_0)$ then we know $T(r)$ for $r > r_0$. Using Eq. 4.42 to calculate $\langle 1/T \rangle$ and estimating $g(T)$ we find that $r_0 = 0$ gives the maximum to $\langle 1/T \rangle^{-1}$ (not too surprising). We conclude from this that the plasma center is the hottest and the temperature decreases with radius. This, given a reasonable model for $g(T)$, leads to a temperature variation which is about $\pm 20\%$ of the measured $\langle 1/T \rangle^{-1}$. Note that if the radial transport time is finite, then, most likely, the temperature error will be less than $\pm 20\%$. Therefore, the largest temperature variation should be for no radial transport, which produces temperature variations of about $\pm 20\%$.

We will now consider the case where the radial energy transport time across the plasma is much faster than the radiation time. For this case the error in the measured temperature is small. Here one needs to balance the total cooling power of the plasma with the total heating power of the plasma and determine that radius which contributes the most heating per cycle, $E_c$.

$$E_c \propto \int \epsilon^2 \left( \frac{\beta}{1+\beta^2} \right) n(r)\, l(r)\, r dr. \tag{5.43}$$

Using $n(r)$ and $N_l(r) = n(r)l(r)$ from Figs. 3.7 and 3.5, and the fact that $\epsilon$ appears not to vary too much for the bulk of the plasma, we find that most of the heating occurs at a radius where $n(r) \approx 0.8\,\langle n \rangle$ ( $\langle n \rangle$ is the average density of the electrons that hit $R_1$ when dumped). This is essentially the radius with the most electrons.

From this analysis we conclude that for very slow radial energy transport time the temperature is known to about $\pm 20\%$ and the density is between $\langle n \rangle$ and $1.2\,\langle n \rangle$. For very fast radial energy transport there is little error in the measured temperature and the density will be about $0.8\,\langle n \rangle$. Since we do not know which of these to choose from we combine the error and say that the density and temperature are known to about $\pm 20\%$.

## 5.6 Conclusions

Our measured relaxation rates are consistent with a Fokker-Planck prediction as calculated by Ichimaru and Rosenbluth when $r_c/b \gg 1$, provided that the prediction is modified by the approximation of Montgomery, Turner and Joyce. When $r_c/b \gg 1$ and $\lambda_D \gg r_c$ (recall that $\lambda_D \gg r_c$ for the plasmas studied in this thesis) Montgomery, Turner and Joyce argue that the coulomb interaction is effectively cut off at a distance of $r_c$ instead of $\lambda_D$.

Our results are also consistent with the O'Neil-Hjorth prediction when $r_c/b \ll 1$. O'Neil and Hjorth predict a rapid decrease in the relaxation rate as $r_c/b$ is decreased below about 1. This, as O'Neil [44] has argued, is most likely due to a many electron adiabatic invariant which constrains the exchange of perpendicular and parallel energy. Our results clearly demonstrate that a rapid decrease in the normalized relaxation rate occurs as $r_c/b$ is decreased when $r_c/b \ll 1$.

A recent calculation [19] of the relaxation rate has yielded rates which are about a factor of 4 larger than the O'Neil-Hjorth prediction when $r_c/b \sim 0.01$. This,

however, does not alter the conclusions we have made regarding the experimental data since the measured low temperatures may have systematic errors as large as 30%. We find good agreement between our results and the newly calculated relaxation rates if we reduce the measured low temperatures by 30%.

# Appendix A

# Appendices

## A.1 Cyclotron Radiation Rate Calculation

In this section we calculate the radiation cooling rate for a pure electron plasma immersed in a large magnetic field. This calculation includes quantum effects (i.e. Landau levels), and assumes that the background radiation is in thermal equilibrium with a temperature $T_w$. We assume that the distribution of perpendicular energy is, at all times, described by a Boltzmann distribution with temperature $T_\perp(t)$. The cyclotron radiation causes $T_\perp$ to decrease, assuming $T_\perp > T_w$, toward $T_w$. For the moment we will ignore the electron spin. At the end of this section, we comment on the electron spin and its effect on the radiation rate.

Let $-R(E_\perp)$ be the energy loss rate for an electron with perpendicular energy $E_\perp$. The energy loss rate per electron for a plasma is then

$$k_B \frac{dT_\perp}{dt} = -\int_0^\infty h(E_\perp) R(E_\perp) dE_\perp \tag{A.1}$$

where $h(E_\perp)$ is the perpendicular energy distribution function. Note that we have assumed that $R$ is unaffected by the electron-electron interactions. This is a valid assumption for a CV plasma since an electron's gyro-orbit is essentially unperturbed by an electron-electron collision. This allows one to calculate $R(E_\perp)$ from a single electron Hamiltonian.

For a single electron immersed in a magnetic field, Landau has shown that the Hamiltonian for the coordinates perpendicular to the magnetic field is reducible to a harmonic oscillator Hamiltonian (see reference [32]). The perpendicular energy is then $E_\perp = E_n = \hbar\Omega(n + 1/2)$. This, together with the assumption that $h(E_\perp)$ is a Boltzmann distribution gives

$$k_B \frac{dT_\perp}{dt} = -\sum_{n=0}^{\infty} \exp(-E_n/(k_B T)) R_n \Big/ \sum_{n=0}^{\infty} \exp(-E_n/(k_B T)) \tag{A.2}$$

where the integral has become a sum over possible states of $E_\perp = E_n$ and $R_n = R(E_n)$.

One must now determine $R_n$. First, $R_n$ can be written as

$$R_n = A_n + B_n I(\Omega)\,[1 - \exp(\hbar\Omega/(k_B T))\,] \tag{A.3}$$

where $A_n$ and $B_n$ are the Einstein coefficients for an electron in state $n$. That is, $A_n$ is proportional to the rate at which an electron in state $n$ spontaneously emits a photon and $B_n$ is proportional to the rate at which an electron in state $n$ is stimulated by the background radiation field into emitting a photon. This gives

$$\frac{dT_\perp}{dt} = \frac{-\sum_{n=1}^{\infty} \exp(-E_n/(k_B T))\{A_n + B_n I(\Omega)\,[1 - \exp(\hbar\Omega/(k_B T))\,]\}}{\sum_{n=0}^{\infty} \exp(-E_n/(k_B T))}. \tag{A.4}$$

Since the Einstein coefficients do not depend on the temperature of the plasma, one can evaluate $B_n$ in terms of $A_n$ for any plasma temperature. Choosing the plasma temperature to be $T_w$ is judicious, since the plasma will be in thermal equilibrium with the background radiation field, which implies

$$0 = A_n + B_n I(\Omega)[1 - \exp(\hbar\Omega/(k_B T_w))] \tag{A.5}$$

for each $n$. This gives

$$\frac{dT_\perp}{dt} = \frac{-\sum_{n=1}^{\infty} A_n \exp(-E_n/(k_B T))}{\sum_{n=0}^{\infty} \exp(-E_n/(k_B T))} \left( \frac{\exp(\hbar\Omega/(k_B T_w)) - \exp(\hbar\Omega/(k_B T))}{\exp(\hbar\Omega/(k_B T_w)) - 1} \right). \tag{A.6}$$

To calculate the spontaneous emission term, $A_n$, we will use Eq. 12 on page 178 in reference [21], which gives $A_n$ as

$$A_n = \frac{4e^2\Omega^4}{3c^3m}\left[|\langle i|x|f\rangle|^2 + |\langle i|y|f\rangle|^2\right]. \tag{A.7}$$

Here, an electron has emitted a photon by making a transition from an initial state $i$ to a final state $f$. Note that $\Omega^2 x = -d^2x/dt^2$ for a harmonic oscillator with frequency $\Omega$ (see pages 191 to 197 in reference [56]). If one substitutes $-\Omega^{-2}d^2x/dt^2$ for $x$ in Eq. A.7, then one recognizes $A_n$ as the quantum equivalent of the classical Larmor formula (see Eq. 4.4).

A calculation of $\langle i|x|f\rangle$ is fairly straightforward. Since the Hamiltonian is that of a harmonic oscillator, one can write $x$ as

$$x = \left(\frac{\hbar}{2m\Omega}\right)^{1/2}(a + a^\dagger) \tag{A.8}$$

where $a$ and $a^\dagger$ are the creation and annihilation operators[1] respectively (see pages 241-242 in reference [32]). The initial state of the electron is $\langle n|$. Since the electron is radiating energy, the final state $f$ must be less than $n$. This implies that only the creation operator contributes to $\langle i|x|f\rangle$. Finally, the creation operator gives zero contribution to $\langle i|x|f\rangle$ unless the final state is $f = n - 1$. Thus, $|\langle i|x|f\rangle|$ becomes

$$|\langle i|x|f\rangle| = \left(\frac{\hbar n}{2m\Omega}\right)^{1/2}. \tag{A.9}$$

Using a similar expression for $|\langle i|y|f\rangle|$, and substituting these into the equation for $A_n$, Eq. A.7, one obtains

$$A_n = \frac{4e^2\Omega^3\hbar n}{3c^3m}. \tag{A.10}$$

After a little more manipulating, one finally obtains

$$\frac{dT_\perp}{dt} = -\frac{4e^2\Omega^3\hbar}{3c^3m}\left(\frac{\exp(\hbar\Omega/(k_B T_w)) - \exp(\hbar\Omega/(k_B T))}{\exp(\hbar\Omega/(k_B T_w)) - 1)(\exp(\hbar\Omega/(k_B T)) - 1)}\right). \tag{A.11}$$

[1] In some books these are called raising and lowering operators.

Substituting this for $\langle dE_\perp/dt \rangle$ in Eq. 4.11 and assuming that the temperature stays isotropic at all times (i.e. using Eq. 4.12 and Eq. 4.13), one finally obtains Eq. 4.17 and Eq. 4.18 for $dT/dt$.

To end this section we will make a few comments about electron spin. In particular, we estimate how much an electron's spin changes the cyclotron radiation rate calculated here. First, if the external magnetic field is uniform in space, then an electron's spin is decoupled from the rest of the electron's motion. In this case the spin has no effect on the cyclotron radiation rate. Second, for time scales of order the cyclotron radiation time, the orientation of an electron's spin does not flip (e.g. go from a spin of -1/2 to a spin of +1/2) except, possibly, through coupling with the gyromotion, and this happens only when the magnetic field has spatial dependence.

For nonuniform magnetic field, the spin energy may be coupled to the perpendicular energy. In this case the perpendicular energy will then have to dissipate some of the electron spin energy as the plasma cools. However, the total spin energy is much less than the total kinetic energy, and thus the calculated radiation rate, as given by Eqs. 4.17 and 4.18, changes only slightly when spin and particle motion are coupled.

When the spin of an electron is included in the Hamiltonian, the total energy of an electron changes by either $\hbar\Omega/2$ or by $-\hbar\Omega/2$, depending on the orientation of the electron's spin to the magnetic field axis. If an electron's spin changes state, the total energy of the electron changes by $\hbar\Omega$, which is equal to the energy difference between two adjacent Landau levels[2]. For a plasma which is described by a Boltzmann distribution, the energy per electron due to spin, energy above the spin

[2]For breivity we have dropped the Landé $g$-factor, which will makes a correction of about 0.1%. The Landé $g$-factor make the energy difference between adjacent Landau levels slightly different than the energy difference between the two spin states.

ground state energy, is

$$E_s = \hbar\Omega \left( \frac{\exp(-\hbar\Omega/(2k_B T))}{\exp(\hbar\Omega/(2k_B T)) + \exp(-\hbar\Omega/(2k_B T))} \right), \tag{A.12}$$

whereas the total kinetic energy is $3k_B T/2$. Thus, the ratio of spin energy to kinetic energy is

$$R_E = \frac{2x}{3(1+\exp(x))} \tag{A.13}$$

where $x = \hbar\Omega/(k_B T)$.

For $k_B T \gg \hbar\Omega$, $R_E$ is much less than 1, and the spin energy can be ignored when calculating the cyclotron radiation rate. In fact, the radiation rate decreases by $1/(1+R_E)$, which is important only for $x \sim 1$. For $x \sim 1$ the radiation rate decreases by about 15% if an electron's gyromotion and its spin are coupled. For $B = 60$ kG, $\hbar\Omega/k_B = 8.1$ K so that $x \sim 1$ implies a plasma temperature of 8.1 K. For $B = 60$ kG and a plasma temperature of 30 K (i.e. the limit of the temperature measurement), the correction to the calculated radiation rate is at most 8%. Such small corrections are probably not noticeable with the present temperature measurement.

## A.2 $\langle dE/dt \rangle = d\langle E \rangle/dt = (k_B/2)dT/dt$

In this section we consider a distribution of particles which are described by a Maxwellian, and where the energy of particle $j$ is given by

$$E_j(t) = E_j(0)C(t). \tag{A.14}$$

Note that $C(t)$ does not depend on the particle's energy and that $C(0) = 1$. This form for the particle's energy comes from a differential equation of the form $dE_j/dt = E_j d(\log(C))/dt$.

Often one is not interested in $E_j(t)$ but $\langle E(t) \rangle$ where the average is over the distribution of particles. For example, from cyclotron cooling one has $C(t) = \exp(-t/\tau_r')$ (see Eq. 4.4) and from the bounce invariant analysis one has $C(t) =$

$(l(0)/l(t))^2$ (see Eq. 4.26). To simplify matters, we treat only the 1-dimensional case (e.g. $E = E_x$). The two dimensional case is handled by writing $\mathbf{E} = E_x\hat{x} + E_y\hat{y}$ and solving for each dimension independently.

We wish to show that $\langle dE/dt\rangle = d\langle E\rangle/dt = (k_B/2)dT/dt$. This occurs since simply increasing all the particles' energies by a common factor does not change the nature of a Maxwellian; it changes only the temperature, or average energy, of the particles. The expression for $\langle dE/dt\rangle$ is

$$\langle dE/dt\rangle = \int_{-\infty}^{\infty} \frac{d}{dt}\left(\frac{mv^2}{2}\right)\exp(-mv^2/(2k_BT))dv \Big/ \int_{-\infty}^{\infty}\exp(-mv^2/(2k_BT))dv. \tag{A.15}$$

Assuming that $T(t) = T(0)C(t)$, one obtains $mv^2(t)/(2k_BT(t)) = E(t)/(k_BT(t)) = E(0)/(k_BT(0))$ which does not depend on time. Thus, the time-derivative can be pulled outside of the integral (note that $dv$ occurs in both the denominator and the numerator, so that changing $dv$ to $dv\sqrt{C(t)}$ also has no effect), and therefore

$$\langle dE/dt\rangle = \frac{d}{dt}\left(\frac{\int_{-\infty}^{\infty}\left(\frac{mv^2}{2}\right)\exp(-mv^2/(2k_BT))dv}{\int_{-\infty}^{\infty}\exp(-mv^2/(2k_BT))dv}\right) = d\langle E\rangle/dt. \tag{A.16}$$

Since $\langle E\rangle = (k_B/2)T$, one obtains

$$\frac{d\langle E\rangle}{dt} = \frac{k_B}{2}\frac{dT}{dt} = \frac{k_BT(0)}{2}\frac{dC(t)}{dt}. \tag{A.17}$$

This gives $T(t) = T(0)C(t)$ which demonstrates that the original assumption and the final solution are self-consistent.

## A.3 Modulated Length Fourier Coefficients

To modulate the plasma length, the potential on one of the confining gates is modulated sinusoidally. In general, a sinusoidal modulation of one of the end gates will not produce a purely sinusoidal modulation of the plasma length. However, the plasma length can be written as a Fourier series. In this appendix, we will estimate

the fundamental amplitude and first harmonic amplitude of this Fourier series. That is, we will estimate $B_1$ and $B_2$ in Eq. 5.6.

We assume that the plasma is well confined (one in which the potentials on the confining gates are much greater than the plasma space charge potential), and consider a plasma that is trapped in $G_7$ (see Fig. 3.1). We take the potential on $G_7$ to be ground and the unmodulated potential on $G_6$ and $G_8$ to be $V_0$. The potential on $G_6$ is modulated as $V(t) = V_0 + \delta V \sin(\omega t)$.

Let $z = 0$ be the boundary between $G_6$ and $G_7$ and let $z' = 0$ be the boundary between $G_7$ and $G_8$. For $r = 0$ and a zero temperature plasma, the plasma stops abruptly at each end. When the modulated potential is turned off, we let the plasma stop near the $G_6$-$G_7$ boundary at the point $z_0$ and near the $G_7$-$G_8$ boundary at the point $z_0'$. This gives a plasma length at $r = 0$ of $l_0 = l_3 - z_0 - z_0'$ where $l_3$ is the length of $G_7$. We now assume that $l_3/R_w \gg 1$, so that we can ignore the potential contribution due to $G_8$ near $z_0$ (similarly, we ignore the potential due to $G_6$ near $z_0'$).

First, consider the plasma end near $G_6$. The vacuum potential $V_v$ from $G_6$ is

$$V_v = V_0 \sum_{k=1}^{\infty} \frac{J_0(r\chi_{0,k})/R_w) \exp(-z\chi_{0,k}/R_w)}{\chi_{0,k} J_1(\chi_{0,k})}. \tag{A.18}$$

where $J_n$ is the Bessel function of order $n$, and $\chi_{0,k}$ is the $k^{th}$ root of $J_0(\chi_{0,k}) = 0$. This formula for the vacuum potential assumes that $G_6$ is semi-infinite in length. By well confined, one means that the plasma ends at a point $z_0/R_w \gg 1$; thus, to a good approximation only the first term ($k = 1$) in Eq. A.18 is needed. This, for $r = 0$ and for $z = z_0$, is

$$V_e \approx V_0 \frac{\exp(-z_0\chi_{0,1}/R_w)}{\chi_{0,1} J_1(\chi_{0,1})}. \tag{A.19}$$

Here, $V_e$ is the potential contribution from $G_6$ at the point $z_0$ where the plasma ends. Note that if the plasma density is changed from $n$ to $n + \delta n$, $V_e$, to lowest order in $\delta n/n$, will change to $(1 + \delta n/n)V_e$.

Now let the potential on $G_6$ change to $V = V_0 + \Delta V$. This causes the plasma length to change, causing, in turn, a plasma density change. The fractional plasma density change is given by

$$\frac{\delta n}{n} \approx \frac{l_0 - l}{l_0} = \varepsilon. \tag{A.20}$$

where $l_0$ is the original length and $l$ is the new length. The new point where the plasma ends is given by

$$(1+\varepsilon)V_e \approx V \frac{\exp(-z\chi_{0,1}/R_w)}{\chi_{0,1}J_1(\chi_{0,1})}. \tag{A.21}$$

Solving for $z$ gives

$$z \approx \left(\frac{R_w}{\chi_{0,1}}\right) \log\left(\frac{V}{(1+\varepsilon)V_e\chi_{0,1}J_1(\chi_{0,1})}\right). \tag{A.22}$$

As for the point where the plasma ends near $G_8$, one has a similar equation for $z'$, except that $V = V_e$,

$$z' \approx -\left(\frac{R_w}{\chi_{0,1}}\right) \log((1+\varepsilon)\chi_{0,1}J_1(\chi_{0,1})). \tag{A.23}$$

The new plasma length is $l = l_3 - z - z'$, which gives

$$\left.\frac{dl}{dV}\right|_{V=V_0} = \frac{-R_w}{l_0\chi_{0,1}(1+2R_w/(l_0\chi_{0,1}))V_0} \tag{A.24}$$

and

$$\left.\frac{d^2l}{dV^2}\right|_{V=V_0} = \frac{R_w}{l_0\chi_{0,1}(1+2R_w/(l_0\chi_{0,1}))V_0^2}. \tag{A.25}$$

Here we have dropped a term of order $(R_w/(l_0\chi_{0,1}))^3$ in the last equation, and we have used

$$\frac{d\varepsilon}{dV} = \frac{-1}{l_0}\frac{dl}{dV} \tag{A.26}$$

and

$$\frac{d^2\varepsilon}{dV^2} = \frac{-1}{l_0}\frac{d^2l}{dV^2}. \tag{A.27}$$

Substituting this into a Taylor expansion for $l(V)$, Eq. 5.7, with $\Delta V = \delta V \sin(\omega t)$ yields

$$l \approx l_0 \left\{ 1 + \frac{R_w}{4 l_0 \chi_{0,1}(1 + 2R_w/(l_0\chi_{0,1}))} \left(\frac{\delta V}{V_0}\right)^2 \right. \tag{A.28}$$

$$- \frac{R_w}{l_0 \chi_{0,1}(1 + 2R_w/(l_0\chi_{0,1}))} \left(\frac{\delta V}{V_0}\right) \sin(\omega t) \tag{A.29}$$

$$\left. + \frac{R_w}{4 l_0 \chi_{0,1}(1 + 2R_w/(l_0\chi_{0,1}))} \left(\frac{\delta V}{V_0}\right)^2 \sin(2\omega t + \pi/2) \right\}. \tag{A.30}$$

Thus, to lowest order in $\delta V/V_0$,

$$B_1 = \frac{-R_w}{l_0 \chi_{0,1}(1 + 2R_w/(l_0\chi_{0,1}))} \left(\frac{\delta V}{V_0}\right), \tag{A.31}$$

and

$$B_2 = \frac{R_w}{4 l_0 (1 + 2R_w/(l_0\chi_{0,1}))} \left(\frac{\delta V}{V_0}\right)^2 = -\frac{B_1}{4} \left(\frac{\delta V}{V_0}\right). \tag{A.32}$$

For the data in this thesis, $\delta V/V_0$ is typically about 1/5 so that $B_2 \sim -B_1/20$, and is indeed small by this estimate.

## A.4 Heating versus $\omega$ including $B_2$

When the plasma length modulation is a pure sinusoid, the compressional heating model (see section 5.2.2) predicts maximum heating per cycle when $\beta = 1$ (i.e. $\omega = 3\nu$). When harmonics are included into the length modulation, the maximum heating no longer occurs at $\beta = 1$. For example, if the first harmonic's amplitude is much bigger than all the other amplitudes, including the fundamental's amplitude, then the maximum heating per cycle occurs when $2\omega = 3\nu$ (i.e. $2\beta = 1$). In this section the modulation frequency which produces the maximum heating per cycle is determined when the fundamental amplitude and the first harmonic amplitude are non-zero (i.e. $B_1$ and $B_2$ are non-zero and $B_n = 0$ for $n > 2$ (see Eq. 5.6)).

The plasma length is assumed to modulate as

$$l(t) = l_0[1 + \epsilon \sin(\omega t) + \delta\epsilon \sin(2\omega t)]. \tag{A.33}$$

Here $B_1 = \epsilon$ and $B_2 = \delta\epsilon$. This results in an average heating per cycle (see the derivation in section 5.2.2) which is given by

$$\Delta T_{\|} = T_{\|} \frac{8\pi}{9} \epsilon^2 \left[ \frac{\beta}{1+\beta^2} + 2\delta^2 \frac{4\beta}{1+(2\beta)^2} \right] \tag{A.34}$$

By cycle we mean a time equal to $2\pi/\omega$. For this case, the peak in the heating lies between $\beta = 1$ and $\beta = 1/2$, depending on the size of $\delta$. Table A.1 lists various values of $\beta_{\max}$ versus $\delta$, where $\beta_{\max}$ is the $\beta$ which produces the most heating per cycle. From this table, we find that one makes less than a 4% error by letting $\beta_{\max} = 1$ (i.e. $\omega = 3\nu$) as long as $\delta$ is less than 0.2. For the data in this thesis we believe that $\delta \lesssim 0.1$, so that we are making less than a 1% error by letting $\beta_{\max} = 1$.

| $\delta$ | $\beta_{\max}$ |
|---|---|
| 0.0 | 1.00 |
| 0.1 | 0.99 |
| 0.15 | 0.98 |
| 0.2 | 0.96 |
| 0.25 | 0.94 |
| 0.3 | 0.92 |
| 0.4 | 0.87 |
| 0.5 | 0.81 |
| 0.7 | 0.71 |
| 1.0 | 0.62 |

**Table A.1:** Corrections to $\beta_{\max}$ due to finite harmonics of the modulated plasma length. $\delta$ is the ratio of the first harmonic's amplitude to the fundamental's amplitude.

## A.5 $\bar{I}$ for Small $r_c/b$

In reference [48], $\bar{I}(r_c/b)$ is given by Eq. 24 (Eq. 2.16 in this thesis). This equation is very difficult to calculate unless $\kappa \gg 1$ (i.e. $r_c/b \ll 1$). In this thesis,

the experimental data is compared to Eq. 2.20, which is much easier to calculate. Equation 2.20 is an approximation to $\bar{I}(r_c/b)$ valid for $r_c/b \ll 1$. In this appendix we derive Eq. 2.20.

Using Eq. 2.17 for $h(\kappa\sigma^3, \eta)$ and Eq. 2.18 for $g(\eta)$, Eq. 2.16 for $\bar{I}$ becomes

$$\bar{I}(r_c/b) \approx 4.39 \int_0^\infty \frac{d\sigma}{\sigma} \exp(-\sigma^2/2) \exp(-\pi\kappa/\sigma^3) \int_0^\infty d\eta\, \eta^3 \frac{\kappa^2}{\sigma^6} \exp(-1.35\kappa\eta^2/\sigma^3). \tag{A.35}$$

It is worth stopping at this point and examining the integral over $\eta$. First, although the $\eta$ integral seems to depend on $\kappa/\sigma^3$, in fact it does not. This can be seen by letting $\eta' = \eta\sqrt{\kappa/\sigma^3}$. Second, for large $\kappa$ the main contribution to the integral comes from small $\eta$. This is fortunate since Eq. 2.17 and Eq. 2.18 are an approximation to $h(\kappa\sigma^3, \eta)$ and $g(\eta)$ respectively, and are only valid for small $\eta$. For the moment, we will assume that $\kappa$ is large enough so that these approximations are valid.

Note that $\eta$ is merely the impact distance $p$ divided by $b_\parallel$. If the magnetic field is small (i.e. $r_c/b \gg 1$), then the main contribution to velocity space scattering occurs for $\eta > 1$ (see section 2.2). However, for large magnetic field (i.e. $r_c/b \ll 1$), the main contribution to the scattering occurs for small $\eta$. This latter case can be understood by considering the time $\tau$ that characterizes the duration of a collision. $\tau$ is about $(p/v_\parallel)^{-1}$ when $\eta \gtrsim 2$. The larger $\Omega\tau$ is, the stronger the adiabatic invariant and consequently the lower the scattering rate. Here, $\Omega\tau = \Omega p/v_\parallel = (\Omega b_\parallel/v_\parallel)(p/b_\parallel) = (\Omega b_\parallel/v_\parallel)\eta$. Therefore, the larger $\eta$ for a given $(\Omega b_\parallel/v_\parallel)$ the larger $\Omega\tau$ will be, and thus the stronger the adiabatic invariant. Consequently, collisions with small $\eta$ contribute the most to the relaxation rate when $r_c/b \ll 1$.

Preforming the $\eta$ integration gives

$$\bar{I}(r_c/b) \approx 3.79 \int_0^\infty d\sigma\, \frac{\exp(-\sigma^2/2)}{\sigma} \exp(-\pi\kappa/\sigma^3). \tag{A.36}$$

For large $\kappa$ (i.e. small $r_c/b$), the $\sigma$ integral can be evaluated using the saddle point method (also called method of steepest descent in some sources; see pages 373-376

in reference [1]).

The saddle point method works well for integrals of the form

$$\int_C g(z)\exp(sf(z))\,dz \tag{A.37}$$

when $s$ is large. In this case, the main contribution to the integral comes from the region in $z$ where $f(z)$ is a maximum. Let $z_0$ be the point where $f(z)$ is a maximum. The saddle point procedure is to Taylor expand $f(z)$ about the point $z_0$ and then to keep only terms to order $(z-z_0)^2$. Also, $g(z)$ is assumed to be essentially constant over this region.

To see that the $\sigma$ integral is of the form of Eq. A.37, let $\sigma' = \sigma/\kappa^{1/5}$. The $\sigma'$ integral then becomes

$$\int_0^\infty \frac{d\sigma'}{\sigma'}\exp(\kappa^{2/5}(-\sigma'^2/2 - \pi/\sigma'^3)). \tag{A.38}$$

Here, $s = \kappa^{2/5}$, $f(\sigma') = -\sigma'^2/2 - \pi/\sigma'^3$ and $g(\sigma') = 1/\sigma'$. If $\kappa^{2/5}$ is large enough, then the main contribution to the integral will come from the region near $\sigma_0' = (3\pi)^{1/5}$, which is where $f(\sigma')$ is a maximum. Taylor expanding $f(\sigma')$ about $\sigma_0'$ gives

$$f(\sigma') \approx \frac{-5(3\pi)^{2/5}}{6} - \frac{5}{2}(\sigma' - \sigma_0')^2 + \vartheta((\sigma' - \sigma_0')^3). \tag{A.39}$$

Substituting this for $f(\sigma')$ gives

$$\tilde{I}(r_c/b) \approx \frac{\exp(-2.04\kappa^{2/5})}{(3\pi)^{1/5}}\int_0^\infty d\sigma' \exp(-(5/2)\kappa^{2/5}(\sigma' - \sigma_0')^2). \tag{A.40}$$

Again, it is worth examining the integral before evaluating it. First, one might guess that $\kappa$ has to be very large in order for the saddle point method to work since $s = \kappa^{2/5}$. In fact, numerical calculations of Eq. 2.19 show that the saddle point method is good as long as $\kappa \gtrsim 1$. This happens mainly because of the 5/2 in $\exp(-(5/2)\kappa^{2/5}(\sigma' - \sigma_0')^2)$, which effectively increases $\kappa$ by a factor of $(5/2)^{5/2} \approx 10$.

Since the integrand is a gaussian function, the main contribution to the integral comes from the region

$$(5/2)\kappa^{2/5}\,(\sigma' - \sigma_0')^2 \lesssim 2. \tag{A.41}$$

This can be written in terms of $v_{||}$ as $v_T\,((3\pi\kappa)^{1/5} - 1) < v_{||} < v_T\,((3\pi\kappa)^{1/5} - 1)$. Therefore, particles with $v_{||} \sim (3\pi\kappa)^{1/5} v_T$ contribute the most to the relaxation rate. Since the equation for $\bar{I}$, Eq. 2.16, was derived using unperturbed orbits (see section 2.3.1), it will be valid only if $r_c/b' > 1$ where $b' = e^2/(mv_T^2(3\pi\kappa)^{2/5})) = b/(3\pi\kappa)^{2/5}$. From this, we conclude that $r_c/b$ must be less than about 0.03 in order for Eq. 2.16 to be a good approximation to $\bar{I}$.

This is not, however, enough to guarantee that Eq. 2.20 is a good approximation to $\bar{I}$ for $r_c/b \lesssim 0.03$. For this equation to be a good approximation, Eq. 2.17 and Eq. 2.18 must also be good approximates to $h(\kappa\sigma^3, \eta)$ and $g(\eta)$ respectively. It is now believed [19] these approximations are possibly good only for $r_c/b \lesssim 10^{-4}$. And, in general, using Eq. 2.20 for $\bar{I}$ underestimates the relaxation rate in the region $10^{-4} \lesssim r_c/b \lesssim 0.1$.

Finally, carrying out the $\sigma'$ integration (here the lower limit of the integral (i.e. 0) is set to $-\infty$) one obtains Eq. 2.20 for $\bar{I}$.

## A.6 Three-Body Collision Rate

In this section the three-body collision rate is estimated. This rate becomes important when $r_c/b \ll 1$, since it may be larger than the relaxation rate. In this case, the parallel velocity distribution relaxes to a Maxwellian on the three-body collision time scale, and not the relaxation time scale (i.e. $\nu^{-1}$).

Consider a collision between two electrons. If there is no exchange between parallel and perpendicular velocity components, conservation of energy and conservation of momentum imply that the parallel velocity components for the two electrons

are not changed by the interaction, or simply interchange (i.e. $v_{1_\parallel} \leftrightarrows v_{2_\parallel}$). This means that the distribution of parallel velocity remains unchanged with time.

On the other hand, for a typical collision there will be an exchange of parallel and perpendicular velocity components. For $r_c/b \ll 1$, however, this exchange may be so small per collision that the parallel velocity relaxes to a Maxwellian on the three-body collision time scale instead of the relaxation time scale.

If there were no magnetic field, the two-body collision rate would relax the distribution to a Maxwellian at a rate of about $\nu' = nb^2 v_{T_\parallel}$. One expects three-body collisions to relax the parallel velocity distribution to a Maxwellian at a rate a factor of the plasma parameter, $g$, slower than $\nu'$. This estimate then gives the three-body rate, $\nu_3$, as

$$\nu_3 \sim g\,(nb^2 v_{T_\parallel}). \tag{A.42}$$

Of course, this is an order of magnitude estimate. Note that $g$ is related to the correlation parameter $\Gamma$ by

$$g = 3^{3/2}\Gamma^{3/2}. \tag{A.43}$$

The above argument is heuristic, and we are not sure that it is correct. Nor have we been able to find a better argument. One might argue that the factor of $g$ that we have introduced into the three-body collision rate should actually be a factor of $\Gamma$. However, for the parameter regime of interest in this thesis, namely $5\,\mathrm{K} < T < 100\,\mathrm{K}$, $g$ and $\Gamma$ are essentially the same (see table A.2).

Table A.2 lists various values of $g$, $\Gamma$, $\nu$ and $\nu_3$ for a pure electron plasma with $n = 10^9 \mathrm{e/cm}^3$ and $B = 60\,\mathrm{kG}$. Here, $\nu$ is calculated from the O'Neil-Hjorth theory (i.e. Eq. 2.11 with Eq. 2.20 used to calculate $\bar{I}$).

| $T$ (K) | $g$ | $\Gamma$ | $\nu$ (Hz) | $\nu_3$ (Hz) |
|---|---|---|---|---|
| 100 | 0.023 | 0.027 | $2.7 \times 10^4$ | $1.7 \times 10^4$ |
| 50 | 0.065 | 0.054 | $6.8 \times 10^3$ | $1.4 \times 10^5$ |
| 20 | 0.27 | 0.14 | 175 | $2.3 \times 10^6$ |
| 10 | 0.73 | 0.27 | 1.2 | $1.7 \times 10^7$ |
| 5 | 2.1 | 0.54 | $4.2 \times 10^{-4}$ | $1.4 \times 10^8$ |

**Table A.2:** Various values of $g$, $\Gamma$, $\nu$ and $\nu_3$ for $n = 10^9 \mathrm{e/cm}^3$ and $B = 60\,\mathrm{kG}$. Here, $\nu$ is calculated from the O'Neil-Hjorth theory.

## A.7 Joule Heating when $n(r,t) = n(r/x(t))/x^2(t)$

In section 4.3.1 we calculated the rate of change of the electrostatic energy per unit length for a plasma which is expanding radially. In that calculation we used a density profile that is uniform; that is, $n(t)$ is independent of raduis for $r < r_\mathrm{p}(t)$, and is zero for $r > r_\mathrm{p}(t)$. Note, to conserve electrons $n(t)r_\mathrm{p}^2(t) = \text{const}$. In this section we calculate the rate of change of the electrostatic energy per unit length for a more general density profile, $n(r,t) = n_0(r/x(t))/x^2(t)$ where $n_0(r) = n(r, t = 0)$ (we assume that the total number of electrons is conserved, hence the factor $x^2(t)$). Here, an electron initially at a radius $r$ is at position $r/x(t)$ a time $t$ later, and $x(0) = 1$. Note that the uniform density used in section 4.3.1 is a special case of this more general density profile. Again, we assume that the plasma is infinitely long and inside a grounded, perfectly conducting cylinder of radius $R_\mathrm{w}$.

We begin this calculation by writing the electrostatic potential energy per unit length, $PE$, in terms of the electric field, $\mathbf{E}$,

$$PE = 2\pi \int_0^{R_\mathrm{w}} \frac{\mathbf{E}^2}{8\pi} r\, dr. \tag{A.44}$$

The rate of change of $PE$ is

$$\frac{d(PE)}{dt} = \frac{1}{2} \int_0^{R_\mathrm{w}} \mathbf{E} \cdot \frac{d\mathbf{E}}{dt} r\, dr. \tag{A.45}$$

The electric field is calculated from the density as

$$\mathbf{E}(r) = \frac{-4\pi e}{r} \int_0^r n\, r'\, dr'\, \hat{r}. \tag{A.46}$$

The rate of change of the electric field is

$$\frac{d\mathbf{E}(r)}{dt} = \frac{-4\pi e}{r} \frac{d(\int_0^r n\, r'\, dr')}{dt} \hat{r}, \tag{A.47}$$

where

$$\frac{d(\int_0^r n\, r'\, dr')}{dt} = \frac{d(\int_0^r n_0(r'/x(t))/x^2(t)\, r'\, dr')}{dt} = -2nr\frac{dx/dt}{x}. \tag{A.48}$$

Here we have used the fact that $n = n(r,t) = n_0(r/x(t))/x^2(t)$.

We can now write Eq. A.45 as

$$\frac{d(PE)}{dt} = -2(2\pi e)^2 \frac{dx/dt}{x} \int_0^{R_w} rn \left( \int_0^r n(r')\, r'\, dr' \right) dr. \tag{A.49}$$

Note that the integral over $r$ can be written as

$$\int_0^{R_w} rn \left( \int_0^r n(r')\, r'\, dr' \right) dr = \int_0^{R_w} \frac{dQ}{dr} Q\, dr = \frac{Q^2(R_w)}{2} \tag{A.50}$$

where $Q(r) = \int_0^r n(r')\, r'\, dr'$. Writing $Q$ in terms of the number of electrons per unit length, $N_p$, one obtains

$$\frac{d(PE)}{dt} = -e^2 N_p^2 \frac{dx/dt}{x} \tag{A.51}$$

as a simple expression for the rate of change of the electrostatic energy per unit length.

Equation A.51 is the same as Eq. 4.20 as long as $(dn/dt)/n$ is evaluated at the radial origin. To show this let us calculate $(dn/dt)/n$ at the radial origin,

$$\begin{aligned} \frac{1}{n}\frac{dn}{dt}\bigg|_{r=0} &= \frac{x^2}{n_0(r/x)} \frac{d}{dt} \left( \frac{n_0(r/x)}{x^2} \right) \bigg|_{r=0} \\ &= \frac{-x^2}{n_0(r/x)} \frac{dx}{dt} \left[ \left( \frac{d(n_0(r/x))}{d(r/x)} \right) \frac{r}{x^2} + \frac{2n_0(r/x)}{x^3} \right] \bigg|_{r=0} \\ &= \frac{-2}{x}\frac{dx}{dt}. \end{aligned} \tag{A.52}$$

Substituting this into Eq. A.51 yields Eq. 4.20.

## A.8 Relaxation Rate Data

In this section, the experimental relaxation rate data is given as well as other relevant data. The actual experimental setup (i.e. the potentials on the confinement gates) is presented.

Table A.3 lists the data for $B = 61.3\,\mathrm{kG}$, Table A.4 lists the data for $B = 40.9\,\mathrm{kG}$, and Table A.5 lists the data for $B = 30.7\,\mathrm{kG}$. In each of these tables we have included the following:

$T_0$ ...The temperature at the beginning of the first heating cycle. Also, when the compressional heating power balances the cyclotron cooling power, the temperature at the beginning of each heating cycle will be $T_0$.

$\nu$ ...measured relaxation rate. $\nu = 2\pi f/3$ where $f$ is the oscillating frequency which produces the most heating.

$r_c/b$ ...calculated from $T_0$ and $B$.

$t'_r/\tau_r$ ...$t'_r$ is the time during each heating set when the heating cycles are turned off, and $\tau_r$ is the radiation time. $t'_r$ is calculated as $t'_r = t_s - N_c/f$ where $f$ is the frequency which produced the most heating. From this, the maximum temperature achieved by a plasma during a heating set can be estimated as $T_{max} \approx T_0(1 + \exp(t'_r/\tau_r))$.

$\nu t'_r$ ...gives the approximate number of relaxation times, $\nu^{-1}$, for which the heating is off during a heating set. When $\nu t'_r \gg 1$, the time $t'_r$ allows the distribution to relax to a Maxwellian before the next set of heating cycles is applied.

$\epsilon'$ ...an experimental estimate for the amount of fractional plasma length modulation which occurs during the heating phase (i.e. $\delta l/l$), which, it is hoped, gives a good estimate to $\epsilon$ in Eq. 5.3. Here, $\epsilon'$ is estimated by balancing the

peak heating power (i.e. setting $\beta = 1$ in Eq. 5.39) with the radiation power, $\epsilon' = \sqrt{9t_s/(4\pi N_c \tau_r)}$.

$\delta V$ ...the modulated potential amplitude (see Eq. 5.5).

| $T_0$ (K) | $\nu$ (kHz) | $r_c/b$ | $t'_r/\tau_r$ (%) | $\nu t'_r$ | $\epsilon'$ (%) | $\delta V$ (V) |
|---|---|---|---|---|---|---|
| 11051.0 | 4.5 | 256 | 2.4 | 19 | 6.3 | 14.4 |
| 9012.8 | 6.0 | 188 | 2.4 | 13 | 5.3 | 12.0 |
| 7204.2 | 8.3 | 135 | 8.0 | 68 | 5.5 | 12.4 |
| 5714.7 | 11.5 | 95 | 1.9 | 11 | 3.7 | 8.60 |
| 5626.1 | 13.4 | 92 | 11 | 154 | 5.5 | 12.5 |
| 4733.4 | 15.7 | 71 | 3.6 | 24 | 3.7 | 8.50 |
| 3973.2 | 17.8 | 55 | 2.3 | 47 | 3.8 | 9.20 |
| 3727.2 | 20.7 | 50 | 4.8 | 106 | 3.7 | 8.40 |
| 2917.1 | 28.7 | 34 | 5.8 | 179 | 3.7 | 8.40 |
| 1857.6 | 46.1 | 17.6 | 2.2 | 114 | 2.3 | 2.45 |
| 1044.0 | 83.8 | 7.4 | 3.1 | 294 | 2.3 | 5.08 |
| 627.8 | 134.0 | 3.5 | 0.3 | 40 | 1.1 | 2.70 |
| 571.0 | 134.0 | 3.0 | 3.7 | 560 | 2.6 | 5.64 |
| 305.3 | 142.4 | 1.2 | 3.7 | 600 | 2.6 | 5.50 |
| 152.2 | 83.8 | 0.41 | 1.3 | 120 | 2.4 | 4.92 |
| 95.5 | 32.5 | 0.21 | 2.0 | 75 | 2.6 | 13.8 |
| 90.3 | 28.3 | 0.19 | 6.2 | 200 | 4.0 | 7.20 |
| 80.8 | 26.2 | 0.160 | 1.1 | 31 | 2.4 | 5.28 |
| 60.2 | 12.4 | 0.103 | 5.0 | 70 | 4.0 | 7.60 |
| 45.6 | 6.7 | 0.068 | 5.3 | 40 | 4.8 | 10.1 |
| 38.7 | 3.0 | 0.053 | 2.5 | 8 | 7.4 | 10.8 |
| 27.5 | 0.9 | 0.032 | 1.2 | 1 | 12 | 13.8 |

**Table A.3:** Relaxation rate, $\nu$, and other relevant data for $B = 61.3$ kG

All of the relaxation data was taken with the same unmodulated gate potentials. The following gates and end collectors are shown in Fig. 3.3. The potential on $G_1$ to $G_5$ was set to $-60$ V. The modulated gate was $G_6$ and, the unmodulated potential on it was set to $-23$ V. The potential on $G_7$ was set to 0 V and the potential on $G_8$ was set to $-80$ V. The potential on $R_2$ to $R_5$ was set to 80 V and the potential

on $R_1$ was set to 103 V.

| $T_0$ (K) | $\nu$ (kHz) | $r_c/b$ | $t'_r/\tau_r$ (%) | $\nu t'_r$ | $\epsilon'$ (%) | $\delta V$ ($V$) |
|---|---|---|---|---|---|---|
| 10922.0 | 3.7 | 377 | 1.1 | 10 | 4.7 | 7.40 |
| 7430.4 | 6.6 | 211 | 1.0 | 17 | 3.5 | 5.64 |
| 5160.0 | 12.8 | 122 | 0.5 | 17 | 2.5 | 60.4 |
| 5065.4 | 9.9 | 119 | 0.2 | 5 | 2.5 | 4.00 |
| 3537.2 | 20.9 | 69.4 | 0.7 | 38 | 2.1 | 3.19 |
| 3517.4 | 18.8 | 68.8 | 0.6 | 44 | 1.8 | 4.80 |
| 3440.0 | 25.6 | 66.6 | 0.6 | 28 | 1.4 | 4.48 |
| 2339.2 | 38.7 | 37.3 | 0.5 | 49 | 2.1 | 3.30 |
| 2322.0 | 34.6 | 36.9 | 0.6 | 55 | 1.6 | 2.22 |
| 1671.8 | 50.3 | 22.6 | 0.6 | 82 | 1.3 | 1.92 |
| 1032.0 | 94.2 | 10.9 | 0.3 | 62 | 1.0 | 1.38 |
| 725.8 | 121.5 | 6.45 | 0.4 | 114 | 1.0 | 1.36 |
| 490.2 | 140.3 | 3.58 | 0.2 | 72 | 0.8 | 1.02 |
| 375.8 | 199.0 | 2.40 | 0.4 | 204 | 0.8 | 1.04 |
| 259.7 | 203.2 | 1.38 | 0.4 | 212 | 0.8 | 1.02 |
| 184.0 | 194.8 | 0.82 | 0.4 | 196 | 0.8 | 1.01 |
| 123.8 | 169.6 | 0.46 | 0.3 | 148 | 0.8 | 1.06 |
| 76.5 | 77.5 | 0.22 | 0.2 | 30 | 1.0 | 1.30 |
| 54.2 | 37.7 | 0.13 | 0.8 | 84 | 1.7 | 1.78 |
| 39.6 | 10.5 | 0.082 | 2.5 | 70 | 4.2 | 3.50 |

**Table A.4:** Relaxation rate, $\nu$, and other relevant data for $B = 40.9$ kG

| $T_0$ (K) | $\nu$ (kHz) | $r_c/b$ | $t'_r/\tau_r$ (%) | $\nu t'_r$ | $\epsilon'$ (%) | $\delta V$ (V) |
|---|---|---|---|---|---|---|
| 7860.4 | 6.7 | 307 | 0.8 | 26 | 2.7 | 4.56 |
| 2808.8 | 24.7 | 65.5 | 0.3 | 40 | 1.3 | 2.20 |
| 894.4 | 121.5 | 11.8 | 0.2 | 122 | 0.7 | 1.15 |
| 464.4 | 209.4 | 4.4 | 0.1 | 124 | 0.5 | 0.76 |
| 341.4 | 224.1 | 2.8 | 0.1 | 152 | 0.5 | 0.65 |
| 256.3 | 261.8 | 1.8 | 0.2 | 224 | 0.5 | 0.592 |
| 168.6 | 272.3 | 0.96 | 0.2 | 244 | 0.5 | 0.625 |
| 126.4 | 272.3 | 0.63 | 0.2 | 244 | 0.5 | 0.625 |
| 85.1 | 157.1 | 0.35 | 0.1 | 102 | 0.5 | 0.75 |
| 72.2 | 83.8 | 0.27 | 0.2 | 202 | 0.8 | 1.07 |
| 61.9 | 67.0 | 0.21 | 0.7 | 222 | 1.2 | 1.25 |
| 49.9 | 41.9 | 0.16 | 0.5 | 102 | 1.2 | 1.30 |

**Table A.5:** Relaxation rate, $\nu$, and other relevant data for $B = 30.7$ kG

## A.9 Frequently Used Symbols and Units

All of the formulas in this thesis are in Gaussian units (information about Gaussian units can be found in reference [7]). The following table describes some of the symbols used in this thesis.

We use the following definitions for $T_{||}$ and $T_{\perp}$;

$$\frac{1}{2}k_{\rm B}T_{||} = \int_0^\infty 2\pi v_\perp \, dv_\perp \int_{-\infty}^\infty dv_{||} \, \frac{mv_{||}^2}{2} f(v_{||}, v_\perp), \tag{A.53}$$

$$k_{\rm B}T_{\perp} = \int_0^\infty 2\pi v_\perp \, dv_\perp \int_{-\infty}^\infty dv_{||} \, \frac{mv_{\perp}^2}{2} f(v_{||}, v_\perp). \tag{A.54}$$

## SYMBOLS

********** Energies **********

| | | |
|---|---|---|
| $E_{||}$ | | energy parallel to magnetic field |
| $E_\perp$ | | energy perpendicular to magnetic field |
| $T$ | | plasma temperature |
| $T_{||}$ | | temperature parallel to magnetic field |
| $T_\perp$ | | temperature perpendicular to magnetic field |
| $T_{\rm w}$ | | experimental apparatus wall temperature |
| $E_n$ | $(n+1/2)\hbar\Omega$ | Energy of an electron in the $n^{\underline{th}}$ Landau level |

********** Frequencies and Times **********

| | | |
|---|---|---|
| $\Omega$ | $eB/(mc)$ | electron gyrofrequency |
| $\omega_{\rm R}$ | (see Eq. 3.10) | plasma rotation rate |
| $\omega_{\rm p}$ | $\sqrt{4\pi ne^2/m}$ | electron plasma frequency |
| $\nu$ | | electron-electron anisotropic temperature relaxation rate |
| $\nu_3$ | | three-body electron-electron collision rate |
| $\tau_{\rm lifetime}$ | $n\,(dn(r=0)/dt)^{-1}$ | plasma lifetime |
| $\tau_{\rm r}$ | | energy e-fold time for a electron plasma cooling via cyclotron radiation when $\nu \gg \tau_{\rm r}^{-1}$ |

# SYMBOLS continued

********** Velocities **********

| | | |
|---|---|---|
| $v_{\|\|}$ | | electron velocity parallel to magnetic field |
| $v_\perp$ | | electron velocity perpendicular to magnetic field |
| $v_{\mathrm{T}}$ | $\sqrt{k_{\mathrm{B}}T/m}$ | electron thermal velocity |
| $v_{\mathrm{T}_{\|\|}}$ | $\sqrt{k_{\mathrm{B}}T_{\|\|}/m}$ | electron thermal velocity parallel to magnetic field |
| $v_{\mathrm{T}_\perp}$ | $\sqrt{k_{\mathrm{B}}T_\perp/m}$ | electron thermal velocity perpendicular to magnetic field |
| $\mathbf{u}$ | $\mathbf{v}_2 - \mathbf{v}_1$ | relative velocity between two electrons |
| $u_{\|\|}$ | | component of $\mathbf{u}$ parallel to magnetic field |
| $u_{0_{\|\|}}$ | | $u_{\|\|}$ when the electrons are not interacting |

********** Others **********

| | | |
|---|---|---|
| $f(\mathbf{x}, \mathbf{v}, t)$ | | distribution function |
| $n$ | | density |
| $N_{\mathrm{l}}$ | $\int n(r,z)dz$ | number of electrons on a field line at radius $r$ |
| $V$ | | electric potential (generally due to confinement gates) |
| $\phi$ | | electric potential (generally due to space charge) |
| $\mathbf{E}$ | | electric field |
| $\mathbf{B}$ | | magnetic field |
| $B$ | $\|\mathbf{B}\|$ | magnitude of magnetic field |
| $\bar{I}$ | $\nu/(nb^2v_{\|\|})$ | |
| $\Lambda$ | $\log(p_{\mathrm{max}}/b)$ | Coulomb logarithm |

## SYMBOLS continued

********** **Lengths** **********

| | | |
|---|---|---|
| $\lambda_D$ | $\sqrt{k_B T/4\pi n e^2}$ | Debye length |
| $b$ | $e^2/(k_B T)$ | classical distance of closest approach |
| $b_{\|\|}$ | $4e^2/(m u_{0_{\|\|}}^2)$ | distance of closest approach that two electrons with initial relative velocity $u_{0_{\|\|}}$ can obtain |
| $\rho$ | $v_\perp/\Omega$ | electron gyroradius |
| $r_c$ | $v_T/\Omega$ | thermal electron gyroradius |
| $p$ | | impact parameter |
| $p_{max}$ | $\approx \lambda_D$, for $r_c > \lambda_D \gg b$, $\approx r_c$, for $\lambda_D > r_c \gg b$ | Coulomb cutoff distance |
| $R_w$ | | radius of gates |
| $r_p$ | | radius of plasma |
| $l$, $l_p$ | | length of plasma |

********** **Dimensionless** **********

| | | |
|---|---|---|
| $g^{-1}$ | $(4\pi/3)\, n\lambda_D^3$ | number of particles in a Debye sphere |
| $\Gamma$ | $(e^2/k_B T)(4\pi n/3)^{1/3}$ | correlation parameter |
| $\kappa$ | $\sqrt{2}\Omega b/v_{T_{\|\|}}$ | Note that, for $T_{\|\|} = T_\perp$, then $v_{T_{\|\|}} = v_{T_\perp}$, and $\kappa = \sqrt{2}b/r_c$ |
| $\sigma$ | $v_{\|\|}/(\sqrt{2}v_{T_{\|\|}})$ | |
| $\eta$ | $p/b_{\|\|}$ | |
| $\epsilon$ | | 1/2 ratio of maximum plasma length variation (due to the modulated confinement gate potential) to plasma length |

# References


[1] G. Arfken. *Mathematical Methods for Physicists.* Academic Press, second edition, 1970.

[2] R. Balescu. Irreversible processes in ionized gases. *Physics of Fluids*, 3:52, 1960.

[3] L. Boltzmann. Weitere studien uber das warmegleichgewicht unter gasmolekulen. *Wien. Ber.*, 66:275, 1872.

[4] R. J. Burke and R. F. Post. Experimental determination of the rate of slowing of fast ions in a dense plasma in a magnetic field. *Physics of Fluids*, 17:1422, 1974.

[5] S. Chapman and D. Cowling. *The Mathematical Theory of Non-Uniform Gases.* Cambridge Univ. Press, 1939. For a comparision between theory and experiments see chapters 12-14.

[6] R. S. Cohen, L. Spitzer, and P. McR. Routly. The electrical conductivity of an ionized gas. *Phys. Rev.*, 80:230, 1950.

[7] D. L. Book ed. *NRL Plasma Formulary.* 1983. (revised edition).

[8] R. C. Davidson. *Theory of Non-Neutral Plasmas.* W. A. Benjamin, 1974.

[9] J. S. deGrassis. *Equilibrium, Waves and Transport in the Pure Electron Plasma.* PhD thesis, University of California at San Diego, 1977.

[10] C. F. Driscoll. Private communication.

[11] C. F. Driscoll. Observation of an $l = 1$ diocotron mode on a hollow electron column. Submitted to *Phys. Rev. Letters.*

[12] C. F. Driscoll and K. S. Fine. Experiments on vortex dynamics in pure electron plasma. *Physics of Fluids.* To be published in 1990.

[13] C. F. Driscoll, K. S. Fine, and J. H. Malmberg. Reduction of radial losses in a pure electron plasma. *Physics of Fluids*, 29:2015, 1986.

[14] C. F. Driscoll and J. H. Malmberg. Hollow electron column from an equipotential cathode. *Physics of Fluids*, 19:760, 1976.

[15] C. F. Driscoll and J. H. Malmberg. Length-dependent containment of a pure electron plasma. *Physical Review Letters*, 50:167, 1983.

[16] D. H. E. Dubin and T. M. O'Neil. Adiabatic expansion of a strongly correlated pure electron plasma. *Physical Review Letters*, 56:728, 1986.

[17] A. D. Fokker. Die mittlere energie rotierender elektrischer dipole im strahlungsfeld. *Annalen Der Physik und Chemie*, xliii:810, 1914.

[18] S. Gasiorowicz, M. Neuman, and R. J. Riddell. Dynamics of ionized media. *Phys. Rev.*, 101:922, 1956.

[19] M. Glinsky, T. M. O'Neil, and K. Tsuruta. Private communication.

[20] H. Goldstein. *Classical Mechanics.* Addison Wesley, 1980. 2nd ed.

[21] W. Heitler. *The Quantum Theory of Radiation.* Oxford, third edition, 1970.

[22] J. R. Hiskes and A. H. Futch. Some observations on mirror losses. *Nucl. Fusion*, 14:116, 1974.

[23] P. G. Hjorth and T. M. O'Neil. Numerical study of a many particle adiabatic invariant. *Physics of Fluids*, 30:2613, 1987.

[24] P. H. Hjorth. *A Many Particle Adiabatic Invariant of Strongly Magnetized Pure Electron Plasmas.* PhD thesis, University of California at San Diego, 1988.

[25] A. W. Hyatt. *Measurement of the Anisotropic Temperature Relaxation Rate in a Magnetized Pure Electron Plasma.* PhD thesis, University of California at San Diego, 1988.

[26] A. W. Hyatt, C. F. Driscoll, and J. H. Malmberg. Measurement of the anisotropic temperature relaxation rate in a pure electron plasma. *Physical Review Letters*, 59:2975, 1987.

[27] S. Ichimaru. *Basic Principles of Plasma Physics.* W. A. Benjamin, 1973.

[28] S. Ichimaru and M. N. Rosenbluth. Relaxation processes in plasmas with magnetic field. temperature relaxations. *Physics of Fluids*, 13:2778, 1970.

[29] J. D. Jackson. *Classical Electrodynamics.* John Wiley and Sons, second edition, 1975.

[30] W. H. Kohl. *Handbook of Materials and Techniques for Vacuum Devices.* Reinhold Publishing Corporation, 1967. Chapter 16.

[31] N. A. Krall and A. W. Trivelpiece. *Principles of Plasma Physics.* San Francisco Press, Inc., 1986.

[32] L. D. Landau and E. M. Lifshitz. *Quantum Mechanics: Non-Relativistic Theory.* Volume 3 of *Course of Theoretical Physics*, Addison-Wesley Publishing Co., Inc., third edition, 1976.

[33] A. Lenard. On bogoliubov's kinetic equation for a spatially homogeneous plasma. *Ann. Phys.*, 10:390, 1960.

[34] E. M. Lifshitz and L. P. Pitaevskii. *Statistical Physics, Landau and Lifshitz Course of Theoretical Physics.* Volume 5, Pergamon Press, third edition, 1980. Part 1.

[35] J. H. Malmberg and J. S. deGrassis. Properties of a nonneutral plasma. *Physical Review Letters*, 35:577, 1975.

[36] J. H. Malmberg, C. F. Driscoll, and W. D. White. Experiments with pure electron plasmas. *Physica Scripta*, T2:288, 1982.

[37] J. H. Malmberg and A. W. Hyatt. Private communication.

[38] J. H. Malmberg and T. M. O'Neil. The pure electron plasma, liquid and crystal. *Physical Review Letters*, 39:1333, 1977.

[39] F. L. Mohler. Resistivity and power input in the cesium discharge at high current density. *Bur. Stnd. J. Res.*, 21:873, 1938.

[40] D. Montgomery, G. Joyce, and L. Turner. Magnetic field dependence of plasma relaxation times. *Physics of Fluids*, 17:2201, 1974.

[41] D. Montgomery, L. Turner, and G. Joyce. Fokker-planck equation for a plasma in a magnetic field. *Physics of Fluids*, 17:954, 1974.

[42] D. C. Montgomery and D. A. Tidman. *Plasma Kinetic Theory.* McGraw-Hill, 1964.

[43] T. G. Northrop. *The Adiabatic Motion of Charged Particles.* Interscience Publishers, 1963.

[44] T. M. O'Neil. Collision operator for a strongly magnetized pure electron plasma. *Physics of Fluids*, 26:2128, 1983.

[45] T. M. O'Neil. A confinement theorem for nonneutral plasmas. *Physics of Fluids*, 23:2216, 1980.

[46] T. M. O'Neil. A new theory of transport due to like-particle collisions. *Physical Review Letters*, 55:943, 1985.

[47] T. M. O'Neil and C. F. Driscoll. Transport to thermal equilibrium of a pure electron plasma. *Physics of Fluids*, 266, 1979.

[48] T. M. O'Neil and P. G. Hjorth. Collisional dynamics of a strongly magnetized pure electron plasma. *Physics of Fluids*, 28:3241, 1985.

[49] A. J. Peurrung and J. Fajans. I would like to thank A. J. Peurrung and J. Fajans; who developed a computer program to analyze the low temperature density profiles.

[50] A. J. Peurrung and J. Fajans. Non-neutral plasma shapes and edge profiles. *Physics of Fluids B*, 4:693, 1990.

[51] M. Planck. On a proposition of statistical dynamics and its extension in the quanta theory. *Sitz. der preuss. Akad*, 324, 1917.

[52] S. A. Prasad and T. M. O'Neil. Finite length thermal equilibria of a pure electron plasma column. *Physics of Fluids*, 22:278, 1979.

[53] C. W. Roberson and C. F. Driscoll, editors. *Non-neutral Plasma Physics*, American Institue of Physics, 1988. See pages 1-74 for a better review of theories and experiments on pure electron plasmas.

[54] M. N. Rosenbluth, W. M. McDonald, and D. L. Judd. Fokker-planck equation for an inverse-square force. *Phys. Rev.*, 107:1, 1957.

[55] S. Lin and E. L. Resler and A. Kantrowitz. Electrical conductivity of highly ionized argon produced by shock waves. *J. Appl. Phys.*, 26:95, 1955.

[56] R. M. Sillitto. *Non-Relativestic Quantum Mechanics.* Quadrangle Books, Inc., Chicago, 1960.

[57] G. R. Smith and A. N. Kaufmann. Stochastic acceleration by an obliquely propagating wave-an example of overlapping resonances. *Physics of Fluids*, 21:2230, 1978.

[58] L. Spitzer and R. Härm. Transport phenomena in a completely ionized gas. *Phys. Rev.*, 89:977, 1953.

[59] W. B. Thompson and J. Hubbard. Long-range forces and the diffusion coefficients of a plasma. *Rev. Mod. Phys.*, 32:714, 1960.